



12-2011

Application of Liquid Chromatography-Tandem Mass Spectrometry Techniques to the Study of Two Biological Systems

Mary E. Eisenhauer
meisenh2@utk.edu

Recommended Citation

Eisenhauer, Mary E., "Application of Liquid Chromatography-Tandem Mass Spectrometry Techniques to the Study of Two Biological Systems." Master's Thesis, University of Tennessee, 2011.
https://trace.tennessee.edu/utk_gradthes/1066

This Thesis is brought to you for free and open access by the Graduate School at Trace: Tennessee Research and Creative Exchange. It has been accepted for inclusion in Masters Theses by an authorized administrator of Trace: Tennessee Research and Creative Exchange. For more information, please contact trace@utk.edu.

To the Graduate Council:

I am submitting herewith a thesis written by Mary E. Eisenhauer entitled "Application of Liquid Chromatography-Tandem Mass Spectrometry Techniques to the Study of Two Biological Systems." I have examined the final electronic copy of this thesis for form and content and recommend that it be accepted in partial fulfillment of the requirements for the degree of Master of Science, with a major in Chemistry.

Shawn R. Campagna, Major Professor

We have read this thesis and recommend its acceptance:

Michael Best, Michael Sepaniak

Accepted for the Council:

Carolyn R. Hodges

Vice Provost and Dean of the Graduate School

(Original signatures are on file with official student records.)

**Application of Liquid Chromatography-Tandem Mass Spectrometry
Techniques to the Study of Two Biological Systems**

**A Thesis Presented for the
Master of Science
Degree
The University of Tennessee, Knoxville**

**Mary E. Eisenhauer
December 2011**

Dedication

For JP, LP, and Olive

Acknowledgements

I would like to first thank my family, for their continuous love, support, patience, and understanding throughout my life and scholastic career. Thank you to my committee members Dr. Best and Dr. Sepaniak, for their support and time spent. I would also like to acknowledge my unofficial committee member and collaborator Dr. Jason Collier, as well as the Collier lab for their hard work. Next, I must thank Dr. Campagna, for helping me realize my potential, but for also helping me reach my career goals as an educator. Thank you to my wonderful group members, Sneha Belapure, Jessica Gooding, Amanda May and Jesse Middleton, for their support and friendship. I could not have asked for a better group of people to work with. A special acknowledgement is owed to Jess and Amanda for teaching me everything I know, but more importantly, for their friendship over the past two years. I would not have made it without them, and I truly appreciate everything they have done for me.

Abstract

Quorum sensing is a type of bacterial cell-cell communication that uses diffusible signaling molecules to allow the regulation of gene expression based on cell density. The two types of signaling molecules discussed here are autoinducer-2 (AI-2) and a class of signaling molecules of the *N*-acylhomoserine lactone type (AHL) also known as autoinducer-1 (AI-1). The biosynthesis of both of these molecules has origins in a metabolic pathway. Although undisputed in some cases, the role of AI-2 and AHLs in bacterial systems has come into question. Here, the functionalities of these molecules were investigated by utilizing isotope-labeled versions of both AI-2 and AHLs in conjunction with liquid chromatography tandem mass spectrometry in order to quantify the natural abundance of these molecules in various bacterial cultures. Presented in this thesis are, a synthesis for doubly-deuterated AHLs as well as chromatographic and spectrometric methods for the detection and quantitation of these molecules. Additionally, a series of relevant biological studies which effectively and prolifically utilize these synthetic and analytical techniques are presented here.

The selective destruction of beta-cell mass in the Langerhans of the pancreas is known to cause Type 1 diabetes mellitus (T1DM). Currently, many key aspects of this autoimmune disease remain unclear, including the exact mechanism of beta-cell death. In a collaborative project with Dr. J. Jason Collier, we sought to test the hypothesis that different mechanisms of cell death will present discrete phenotypic profiles which can be distinguished by a specific metabolic response in response to the appropriate stimuli. A second project presented in this thesis is the development and implementation of a method to profile the metabolic signatures of two types of pancreatic beta-cell death using tandem mass spectrometry techniques. Using 832/13 rat insulinoma cells, the metabolite pools of cells exposed to either pro-inflammatory cytokines or known apoptosis inducers, such as camptothecin, were analyzed. In this investigation, it was found that this method was effective in defining reproducible metabolic differences in each sample tested. Taken together with complementary methods used in the Collier lab, the results collectively demonstrate that pancreatic beta-cells undergo apoptosis in response to camptothecin, but not pro-inflammatory cytokines.

Table of Contents

Introduction	1
<u>Chapter I</u>	
Achieving a Quantitative Understanding of Quorum Sensing	2
Abstract.....	3
Background and Significance	4
Quorum Sensing	5
AI-2 Mediated Quorum Sensing	6
<i>N</i> -Acylhomoserine Lactone Mediated Quorum Sensing	7
Biosynthesis of Quorum Sensing Molecules.....	8
<i>Vibrio harveyi</i> and <i>Escherichia coli</i> Background	9
Analytical Methods	11
High Performance Liquid Chromatography Tandem Mass Spectrometry	12
Isotope Dilution Tandem Mass Spectrometry	14
Results and Discussion	14
Design Rationale for the Synthesis of Stable Isotope Labeled AHLs	15
Synthesis of Deuterated <i>N</i> -Acyl Homoserine Lactones	15
Separation and Detection of AHLs and AI-2	18
Profiling Bacterial Species for Autoinducer Production	20
Results: <i>Vibrio fischeri</i>	21
Results: <i>Edwardsiella tarda</i>	23
Characterization of an Enteropathogen	24
Results: <i>Yersinia enterocolitica</i>	24
Methods and Materials	30
General Methods.....	30
Bacterial Growth Conditions	30
Chromatographic Details	30
General Mass Spectrometric Detection Parameters for AI-2 and AHLs	31
Measurement of AI-2 Concentration [AI-2]	31
Measurement of AHL Concentration(s) [AHL(s)]	32
Data Handling for the Calculation of [DPD].....	32
Data Handling for the Calculation of [AHL(s)]	33
Measurement of Glucose Concentration by Colorimetric Glucose Oxidation Assay.....	34
<i>N</i> -Boc-(4,4- ² H ₂)homoserine- α -OtBu ester, 2	34
<i>N</i> -Boc-(4,4- ² H ₂)homoserine- γ -OMs- α -OtBu ester, 3	35
<i>N</i> -Boc-(4,4- ² H ₂)methionine-OtBu ester, 4	36
(4,4- ² H ₂)methionine, 5	36
<i>N</i> -Fmoc-(4,4- ² H ₂)methionine, 6	37
Representative <i>N</i> -Fmoc-(4,4- ² H ₂)methionine resin loading protocol	37
Representative Synthesis of (² H ₂) AHLs, <i>N</i> -octanoyl-(4,4- ² H ₂) acylhomoserine lactone	38
<u>Chapter II</u>	
Determining Metabolic Profiles of Rat Insulinoma Cells.....	41
Abstract.....	42
Background and Significance	43
Metabolomics Background	43
Metabolic Profiling vs. Metabolic Fingerprinting	44
Sample Type	44
Sampling and Extracting.....	45

Analytical Methods	46
Mass Spectrometry Based Metabolomics.....	46
Data Analysis	47
Pancreatic β -cell Death	47
Pancreatic β -cell Death is likely the Result of a Non-Apoptotic Mechanism	48
Results and Discussion	50
Distinction between Cell Death	50
Metabolic Profiling by Tandem Mass Spectrometry	51
Methods and Materials	53
General Methods.....	53
Cell Extraction Procedure.....	53
Chromatographic Details	53
Mass Spectrometric Detection Parameters.....	54
Data Handling and Statistical Analysis	55
Conclusion	56
References.....	57
Appendix	65
NMR Spectra.....	66
Tabulated Data.....	79
Metabolites Measured.....	106
Vita.....	110

List of Tables

Table 1: Structure, Abbreviations and SRMs for AHLs	18
Table 2: Strains Profiled.....	20
Table 3: <i>V. fischeri</i> strain ES114 [AHLs] Used in Figure 6A and 7B	79
Table 4: <i>V. fischeri</i> strain MJ-1 [AHLs] Used in Figure 6B and 7A.....	80
Table 5: <i>V. fischeri</i> strain CL21 [AHLs] Used in Figure 6C	81
Table 6: <i>V. fischeri</i> strain VCW2G7 [AHLs] Used in Figure 6D.....	82
Table 7: <i>V. fischeri</i> Cell Densities Used in Figure 6E	83
Table 8: <i>V. fischeri</i> strains MJ-1 and ES114 [DPD] Used in Figure 7	84
Table 9: <i>E. tarda</i> No Added Glucose and 0.14% Glucose Cell Density and [DPD] Figure 8	85
Table 10: <i>Y. enterocolitica</i> No Added Glucose Cell Density and [DPD]/OD Used in Figure 9.....	86
Table 11: <i>Y. enterocolitica</i> 0.08% Glucose Cell Density and [DPD]/OD Used in Figure 9.....	87
Table 12: <i>Y. enterocolitica</i> 0.14% Glucose Cell Density and [DPD]/OD Used in Figure 9.....	88
Table 13: <i>Y. enterocolitica</i> 0.20% Glucose Cell Density and [DPD]/OD Used in Figure 9.....	89
Table 14: <i>Y. enterocolitica</i> No Added Glucose [DPD] and % Glucose Used in Figure 10A.....	90
Table 15: <i>Y. enterocolitica</i> 0.08% Glucose [DPD] and % Glucose Used in Figure 10B	91
Table 16: <i>Y. enterocolitica</i> 0.14% Glucose [DPD] and % Glucose Used in Figure 10C	92
Table 17: <i>Y. enterocolitica</i> 0.20% Glucose [DPD] and % Glucose Used in Figure 10D	93
Table 18: <i>Y. enterocolitica</i> No Added Glucose Cell Density and [DPD]/OD Used in Figure 11 ..	94
Table 19: <i>Y. enterocolitica</i> 0.08% Glucose Cell Density and [DPD]/OD Used in Figure 11.....	95
Table 20: <i>Y. enterocolitica</i> 0.14% Glucose Cell Density and [DPD]/OD Used in Figure 11.....	96
Table 21: <i>Y. enterocolitica</i> 0.20% Glucose Cell Density and [DPD]/OD Used in Figure 11.....	97
Table 22: <i>Y. enterocolitica</i> 0.30% Glucose Cell Density and [DPD]/OD Used in Figure 11.....	98
Table 23: <i>Y. enterocolitica</i> 0.50% Glucose Cell Density and [DPD]/OD Used in Figure 11.....	99
Table 24: <i>Y. enterocolitica</i> No Added Glucose [DPD] and % Glucose Used in Figure 12A.....	100
Table 25: <i>Y. enterocolitica</i> 0.08% Glucose [DPD] and % Glucose Used in Figure 12B	101
Table 26: <i>Y. enterocolitica</i> 0.14% Glucose [DPD] and % Glucose Used in Figure 12C	102
Table 27: <i>Y. enterocolitica</i> 0.20% Glucose [DPD] and % Glucose Used in Figure 12D	103
Table 28: <i>Y. enterocolitica</i> 0.30% Glucose [DPD] and % Glucose Used in Figure 12E	104
Table 29: <i>Y. enterocolitica</i> 0.50% Glucose [DPD] and % Glucose Used in Figure 12F.....	105
Table 30: Metabolites Measured	106
Table 31: Metabolites Measured	108

List of Figures and Schemes

Figure 1: Quorum sensing is cell density dependent	5
Scheme 1: (S)-4,5-dihydroxy-2,3-pentandione (DPD)	6
Scheme 2: Biosynthesis of <i>N</i> -acylhomoserine lactones (AHL)	7
Figure 2: <i>N</i> -acylhomoserine lactones (AHLs)	8
Figure 3: The Activated Methyl Cycle	9
Figure 4: Landscape depictions of AI signal/cell density ratios, and AI synthesis rates	10
Scheme 3: Fragmentation reactions of AHLs and derivitizaion of DPD	13
Scheme 4: Solution phase synthesis of (S)-[4,4,2H ₂]- <i>N</i> -Fmoc-methionine	16
Scheme 5: Solid phase synthesis of various AHLs.....	17
Figure 5: Chromatographic separation and detection of AHLs	19
Figure 6: Production of 3OC6, C6, C7 and C8 AHLs in <i>V. fischeri</i>	22
Figure 7: Cascade depictions of all autoinducers produced by <i>V. fischeri</i>	23
Figure 8: Growth kinetics and DPD production in <i>Edwardsiella tarda</i>	24
Figure 9: Average growth kinetics and [DPD]/cell # for <i>Yersinia enterocolitica</i> in BHI.....	26
Figure 10: Average [DPD] and [glucose] for <i>Yersinia enterocolitica</i> in BHI	27
Figure 11: Average growth kinetics and [DPD]/cell # for <i>Yersinia enterocolitica</i> in LB	28
Figure 12: Average [DPD] and [glucose] for <i>Yersinia enterocolitica</i> in LB.....	29
Figure 14: Representative heatmap displaying metabolite fold changes	52

Introduction

Life in all of its forms is fundamentally chemical in nature. At the unique intersection of chemistry and biology, chemistry is the universal language which governs all biological systems. Over the years, the discipline of chemical biology has grown to include the tools of the core disciplines of chemistry such as analytical and synthetic chemistry. Applications of these tools have been essential for the probing and understanding of relevant biological problems and questions because many of them are in fact rooted in chemistry. The two systems, whose studies provided the subsequent results detailed in this thesis, were investigated principally by variations of liquid chromatography-tandem mass spectrometry techniques.

The first system presented is the primary cell-cell communication systems of bacterial species. These systems, termed quorum sensing, are a method by which bacteria use small molecules to send information about the status of their population density and possibly their immediate environment. The variety of platforms used to study these systems are expansive, ranging anywhere from genomics to classical analytical techniques. The immediate goal surrounding research of these systems also varies. Quorum sensing pathways continue to be newly identified in different species of bacteria and in different environments. Alternatively, the purpose for studying quorum sensing could be to determine why these systems are present and for what purpose they ultimately serve. The studies presented in Chapter I of this thesis will focus on the quantitation of the small molecules involved in quorum sensing in different bacterial species in an effort to better define the exact nature of quorum sensing systems.

The second system of interest is the global metabolism of rat insulinoma cells. These cells will serve as a model for the human pancreatic islet cells affected by the autoimmune disease, Type 1 Diabetes mellitus (T1DM). Although the destruction of these cells is known to cause T1DM, the exact mechanism of death is unknown. Consequently, the delineation of this mechanism is essential for the advancement toward a cure. Most of the current studies focus on the genomic manipulation of pathways which are known to be involved in T1DM. From a chemical standpoint, the studies presented in Chapter II will focus on profiling the metabolism of rat insulinoma cells in order to better understand possible mechanisms thought to be responsible for pancreatic islet cell death.

Chapter 1

Achieving a Quantitative Understanding of Quorum Sensing

Abstract

The quorum sensing signal Autoinducer-2 (AI-2) is thought to be an interspecies signal, and while its signaling abilities are not disputed in all cases, there has been evidence of an alternative use for AI-2. Its biosynthesis is linked to the activated methyl cycle, which has raised the question as to whether its function is strictly signaling, metabolic or a combination of the two. Conversely, only gram negative bacteria are known to produce the quorum sensing signals *N*-acyl homoserine lactones (AHLs) or Autoinducer 1 (AI-1). These molecules are produced by an intersection of two biosynthesis pathways that ordinarily serve unrelated metabolic functions. Often, one species will produce more than one AHL and/or integrate a different class of quorum sensing molecules such as AI-2. Our lab has designed a strategy for the determination of the role of AI-2 through detection and quantification, and previous studies employing these strategies have led to a basic definition of quorum sensing. Currently, there are no such tools available for the quantitation of AI-1s. From here we aimed to develop a similar set of tools for the detection and quantitation of AHLs. First, we have designed and carried out a synthesis of stable isotope labeled AHLs that incorporates the use of solid phase techniques, and can produce any AHL sought-after, due to the strategic placement of the isotope into the conserved lactone core. With these stable isotope labeled standards in hand, we then sought to develop chromatographic and spectrometric methods in order to use the technique of isotope dilution tandem mass spectrometry. Using all the tools developed by our lab, we were able to accurately quantitate exact concentrations of AHLs from biological samples, as well as continue to probe these species for AI-2 production, to begin to understand the relationship between these different quorum sensing systems.

Background and Significance

For many years it had been postulated that the bacterial world possessed a means by which cooperative behaviors could ensure that the efforts of many outweighed the efforts of few. It was noted that the communal nature of bacteria was beneficial for survival.¹ While intrinsically interesting, the methods by which many bacteria communicate with each other are of particular interest because of their physiological implications. One of these methods consists of the synthesis, accumulation, and recognition of small diffusible molecules that has been termed quorum sensing.²⁻⁴ Quorum sensing was first discovered decades ago, but it has gained interest recently due to the role this mechanism plays in biofilm formation.⁵⁻⁷ Understanding the underlying mechanisms of biofilm formation is of importance because of the role they play in chronic infections persistent in diseases such as cystic fibrosis.⁸⁻¹⁰ Several pathogenic bacteria have been found that produce quorum sensing-dependent biofilms, and many of them are antibiotic resistant. The ability to interrupt these quorum sensing pathways could potentially lead to novel anti-infective agents that have several advantages over traditional agents.^{11, 12}

Though many significant discoveries have been made, there is still more to be understood about quorum sensing and the molecules involved. One basic problem is the lack of a definition of the term quorum sensing. Currently, the term is used to encompass all phenotypic expressions which are found to be regulated by the production and recognition of diffusible chemical signals, regardless of whether the purpose is to transmit information on local cell density. However, it is becoming more evident with increasing interest, that the pathways and mechanisms of quorum sensing circuits are more dynamic, diverse and complex than originally thought.¹³⁻¹⁵ For example, there are now many reports of bacteria that possess quorum sensing machinery, yet do not employ quorum sensing molecules in order to measure cell density. Conversely, other bacteria utilize multiple quorum sensing molecules and systems in order to regulate a single behavior. There are many questions about this sometimes oversimplified mechanism that need to be answered if a definite and comprehensive understanding of quorum sensing molecules and pathways is to be achieved.

The analytical techniques that have been used previously have been focused toward the detection of these quorum sensing molecules in biological systems. If the original thought that the production of these molecules is strictly a means for bacteria to essentially “count” cell

numbers, then quantifying these molecules should be the next logical step in determining the information content of signaling molecules. It is our belief that characterizing the function of quorum sensing on an individual basis will begin with the quantitation of quorum sensing molecules. The work presented in this chapter is built upon the tools previously employed by our lab for the quantitation of quorum sensing molecules, and demonstrates the effectiveness of synthetic isotopically labeled internal standards coupled with unbiased and sensitive analytical techniques for quantitation in a variety of bacterial species.

Quorum Sensing

Quorum Sensing is the term that has been given to the unique capability by which bacterial communities monitor population and adjust behaviors accordingly, allowing them to adapt to different environmental factors and cues. This is accomplished by a variety of small diffusible signaling molecules, and there are now many known examples of signaling mechanisms in a broad range of bacteria that act as quorum sensing systems. The mechanisms have been shown to be cell density dependent; while each single cell may emit a low concentration of these small molecules, at high cell densities high concentrations of signal will consequently be reached^{4, 6} (Figure 1). Thus, a quorum is necessary for the community to recognize its own minimal population density in order to regulate gene expression. The physiological processes and behaviors that are regulated by the gene expression resulting from quorum sensing are usually thought to be beneficial to the population and can range anywhere from biofilm formation to virulence depending on the species.¹⁶ Other examples include motility, bioluminescence, and anti-biotic resistance.¹⁷⁻¹⁹ One of the genes regulated by quorum sensing, discovered in early studies, is the production of the signaling molecules themselves which gives them their common name autoinducers (AI).

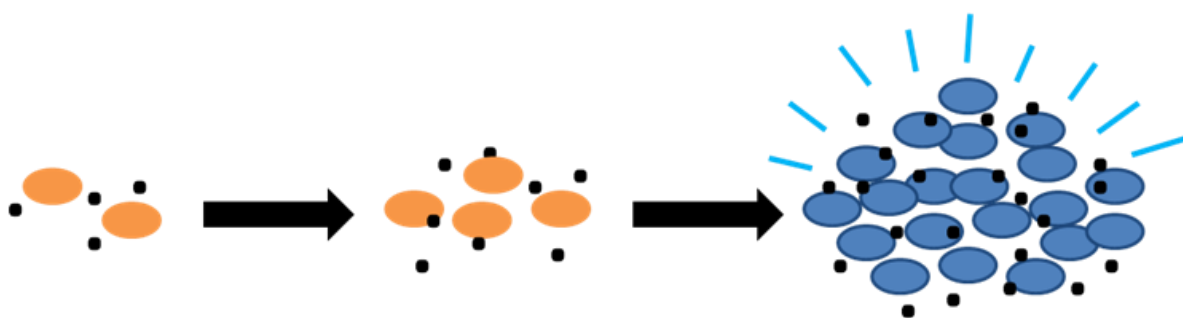
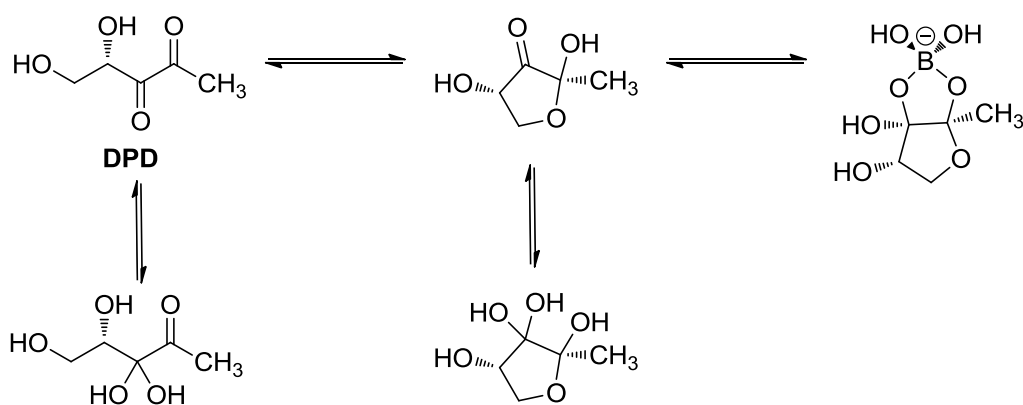


Figure 1: Quorum sensing is cell density dependent.

Quorum sensing can be interspecies or intraspecies. Major classes of intraspecies signaling systems include those of gram negative bacteria, which produce *N*-acyl homoserine lactones (AHLs), or autoinducer 1 (AI-1s)¹, and gram positive bacteria, which produce cyclic peptides (AIPs)²⁰. The interspecies signals that are variations of (*S*)-4,5-dihydroxy-2,3-pentandione (DPD), are known as AI-2, and have been found in both gram positive and gram negative bacteria²¹. Both types function similarly. The work presented in this thesis will focus on intraspecies AI-1 molecules as well as the interspecies AI-2 signaling molecule. All AIs will be profiled in strains that utilize one or both signaling systems. The relationship between the two signaling pathways will be examined in species possessing both systems.

AI-2 Mediated Quorum Sensing

Initially, it was thought that a quorum sensing molecule produced by a particular species was the primary means by which that species “talked” among its own kind. However, the only known quorum sensing signal common to both gram negative and gram positive bacteria, AI-2, is used throughout a wide variety of bacteria. The molecule was first discovered in the bioluminescent marine organism *Vibrio harvey*²², and its structure was finally elucidated in 2002.²³ AI-2 in its active form has many different chemical forms. Each species may recognize a different chemical form. As shown in Scheme 1, it can spontaneously rearrange and can also hydrate or borate. Its synthetic precursor, DPD, is synthesized by the enzyme (*S*) ribosyl homocysteinase,

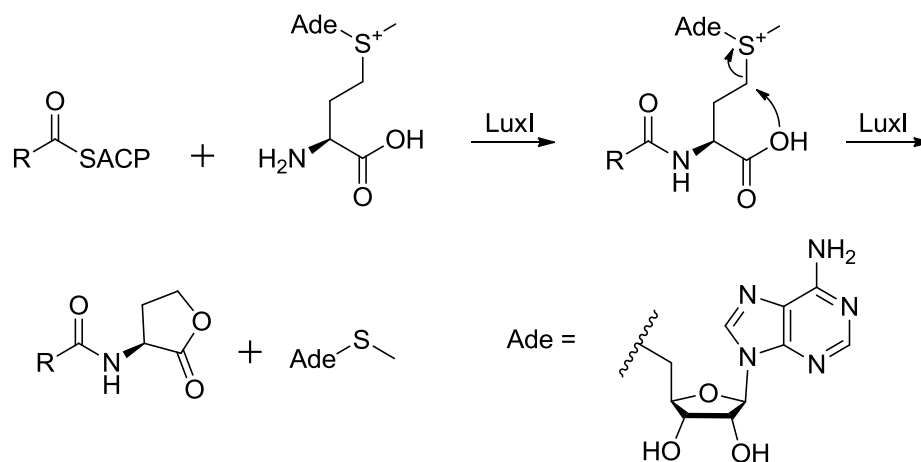


Scheme 1: (*S*)-4,5-dihydroxy-2,3-pentandione (DPD) can spontaneously rearrange, hydrate, or borate to form multiple chemically active forms.

(LuxS).²⁴ LuxS was identified as the AI-2 synthase in 1999, although this enzyme had previously been described in 1968 as a part of the activated methyl cycle.²⁵ This enzyme is well conserved; nearly half of all sequenced bacteria, both gram positive and gram negative, contain a LuxS homologue lending support to the idea that AI-2 is an interspecies signal.²¹ Throughout this text, the terms DPD and AI-2 will be used interchangeably.

***N*-Acylhomoserine Lactone Mediated Quorum Sensing**

Many gram negative bacteria produce one or more acylated homoserine lactone molecules to be utilized as signaling molecules. AHL-mediated quorum sensing was first identified in *V. fischeri*.²⁶ The molecule produced was identified as (3*S*)-*N*-[3-oxo-hexyl]-homoserine lactone. From here, several other signaling systems were identified in a wide range of species.¹ Once thought to be unique to marine bacteria, it is now clear that AHL signaling is a well conserved regulatory system that is widespread throughout proteobacteria.^{27, 28} The process by which quorum sensing bacteria produce and utilize AHLs has been extensively studied and is relatively well characterized. Mechanistically, it is fairly simple. Acyl homoserine lactones are synthesized by a family of proteins of the LuxI-type. When the quorum is reached, another protein, encoded in the same lux operon, of the LuxR-type detects and interacts with



Scheme 2: A proposed mechanism for the biosynthesis of *N*-acylhomoserine lactones (AHL).

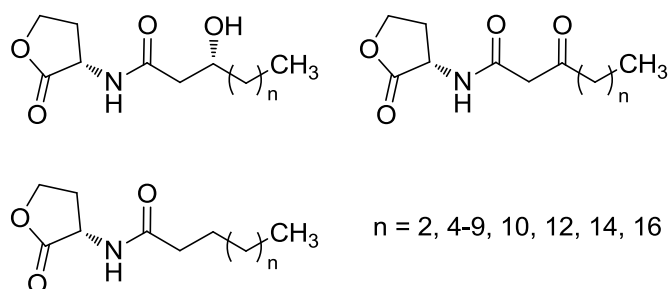


Figure 2: *N*-acylhomoserine lactones (AHLs). AHLs are named by their chain length and by substituent in the 3 position.

the AHLs, which then causes changes in genotypic and phenotypic expression by transcriptional activation.²⁹ These complexes catalyze the formation of the amide bond between the amino group of *S*-adenosyl methionine (SAM) and the acyl chain from an acyl carrier protein (ACP).⁶ Scheme 2 depicts a proposed mechanism by which AHLs are synthesized by LuxI. The acyl chains can vary in length but are usually even numbered due to the fact that they originate in lipid synthesis pathways. They may also be unsaturated, have branching or be oxidized in the 3 position (Figure 2). AHLs are named by the chain length and by additional substitution in the 3 position. Given that the synthesis of these molecules involves the integration of two biological pathways that ordinarily serve different purposes, it raises the question as to whether quorum sensing is strictly that, or if there is a metabolic implication for the production of AHLs.

Biosynthesis of Quorum Sensing Molecules

The activated methyl cycle (AMC) is a major metabolic pathway responsible for the recycling of sulfur containing amino acids as well as the methylation of important biomolecules such as DNA and RNA.³⁰ In this cycle *S*-adenosyl methionine (SAM) is produced by a reaction with methionine and adenosine triphosphate (ATP), catalyzed by the enzyme MetK. SAM is then converted into *S*-adenosyl homocysteine (SAH), and then detoxified to generate *S*-ribosyl homocysteine (SRH). The pinnacle enzyme LuxS, which catalyzes the conversion of SRH to homocysteine, is consequently responsible for the production of AI-2 in the same process. The conversion of homocysteine back to methionine then completes the cycle, as shown in Figure 3.

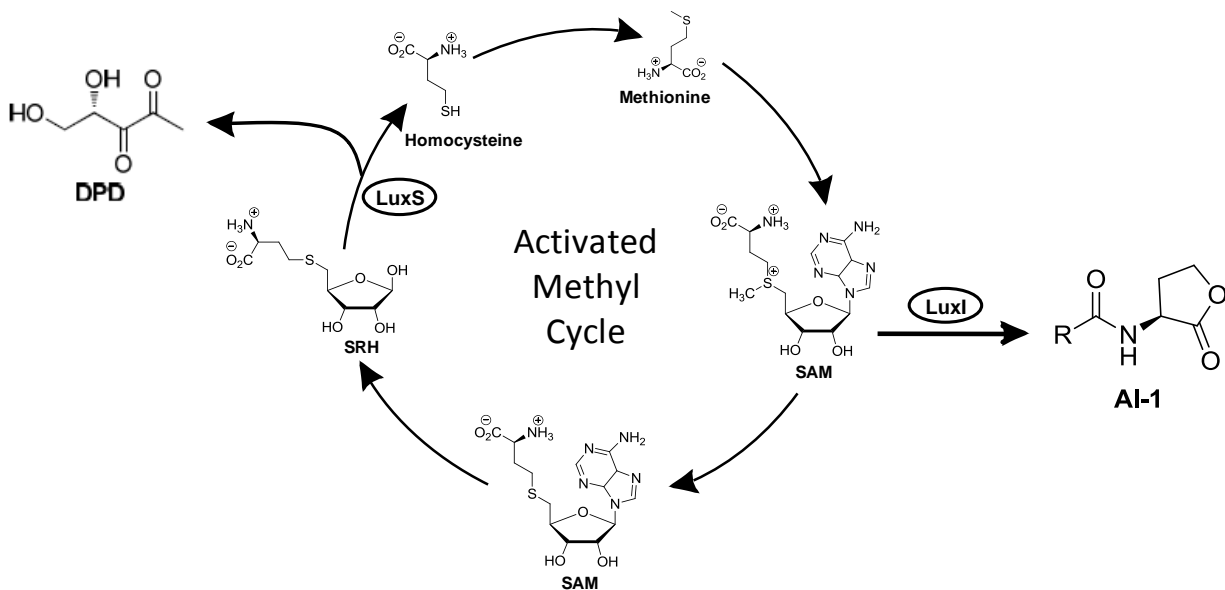


Figure 3: The Activated Methyl Cycle. Both AI-2 and AHL production are linked to the activated methyl cycle. LuxS catalyzes the formation of homocysteine from SRH while also producing DPD. AI-1s, or AHLs, are produced from SAM by the enzyme LuxI.

AI-1 or AHL production is also linked to the activated methyl cycle, as it is synthesized directly from SAM by LuxI. Further, the acyl chain of ALHs is delivered directly from an acyl carrier protein either from lipid synthesis pathways. The realization that both of these quorum sensing molecules are tied to biological pathways that ordinarily serve an alternative purpose, has raised questions as to the purpose of these molecules in various bacterial species. An alternative thought is that the production of these molecules is simply a metabolic side product.

***Vibrio harveyi* and *Escherichia coli* Background**

The quorum sensing circuit that utilizes AI-2 was first discovered in *Vibrio harveyi*, and since then, several homologues of LuxS have been identified in a wide variety of bacteria.²³ *V. harveyi* also utilizes AI-1 quorum sensing. It has been shown that this species uses both of these systems to regulate bioluminescence and that their biological pathways converge. Because of this unique intersection it has been hypothesized that the integration of these two different systems allows *V. harveyi* to identify itself from other species.³¹

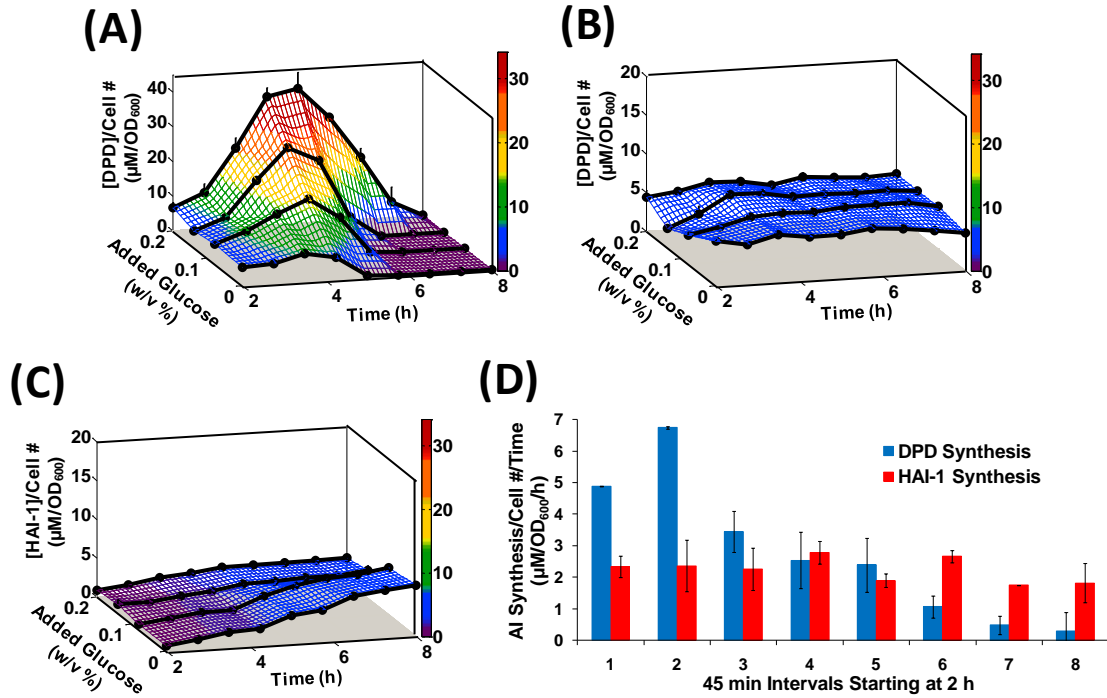


Figure 4: Landscape depictions of AI signal/cell density ratios, and AI synthesis rates. **(A)** *E. coli* is unable to regulate [DPD]/cell density ratio. **(B)** *V. harveyi* maintains this ratio. **(C)** [HAI-1]/cell density ratio increases slightly for *V. harveyi*. **(D)** Over 45 minute intervals, the rate of production of DPD decreases, while the rate of production of HAI-1 is constant for *V. harveyi*.

Escherichia coli is of interest due to the fact that it is known to contain AI-2 producing and transporting enzymes, although it does not appear to use them for quorum sensing signaling.²¹ Of interest is the AI-2 receptor, LsrB, which upon recognition of AI-2, upregulates the importation and catabolism of AI-2.^{21, 32} This has led to the belief that AI-2 has a strictly metabolic purpose in *E. coli*. In studies conducted by our lab, these two species were selected for investigation in order to gain a molecular definition of quorum sensing.³³ The central hypothesis was that if the bacterial species of interest was indeed using AI-2 to transmit information about cell density, then the concentration of AI-2 per cell number should remain constant under all conditions, including time, growth phase and most importantly, nutrient conditions. DPD concentrations in *E. coli*, and DPD and HAI-1 (AI-1 produced by *V. harveyi*) concentrations in *V. harveyi* were monitored as cultures grew from exponential to stationary phase. Each species was grown with one of four different glucose concentrations, 0.0, 0.08,

0.14, or 0.20% (w/v). As glucose concentrations increased, *i.e.* added nutrients increased, neither *E. coli* nor *V. harveyi* demonstrated a considerable increase in cell density. It was found that [DPD]/cell density in *E. coli* varied from 4.8 ± 0.5 to 39 ± 4.8 $\mu\text{M}/\text{OD}_{600}$, indicating that *E. coli* is not capable of regulating cell density information without regulation of metabolism (Figure 4A). Conversely, [DPD]/cell density in *V. harveyi* remained nearly constant under all the glucose concentrations (Figure 4B), indicating its use as a quorum sensing signal. When [HAI-1]/cell density was examined, the ratio did increase from 0.7 ± 0.2 to 6.6 ± 0.4 $\mu\text{M}/\text{OD}_{600}$. (Figure 4C), however with added glucose concentrations, [HAI-1] showed no significant changes during exponential phase. This led us to believe that HAI-1 is not used as a quorum sensing signal in *V. harveyi*. Additionally, the rate at which *V. harveyi* produces DPD decreased over time, while the rate of production of HAI-1 stayed constant (Figure 4D). The initial studies of these two species are what led to the following definition of quorum sensing³³:

$$\frac{\text{extracellular signal concentration}}{\text{cell density}} = \text{constant}$$

These studies effectively validated a method by which future studies on a wide variety of bacteria could be studied. Using this definition of quorum sensing, [AI-2] can be quickly screened for in various bacteria to determine if the species of interest uses AI-2 as a quorum sensing signal.

Analytical Methods

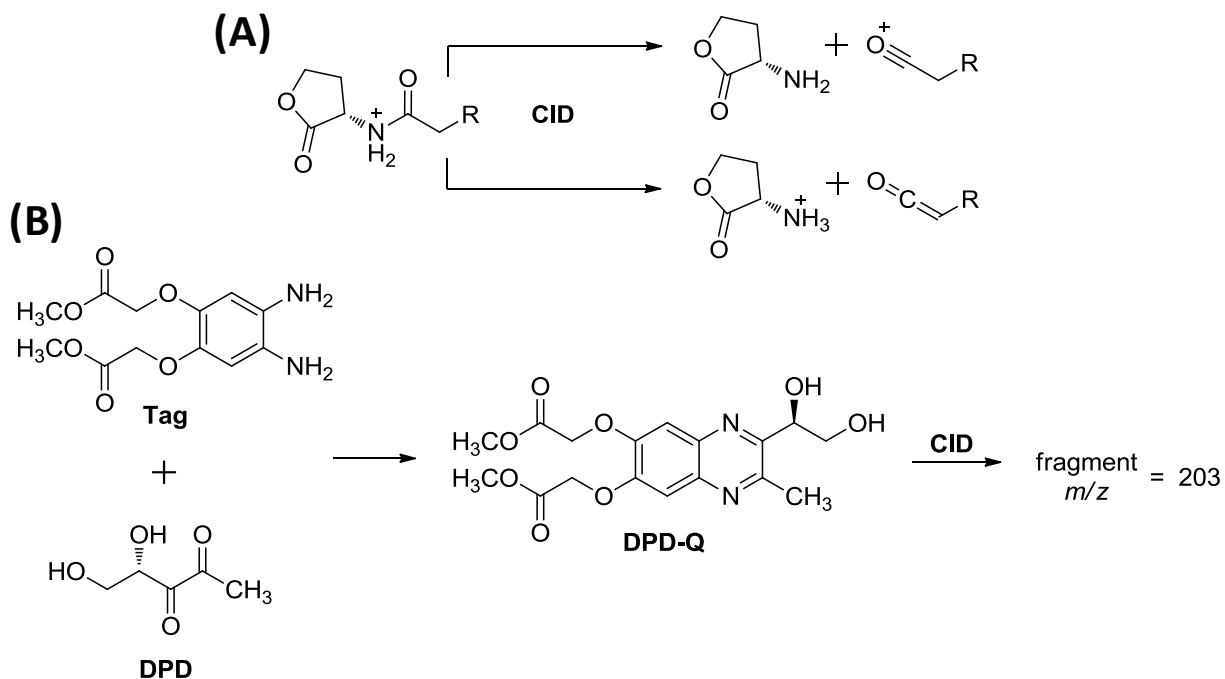
Methods of detection for both AI-2 and AHLs have included bioassays, chromatography, and spectrometry.⁶ Previously, many of the reported studies had focused on genomics and proteomics, or the genotypic and phenotypic expression of quorum sensing-dependant behaviors such as the observation of bioluminescence in order to detect the presence of autoinducers in biological samples. The function of AI-2 and other autoinducers has also been studied by constructing and utilizing *luxS* and other genetic mutants.

Bioassays are used mainly for detection and often rely on reporter strains to obtain quantitation.^{34, 35} Several different methods of detecting and even quantifying AI-2 and AHLs have been reported. Up until now, the most widely used method for detecting AI-2 was the *V.*

harveyi bioassay. Quantitation with this method is problematic as this method has a very small linear range and is not very reproducible. Other problems with detecting AI-2 are that it has many chemical forms, it degrades upon concentration and has no chromophore. In the case of AHL detection, crucial drawbacks of bioassay methods are that sensitivity varies greatly between different AHLs, and a different assay is needed for different species of bacteria. Although these methods were initially useful in determining the presence of AIs, they are lacking in the ability to produce a quantitative understanding of quorum sensing molecules. One of the earliest quantitative methods developed was a radioactive assay in which [1-¹⁴C]-L-methionine is incorporated into production of AHLs via SAM.³⁶ Using this method, relative amounts of AHLs can be quantified, however the use of [1-¹⁴C]-L-methionine is costly, and this method failed to identify all of the AHLs previously reported for the bacteria of interest suggesting a lack of sensitivity. Gas chromatography combined with mass spectrometry has also been implemented for the identification and quantitation of [AHL].^{37, 38}

High Performance Liquid Chromatography Tandem Mass Spectrometry

Profiling of AHLs have been completed using LC/MS techniques and have been successful in establishing a methodology in which semi-quantitative information can be rapidly produced.^{39, 40} While our approach uses similar technology, it ultimately provides direct quantitation that combines a number of preferred attributes not previously seen before in the field. Using high performance liquid chromatography tandem mass spectrometry (LC-MS/MS) in conjunction with selected reaction monitoring (SRM) produces a method that is adequately sensitive, facile and universal. This method was first used for the detection and quantitation of [AI-2] by our lab in the *V. harveyi* and *E. coli* experiments with good results.⁴¹ After separation by liquid chromatography, samples can be analyzed by the method of selected reaction monitoring events (SRM) on a triple quadrupole mass spectrometer. In this method a precursor ion of m/z is selected in the first quadrupole. This parent ion is then fragmented by collisionally-induced dissociation (CID) in the second quadrupole, and a characteristic fragment of the ion is selected in the third. This allows compounds of the same mass to be separated as well as co-eluting compounds. This method is perfectly suited for detection of AHLs as they have two specific fragmentations reactions, both of which can be detected by SRM (Scheme 3A).



Scheme 3: Fragmentation reactions of AHLs and derivitization of DPD. **(A)** AHLs can undergo two collisionally induced fragmentations while DPD must be first derivitized to the stable quinoxaline (DPD-Q) prior to detection **(B)**.

In the case of AI-2, the chemical properties of DPD have made its detection difficult. Our lab has designed a method by which DPD is first derivitized (Scheme 3B).⁴¹ As a stable quinoxaline, it can then be detected with ease by the techniques just described.

Another advantage to the use of these techniques is the availability of metabolomics methods previously developed by our laboratory (see Chapter II). If desired, approximately 350 known metabolites, at least one from every major biosynthetic pathway, could be detected and measured. Being able to monitor concentrations of metabolites would be useful in answering questions concerning AI's role in metabolism because of their links to specific metabolic pathways. Major disturbances in important biological pathways could result in changes in metabolite concentrations which would be detectable by LC-MS/MS.

Isotope Dilution Tandem Mass Spectrometry

Quantitative analysis of naturally occurring AI-2 and/or AHL(s) from biological samples is best accomplished by addition of isotope labeled internal standards in conjunction with the techniques just described. This technique, called isotope dilution mass spectrometry (IDMS), is a useful tool for exact quantification due to its high accuracy and sensitivity at low concentrations, and eliminates the need to construct an external calibration curve. Isotope labeled versions of autoinducers of interest were added to the collected biological samples and analyzed by LC-MS/MS techniques described. Difficulties arise with attempts to quantitate without the use of isotope labeled internal standards. Differences in factors such as media, bacteria, and phases of growth contribute to matrix effects.³⁹ Because isotope dilution involves isotopologues of the compound to be analyzed, chemical and biological matrix effects are eliminated as both compounds are affected equally. Using SRMs, compounds can be separated by mass, and the relative ratio of unlabeled to labeled provides accurate quantitation of the natural product.

Results and Discussion

To move away from phenotypic observation-based methods, we sought to first profile different bacterial strains of interest for AHLs as well as AI-2 and then quantitate their concentrations. The backbone of the work presented in this thesis implements the use of LC-MS/MS spectrometry techniques to obtain direct quantitation of various natural autoinducers produced by multiple bacterial species during normal growth cycles. Combining the use of stable isotope labeled versions of autoinducers and IDMS, we were able to quantify AI-2 and/or any desirable AHL, and through relatively straight forward and well detailed experiments, piece together the role that these molecules play in bacterial species that contain quorum sensing pathways. The preferred tools necessary for detection and quantitation include: the synthesis of stable isotopically labeled internal standards, and the ability to detect and separate these compound by LC-MS/MS techniques. Stemming from the initial *V. harveyi* and *E. coli* studies conducted by our lab, the work presented in this thesis uses similar methods and protocols with slight modification. A synthesis of ¹³C-labeled AI-2 has previously been developed.⁴² Therefore, the synthetic work pertaining to this thesis focuses on the development of a method for

detecting and quantitating AHLs, although the bacterial species studied were indeed profiled for both AI-2 and AHLs. A logical design for the synthesis of doubly deuterated AHLs was proposed and completed, and these molecules have been implemented in several biological studies. Further, chromatographic and spectrometric techniques for the detection of AI-2 have been improved. Methods for AHLs have been developed and refined to the point that future experiments can be executed with ease.

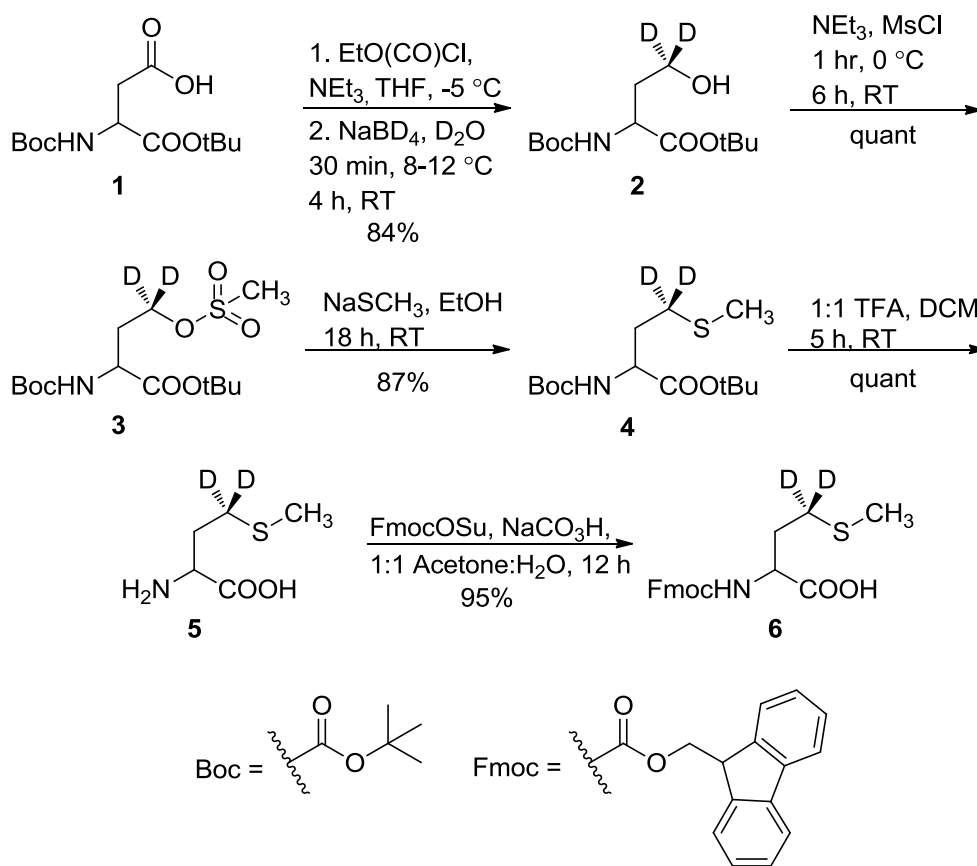
Design Rationale for the Synthesis of Stable Isotope Labeled AHLs

There were several specific goals when we considered the synthesis of stable isotope labeled AHLs. In order to easily produce any AHL desirable with minimal steps, the isotope should be incorporated in the conserved part of the molecule, in this case, the lactone ring. Additionally, the use of two deuteriums, as opposed to the use of one, allows the resulting internal standard to be distinguishable from the appearance of a natural ^{13}C isotopomer. The next objective was to easily and effectively produce all AHLs by using solid phase synthesis techniques. The reason for the use of solid phase chemistry was to increase yields and eliminate the need for further purification. Using this technique also enables the synthesis to be biomimetic. The proposed synthesis should have also yielded an enantiomerically pure product, which would further reduce the chance of the occurrence of matrix effects leading to invalid measurements. Although *N*-acyl-homoserine lactones have been made previously, most reports have either used synthetic C7AHL as reference compound, as it is not thought to be biologically present in most systems,³⁸ or incorporated a ^{13}C into the acyl chain.⁴³ A synthesis of tetra-deuterated acyl-homoserine lactones has been reported⁴⁴, however this synthesis did not take advantage of solid phase techniques, and therefore required extensive purification of both intermediates and AHLs.

Synthesis of Deuterated N-Acyl Homoserine Lactones

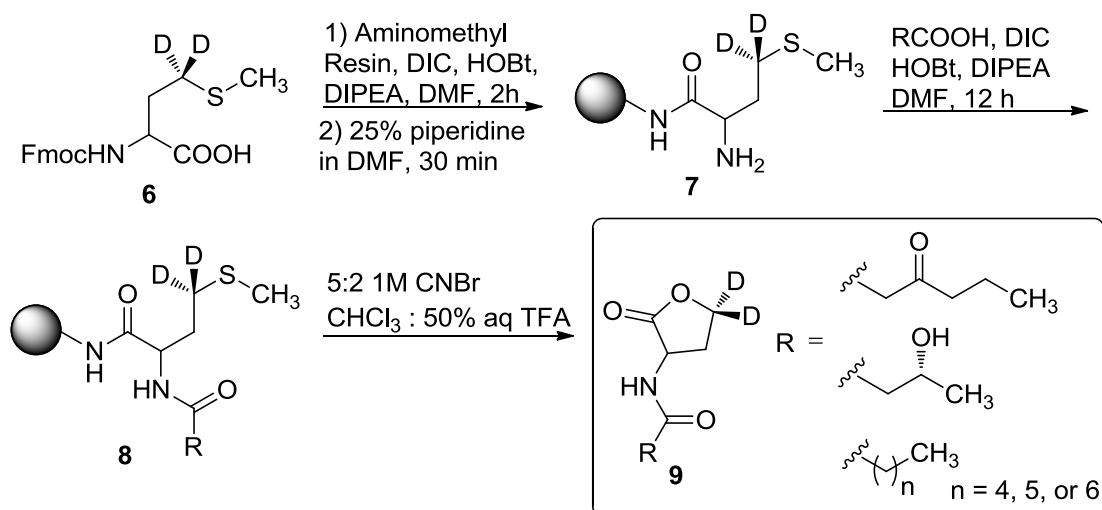
In order to implement the chosen method of incorporating any acyl chain into AHLs by use of solid phase chemistry, we determined that (S)-[4,4, $^2\text{H}_2$]-*N*-Fmoc-methionine **6** would be a useful common intermediate. Synthesis of **6** began with protected aspartic acid derivative, **1**. This molecule was synthesized by a series of known steps.⁴⁵ Protecting groups were chosen by

ability to survive the basic conditions used in Scheme 4, and the steric bulk of the *t*-Bu ester was critical for the conversion of **1** to **2**. Introduction of the isotopes began with converting the free acid of **1** with ethylchloroformate to the acyl ethyl carbonic anhydride. This intermediate allowed us to selectively reduce the anhydride over the *t*-Butyl ester using NaBD₄ in D₂O to give **2** in 84 % yield.⁴⁶ Mesylation of the resulting alcohol to (**3**), followed by a displacement reaction with NaSMe gave **4**. Global deprotection of **4** with TFA gave **5**. In order to introduce this molecule to the solid phase using standard solid phase conditions, protection with 9-Fluorenylmethyl succinimidyl carbonate gave (*S*)-[4,4,²H₂]-*N*-Fmoc-methionine **6**.



Scheme 4: Solution phase synthesis of (*S*)-[4,4,²H₂]-*N*-Fmoc-methionine

Coupling of **6** to an aminomethyl polystyrene resin was accomplished with diisopropylcarbodiimide (DIC), hydroxybenzotriazole (HOBt) and Hünig's Base (DIPEA) in DMF as shown in Scheme 5. The Fmoc group was then deprotected with 25% piperidine in DMF to give **7**, followed directly by coupling of the acyl side chain using the same coupling conditions to afford **8**. Acyl chains that were fully oxidized in the 3 position were protected with an ethylene glycol acetal. Protection of the 3-OH-C4 was unnecessary. Treatment of **8** with 5:2 1M CNBr in CHCl₃:50% aqueous TFA for 24 hours allowed cyclization to form the homoserine lactone moiety and provided cleavage from the resin to give **9** without further purification. In syntheses involving acetal protection, cleavage conditions were sufficient for removing the protecting group. Although it was originally proposed to obtain enantiomerically pure product, initial results proved that racemization occurred readily, and at many points in the reaction scheme. This could be attributed to the basic conditions of the coupling reactions. An attempt to modify the synthesis and avoid these conditions was carried out. However, it was ultimately decided that the elegant nature of the original synthesis outweighed the one downfall of failing to obtain enantiomerically pure product.

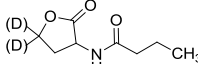
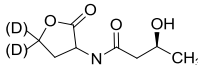
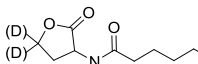
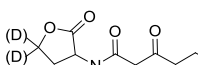
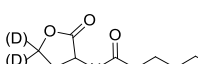
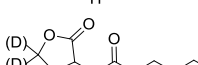
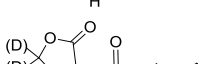
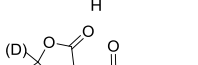


Scheme 5: Solid phase synthesis of various AHLs

Separation and Detection of AHLs and AI-2

As previously stated, the chemical properties of DPD and its various active forms have made its detection problematic. A simple derivatization, developed by our lab,⁴¹ allows such complications to be avoided. Although it was not an initial focus of this project, a shorter 4 min LC-MS/MS method was developed for the quantitation of AI-2. Using this isocratic gradient, the throughput for the analysis of biological samples was subsequently increased. Previous methods for AHL separation have been long, ranging from ~30-50 minutes.^{45, 47} Two shorter methods have been reported⁴⁰, although these methods used high column temperatures or atypical additives in the mobile phase such as ethylenediaminetetraacetic acid (EDTA).⁴⁸ These conditions are often not suitable for most LC-MS methods. To ensure a high throughput for the detection and quantitation of multiple AHLs, a shorter, 7 min, liquid chromatography method was developed using a high-efficiency Kinetex core-shell C18 column. The mobile phases used

Table 1: Structure, Abbreviations and SRMs for AHLs

Structure	Abbreviation	SRM Parent-fragment (<i>m/z</i> - <i>m/z</i>)
	C4 (D ₂)C4	172-102 174-104
	3OHC4 (D ₂)3OHC4	188-102 190-104
	C6 (D ₂)C6	200-102 202-104
	3OC6 (D ₂)3OC6	214-102 216-104
	C7 (D ₂)C7	214-102 216-104
	C8 (D ₂)C8	228-102 230-104
	C10 (D ₂)C10	284-102 286-104
	C12 (D ₂)C12	312-102 314-104

(D) indicates position occupied either by a proton or deuterium

were 1% acetic acid (AcOH) solution in water and acetonitrile (ACN). This provided the separation of 8 different AHLs, and most importantly, the separation of the 3OC6 and C7, which have the same mass. Table 1 shows the structure, abbreviations and SRMs of each AHL analyzed in these studies. Some bacteria only make short chain AHLs, while others make longer ones such as C12 and C14 AHLs. Addition of additives to the mobile phase such as EDTA was most likely done to prevent the formation of aggregates that the long hydrophobic chains of AHLs can form. To address this issue, 0.1% AcOH was included in the ACN of the mobile phase, and the run time was extended to 12.5 min. This slowed analysis but allowed the separation of AHLs ranging from C4 to C14 in length (Figure 5).

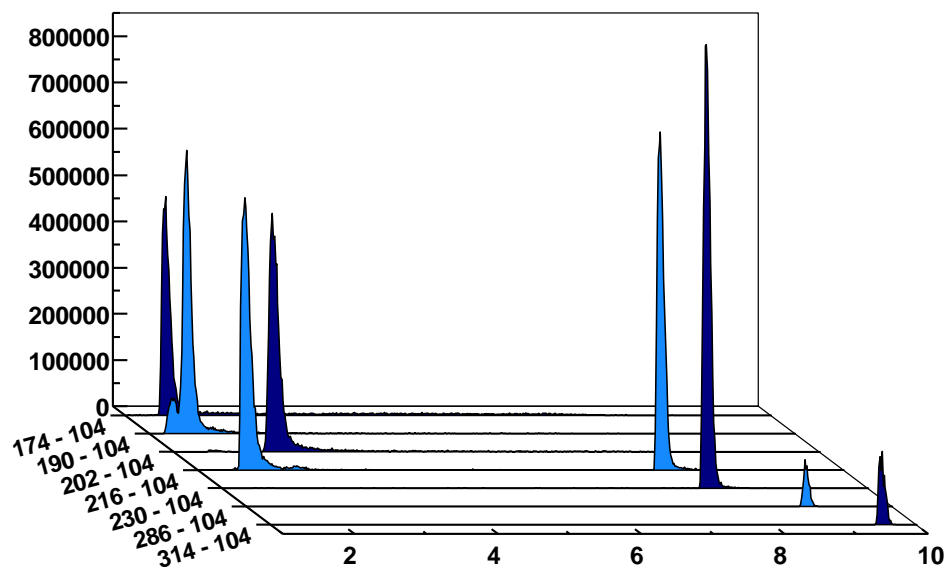


Figure 5: Chromatographic separation and detection of AHLs. Selected ion chromatograms for the (D2)AHLs C4, 3OHC4, C6, 3OC6, C7, C8, C12, C14 showing separation in both the time and mass domain. Of importance, the 3OC6 and C7, which have the same mass, are separated by retention time.

Profiling Bacterial Species for Autoinducer Production

There are a variety of species of bacteria known to produce AI-1s and AI-2. Table 2 summarizes the strains that have been profiled as well as which have been profiled for AHLs and/or AI-2. These species were selected for analysis based on whether they possess a LuxS or LuxI homologue, availability, as well as the ability to grow them in the lab. Two wild type strains of *Vibrio fischeri* have been profiled for both AI-2 and AHL production. The *ainS* mutant of *Vibrio fischeri*, CL21, which lacks the ability to produce the C8 AHL as well as VCW2G7, the LuxI mutant of ES114 were profiled for AHL production. Again, LuxI is responsible for producing the 3OC6 AHL; therefore, this mutant lacks the ability to produce the 3OC6 AHL. *Ralstonia pickettii* (data not shown), *Edwardsiella tarda* and *Yersinia enterocolitica* have all been profiled for AI-2 production. In each of these studies, AI production was monitored as cultures grew from exponential to stationary phase. Optical density was taken for each culture to measure growth, and cultures were studied with added glucose concentrations of 0, 0.08, 0.14 % (w/v), or a combination of these. Measured concentrations of AI-2 and AHLs are denoted as [DPD] and [AHL(s)], respectively.

Table 2: Strains Profiled

Organism	Strain	Genotype	AI-1s	AI-2
<i>Edwardsiella tarda</i>	15947	WT		✓
<i>Vibrio fischeri</i>	MJ-1	WT	✓	✓
<i>Vibrio fischeri</i>	ES114	WT	✓	✓
<i>Vibrio fischeri</i>	VCW2G7	<i>luxI</i> -	✓	
<i>Vibrio fischeri</i>	CL21	<i>ainS</i> -	✓	
<i>Ralstonia pickettii</i>	49129	WT	-	✓
<i>Yersinia enterocolitica</i>	9610	WT		✓

WT = wild type

Results: *Vibrio fischeri*

Initial studies were conducted on wild type strains ES114 (Figure 7A), and MJ-1 (Figure 7B) of *V. fischeri*. Concentrations of various AHLs were calculated and plotted to visualize their production and degradation. Of particular interest were the identification of two unreported AHLs, C6 AHL and C7 AHL. The maximum concentrations of the C6 and C7 AHLs found for MJ-1 and ES114 were $0.047 \pm 0.005 \mu\text{M}$ and $0.034 \pm 0.007 \mu\text{M}$, and $158 \pm 1.00 \text{ nM}$ and 0.118 ± 0.013 respectively. Maximum concentrations of 3OC6 AHL and C8 AHL reached $0.287 \pm 0.041 \mu\text{M}$ and $250 \pm 10.00 \text{ nM}$, and $0.00 \mu\text{M}$ and $2.474 \pm 0.211 \mu\text{M}$, in MJ-1 and ES114, respectively. While probing ES114 and MJ-1 for AHLs, production of AI-2 was also examined as wild type *V. fischeri* is known to produce DPD. Results for ES114 and MJ-1 show an expected increase in DPD concentration ([DPD]) during exponential phase with maximum [DPD] reaching 1.79 and 1.29 μM , respectively. Figure 6 shows all of the autoinducers produced by MJ-1 and ES114. Notably, the onset of the production of the C6 and C7 AHLs occurred later in growth during stationary phase. In fact, the production of all AHLs in both MJ-1 and ES114 seem to happen sequentially with production of every AHL occurring during stationary phase after AI-2 production has ceased. This was an interesting result as we typically reason that AI production will increase as cell numbers are increasing exponentially. This result was unexpected and has brought forth further questions about production and utilization of multiple AHLs. Further AHL studies were conducted on strains CL21, *ainS* mutant, (Figure 7C), and VCW2G7, *luxI* mutant, (Figure 7d) of *V. fischeri*. Expected results for CL21 should indicate an absence in the production of C8 AHL. Surprisingly, results showed that no other AHL was produced. This could be a consequence of the absence of the C8 AHL, if they were indeed produced in a step-wise manner. Results for the *luxI* mutant indicated that the 3OC6 AHL was not produced in sufficient amounts however; the *luxI* mutant is a mutant of the ES114 strain of *V. fischeri* which also produces negligible concentrations of the 3-oxo-C6 AHL. Taken together, these preliminary studies of *V. fischeri* have introduced the idea that the production of certain autoinducers in *V. fischeri* may implicate a different means of communication, one not reliant on cell numbers.

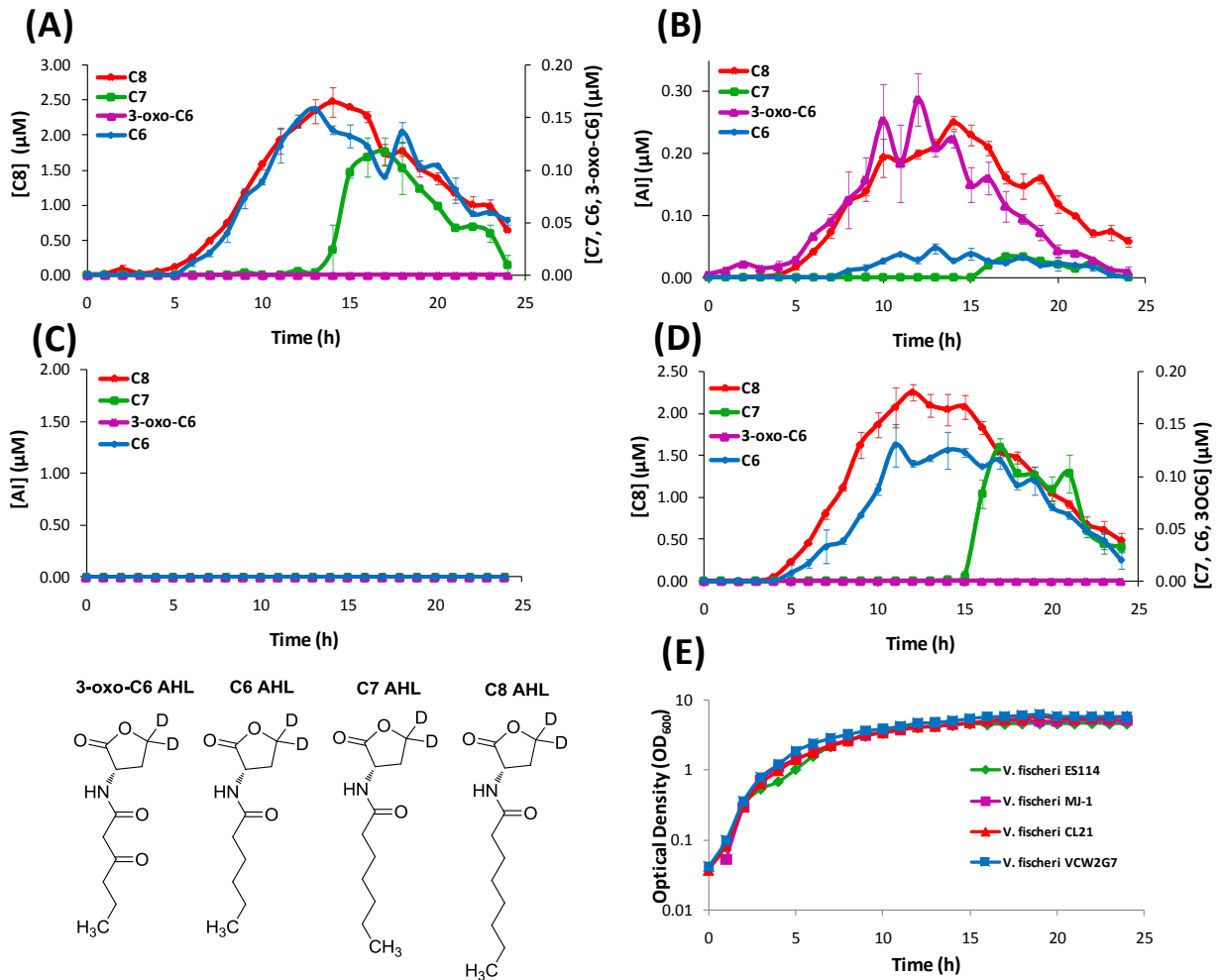


Figure 6: Production of 3OC6, C6, C7 and C8 AHLs in *V. fischeri* WT strains (A) ES114, and (B) MJ-1, and *V. fischeri* mutant strains (C) CL21 and (D) VCW2G7. (E) Growth kinetics of all *V. fischeri* strains studied.

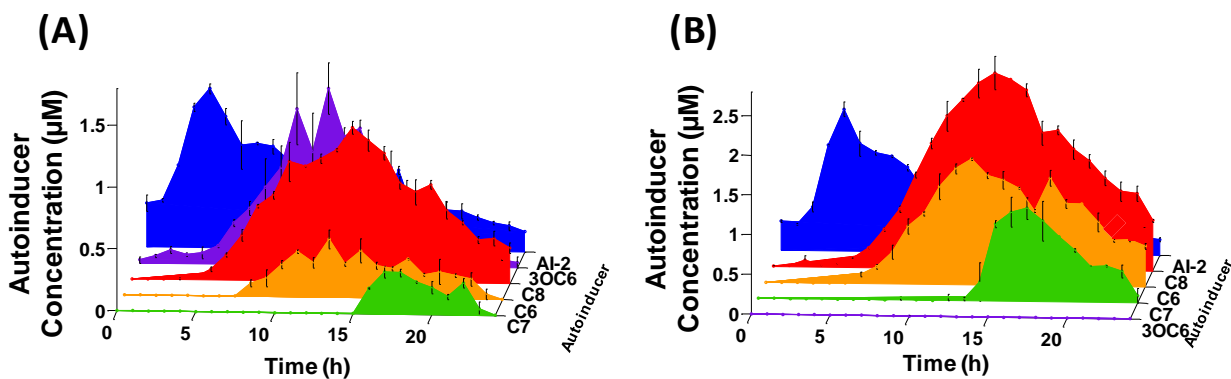


Figure 7: Cascade depictions of all autoinducers produced by *V. fischeri* strains ES114 and MJ-1. Data for Al-2, 3OC6, C6, C7, C8 AHL production in **(A)** MJ-1 and **(B)** ES114

Results: *Edwardsiella tarda*

Edwardsiella tarda is a gram negative pathogen. This particular species infects fish but is also found as a human pathogen.^{49, 50} *E. tarda* was profiled for Al-2 production for 24 hours with added glucose concentrations of either 0.0% or 0.14% (w/v). Results showed that [DPD] reached a maximum concentration of 34.65 µM and 112.1 µM at 12 and 17 h for the 0% and 0.14% glucose concentrations, respectively (Figure 8). It was also noted that *E. tarda* grew at a slightly faster rate with the added glucose (Figure 8A). Also, the duration of Al-2 production was extended for the culture with added glucose. No detectable concentration of Al-2 was found after 15 h for the culture with no added glucose, while Al-2 production continued for an additional 5 h in the culture with 0.14% (w/v) glucose (Figure 8B). In both cultures, the detectable amounts of [DPD] were found as both cultures entered stationary phase at approximately 6 h.

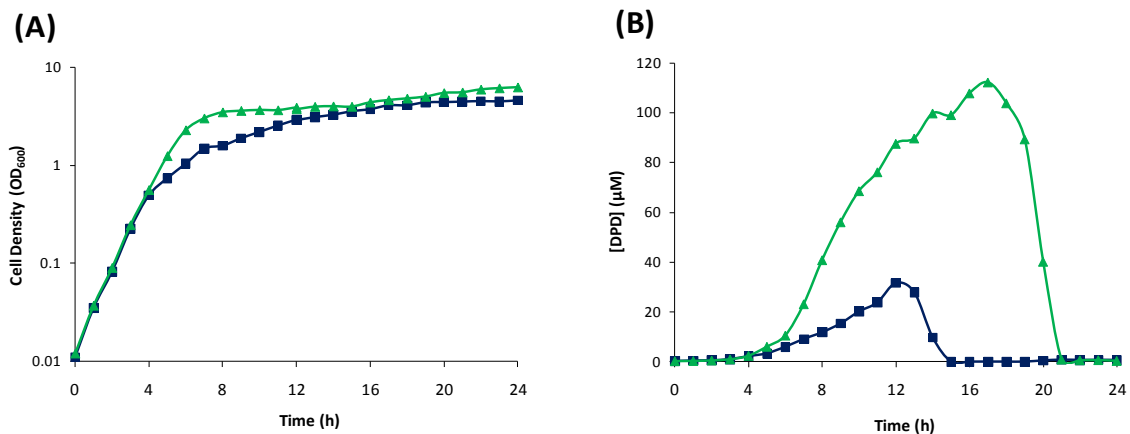


Figure 8: Growth kinetics and DPD production in *Edwardsiella tarda*. Data for cultures spiked with either 0.0 (■), 0.14 (▲) % (w/v) glucose. **(A)** Growth kinetics measure by OD₆₀₀. **(B)** [DPD] monitored over 24 hours in each glucose concentration.

Characterization of an Enteropathogen

Yersinia enterocolitica was the second pathogen that was studied. This species is a mammalian pathogen,⁵¹ and because it belongs to the same genus as *Yersinia pestis*, otherwise known as the plague, it is of particular interest in the research community. Preliminary studies on *Y. enterocolitica* found that this species produced AI-2 in the µM range at a maximum of approximately 100 µM, a result not typical in AI-2 quantitation. As a focus, AI-2 production in the species *Y. enterocolitica* was characterized in two different media, and in all four different glucose concentrations. In each experiment, all measurements were taken in duplicate.

Results: *Yersinia enterocolitica*

Y. enterocolitica was first profiled for AI-2 production in a brain and heart infusion (BHI) media, the standard for this species. *Y. enterocolitica* was profiled for 16 h as it was found in the preliminary studies that this species reached stationary phase at approximately 8 h and continued to produce DPD until 14 h. Four separate experiments were conducted in duplicate. Glucose concentrations of 0, 0.08, 0.14, and 0.20 % (w/v) were added to the media prior to inoculation. Growth kinetics were identical for all cultures (Figure 9A). In all of the cultures, DPD production began as the cultures began to enter stationary phase and continued for a total of 14 h. In *Y. enterocolitica*, [DPD] increased with any concentration of glucose added and a

maximum concentration of $115.12 \pm 4.09 \mu\text{M}$ DPD was found at 12 h. Concentrations of DPD in the 0.0 % glucose culture reached a maximum of $78.62 \pm 0.24 \mu\text{M}$. The maximum $[\text{DPD}]/\text{OD}_{600}$ in all of the glucose concentrations was relatively small range, from $28.75 \pm 0.54 \mu\text{M}$ to $36.54 \pm 0.39 \mu\text{M}$ (Figure 9B). Results from the colorimetric glucose oxidation assay revealed that glucose levels in each culture dissipated to 0 % over the course of ~2-3 h during the time that [DPD] were increasing (Figure 10A-D). These data seemed to indicate that a *Y. enterocolitica* reached a maximum [DPD] with any concentration of added nutrients. Because BHI contains 3 g glucose per 1 L, it was attempted to repeat these experiments, with the same conditions, in a medium that contained low glucose and sugar carbon sources such as LB. Results, as indicated by measurement of OD_{600} showed that *Y. enterocolitica* grew similarly in LB as in BHI (Figure 11A). When experiments were repeated with identical glucose concentrations, it was noted that the $[\text{DPD}]/\text{OD}_{600}$ increased both in maximum amount and with time as glucose concentrations increased as shown in Figure 11B. Again, DPD production began as *Y. enterocolitica* entered stationary phase. In the 0.0 % (w/v) glucose culture, the $[\text{DPD}]/\text{OD}_{600}$ reached a maximum of $6.391 \pm 0.380 \mu\text{M}$ at 8 h; the 0.08 % (w/v) glucose culture reached a maximum the $[\text{DPD}]/\text{OD}_{600}$ of $25.11 \pm 2.203 \mu\text{M}$ at 9 h; the 0.14 % (w/v) glucose culture reached a maximum the $[\text{DPD}]/\text{OD}_{600}$ of $28.56 \pm 0.069 \mu\text{M}$ at 10 h; and the 0.08 % (w/v) glucose culture reached a maximum the $[\text{DPD}]/\text{OD}_{600}$ of $32.92 \pm 1.115 \mu\text{M}$ at 11 h. Two additional glucose concentrations were used in the LB studies in an attempt to locate a threshold concentration at which *Y. enterocolitica* would produce a maximum [DPD].

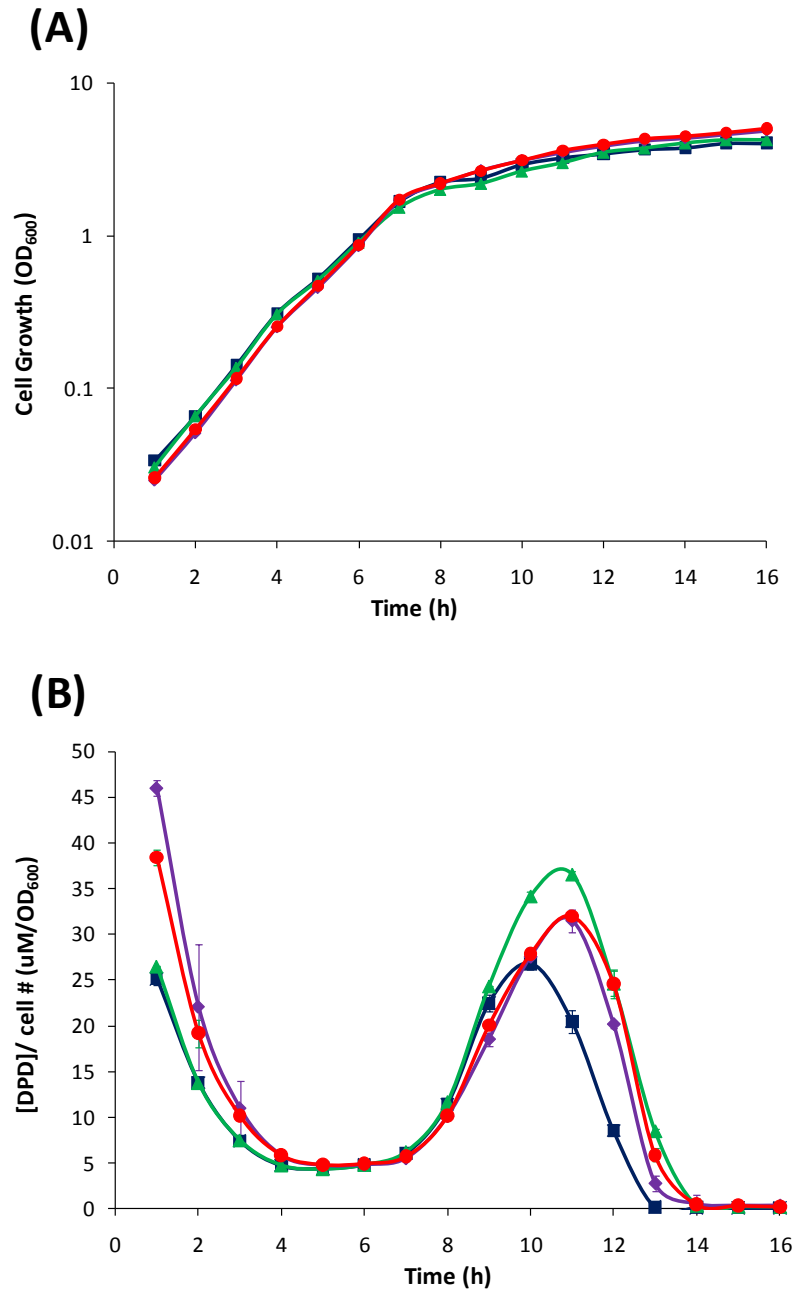


Figure 9: Average growth kinetics and average [DPD]/cell # for *Yersinia enterocolitica* in BHI. Data for culture spiked with either 0.0 (■), 0.08 (▲), 0.14 (◆), or 0.20 (●) % (w/v) glucose. **(A)** Average cell density measured by OD₆₀₀. **(B)** Average [DPD]/cell # (µM/OD₆₀₀) measured over 16 hours for each glucose concentration. Measurements were performed in duplicate and error bars represent the range of data.

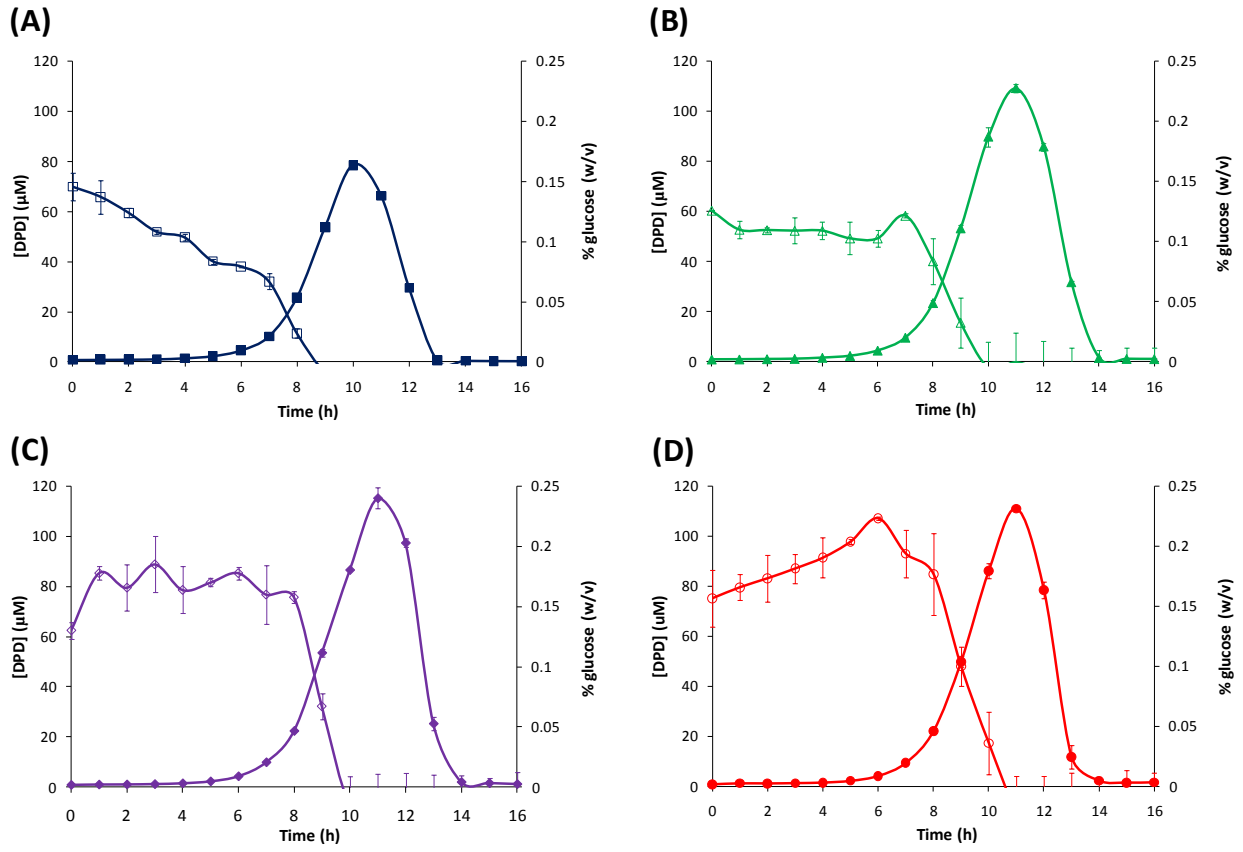


Figure 10: Average [DPD] and average [glucose] for *Yersinia enterocolitica* in BHI. Filled markers represent [DPD] (μM) and open markers represent % glucose (w/v). Data for cultures spiked with either (A) 0.0 (■), (B) 0.08 (▲), (C) 0.14 (◆), or (D) 0.20 (●) % (w/v) glucose. All measurements were performed in duplicate and error bars represent the range of data. Glucose concentrations are represented as total % (w/v) in the culture.

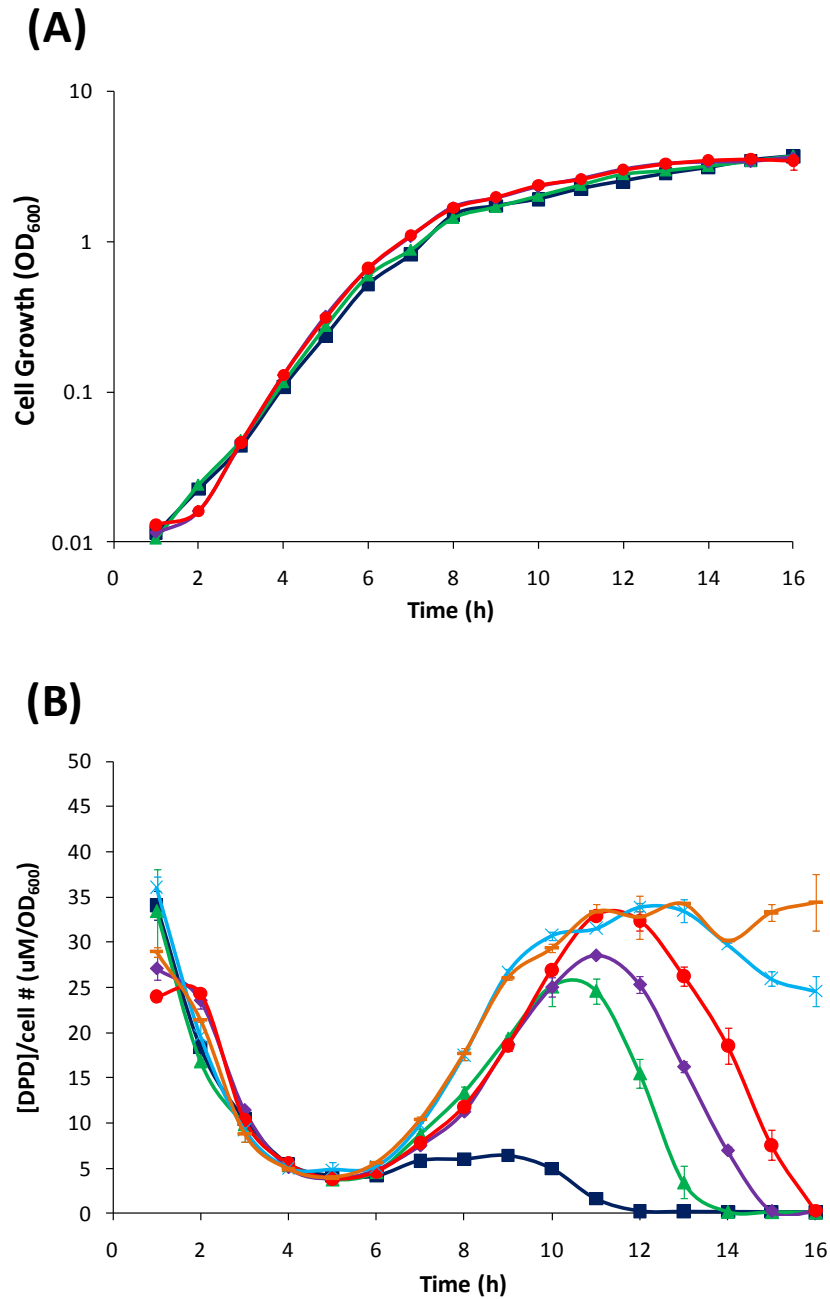


Figure 11: Average growth kinetics and average [DPD]/cell # for *Yersinia enterocolitica* in LB. Data for culture spiked with either 0.0 (■), 0.08 (▲), 0.14 (◆), or 0.20 (●) % (w/v) glucose. **(A)** Average cell density measured by OD₆₀₀. **(B)** Average [DPD]/cell # (µM/OD₆₀₀) for each glucose concentration. All measurements were performed in duplicate and error bars represent the range of data.

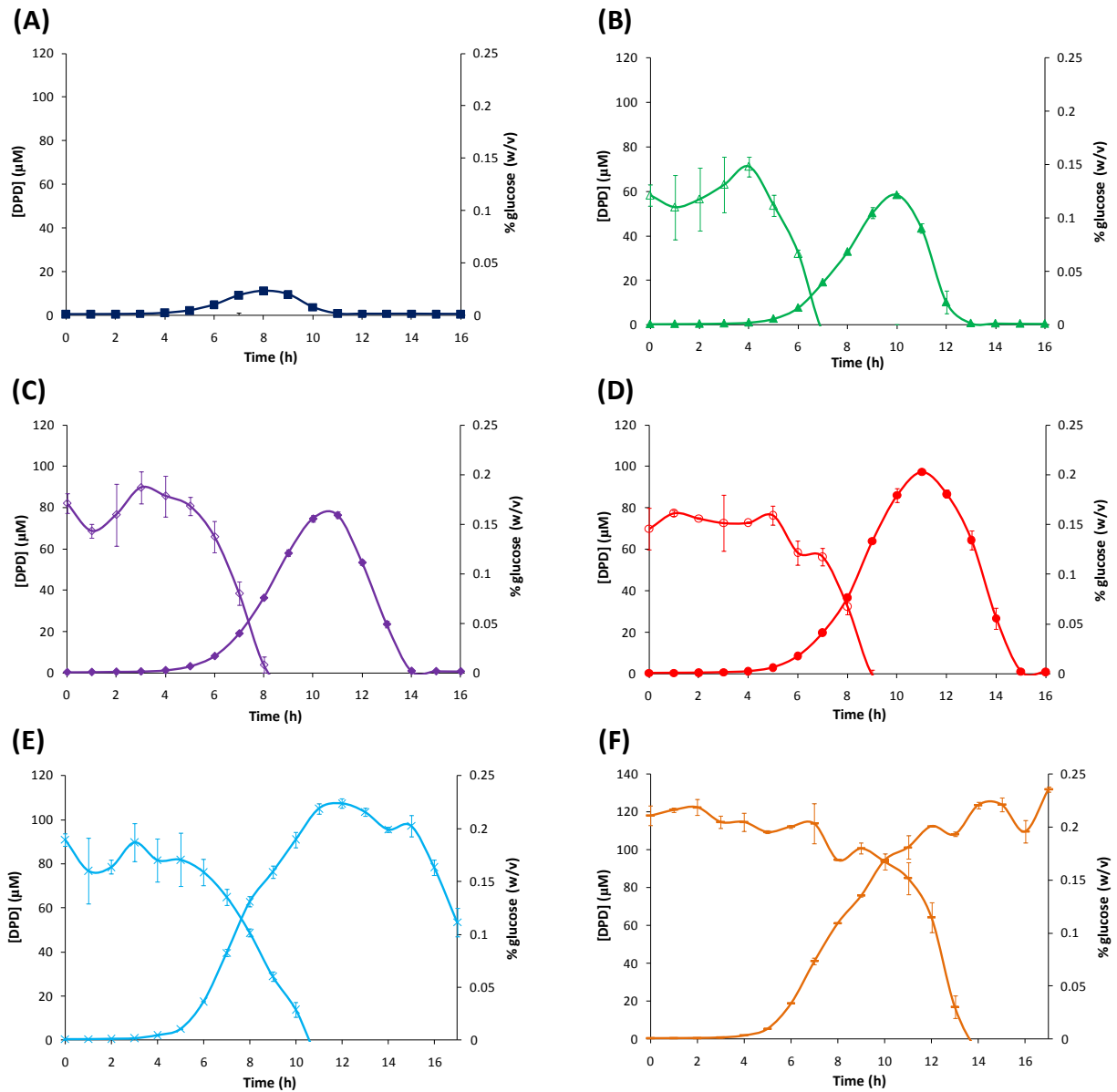


Figure 12: Average [DPD] and average [glucose] for *Yersinia enterocolitica* in LB. Filled markers represent [DPD] (μM) and open markers represent % glucose (w/v). Data for cultures spiked with either (A) 0.0 (■), (B) 0.08 (▲), (C) 0.14 (◆), (D) 0.20 (●), (E) 0.30 (✕) or (F) 0.50 (—) % (w/v) glucose. All measurements were performed in duplicate and error bars represent the range of data. Glucose concentrations are represented as total % (w/v) in the culture.

Methods and Materials

General Methods

Optical densities were measured on a BioPhotometer (Eppendorf), and all absorbance measurements for the colorimetric glucose oxidase assay were performed on a μ QUANT Universal Microplate Spectrophotometer (Bio-Tek Instruments, Inc.). The liquid chromatography-tandem mass spectrometer (LC-MS/MS) used for detection of both AI-2 and AHLs consisted of a Thermo Electron Surveyor Autosampler Plus, a Surveyor MS Pump Plus, and a TSQ Quantum Discovery Max triple quadrupole MS. All separations were performed on a Kinetex reverse phase C₁₈ core-shell column (5 μ m pore size, 100 Å particle size, 100 x 2 mm) supplied by Phenomenex. All MS spectra were collected and analyzed using the Xcalibur MS v 2.0.7 software package (Thermo Electron Corporation). All chemicals and solvents were purchased from Fisher Scientific, VWR, or Chem Impex and were used without further purification. Deuterated solvents used for NMR analysis were purchased from Cambridge Isotope Laboratories, Inc. Silica gel (230 x 400 mesh) and TLC plates were purchased from Sorbent Technologies. All NMR spectra were recorded on either a Varian Mercury 300 MHz, or Varian INOVA 500 MHz spectrometer. All high accuracy mass spectra were taken on a JEOL AccuTOF mass spectrometer with a DART ion source. IR spectra were recorded on a Thermo Electron Nicolet IR 100 FT-IR.

Bacterial Growth Conditions

Cultures of *Vibrio fischeri* wild type strains ES114 and MJ-1, as well as cultures of mutant strains CL21 and VCW2G7 were grown aerobically in Luria marine medium (LM)²² at 25 °C with shaking. *Edwardsiella tarda* cultures were grown aerobically in Luria broth (LB)⁵² at 28 °C with shaking. *Yersinia enterocolitica* cultures were grown aerobically in either LB or Brain Heart Infusion (BHI)⁵³ at 28 °C with shaking.

Chromatographic Details

For all samples, 10 μ L was injected onto the column via delivery by autosampler. The column temperature was 25 °C. High performance liquid chromatography (HPLC) was performed

utilizing a quaternary pump to generate a gradient for the elution of compounds from the stationary phase as listed below:

AI-2

A flow rate of 200 $\mu\text{L}/\text{min}$ was used. The mobile phases were 0.1% acetic acid in water (solvent A) and HPLC grade acetonitrile (solvent B) and a 4 min isocratic method was created using 5% solvent A, and 95% solvent B.

AHL(s)

A flow rate of 200 $\mu\text{L}/\text{min}$ was used. The mobile phases used were 0.1% Acetic Acid in water (solvent A) and HPLC grade Acetonitrile (solvent B). These were used to develop the following 12.5 minute gradient elution profile: $t = 0$ min, 99% solvent A, 1% solvent B; $t = 0.5$ min, 95% solvent A, 5% solvent B; $t = 3$ min, 90% solvent A, 10% solvent B; $t = 5$ min, 25% solvent A, 75% solvent B; $t = 6$ min, 25% solvent A, 75% solvent B; $t = 6.5$ min, 99% solvent A, 1% solvent B; $t = 7$ min, 99% solvent A, 1% solvent B.

General Mass Spectrometric Detection Parameters for AI-2 and AHLs

After delivery by HPLC, samples were introduced into the electrospray ionization chamber (ESI) through a 0.1 mm diameter fused silica capillary. The voltage for the ESI source was set to 4500 V. Detection of both AI-2 and AHL(s) occurred in positive mode. Nitrogen was used as the sheath gas (40 psi) and the inlet capillary temperature was 290 °C. Argon was used in the second quadrupole as the collision gas at a pressure of 1.5 mTorr. Samples were analyzed using selected reaction monitoring (SRM) with a scan time set to 0.05 s and a scan width of 1 m/z .

Measurement of AI-2 Concentration [AI-2]

In each experiment, the AI-2 concentration ([AI-2]) was measured as cultures grew from exponential phase through stationary phase. A preliminary growth curve was constructed in order to determine the time needed to reach stationary phase and cell density was measured by optical density at 600 nm (OD_{600}). Once determined, the following procedure was used for each biological experiment conducted with limited modification necessary. Incubation temperature,

growth medium, and duration of the experiment varied with the bacteria. Cell cultures were grown in duplicate. Incubation temperature, growth medium, and duration of the experiment varied with the bacteria. Cell cultures were grown in duplicate, unless otherwise noted. Every hour, a 300 μL sample was taken from each culture and placed into a 1.5 mL microcentrifuge tube containing 10 μL a solution of ^{13}C -DPD (341 μM). The contents were then mixed thoroughly by vortexing and centrifuged to remove cells and other particulates. A portion of the supernatants (260 μL) were placed in a subsequent microcentrifuge tube containing 26 μL of DPD-Tag (5 mg/mL). The contents were allowed to react for 45 minutes before extraction with ethyl acetate (2 x 130 μL), followed directly by LC-MS/MS analysis.

Measurement of AHL Concentration(s) [AHL(s)]

In each experiment, the AHL concentration ([AHL]) was measured as cultures grew from exponential phase through stationary phase. A preliminary growth curve was constructed in order to determine the time needed to reach stationary phase and cell density was measured by OD_{600} . Once determined, the following procedure was used for each biological experiment conducted with limited modification necessary. Incubation temperature, growth medium, and duration of the experiment varied with the bacteria. Cell cultures were grown in duplicate. Every hour, a 300 μL sample was taken from each culture and placed into a 1.5 mL microcentrifuge tube containing 10 μL of a solution of respective deuterated AHLs (6.2 μM). The contents were mixed thoroughly by vortexing and centrifuged to remove cells and other particulates. The resulting supernatants (260 μL) were extracted two times with half volume of ethyl acetate and transferred to 300 μL autosampler vials. If an extraction could not be performed, supernatants were taken directly after centrifugation for analysis.

Data Handling for the Calculation of [DPD]

Data from the SRMs 381-202 and 382-203 (parent-product ion) at a collision energy of 41 eV were selected and analyzed by manual integration of chromatographic peak area to obtain [DPD]. The SRM 381-202 and 382-203 corresponds to the DPD-Quinoxalines, (^{12}C)DPD-Q and (^{13}C)DPD-Q signal respectively. One of two correction factors was applied to integration values based on the ratio of (^{12}C)DPD-Q to (^{13}C)DPD-Q signal and are stated below. A full discussion of these correction types has been previously reported by our lab.⁴¹

Correction type 1 is a correction for the naturally occurring (¹³C)DPD and was applied when the ratio of (¹²C)DPD-Q to (¹³C)DPD-Q signal was greater than 0.3:

$$\text{Observed } (^{13}\text{C})\text{DPD-Q} - 0.144 \times \text{Observed } (^{12}\text{C})\text{DPD-Q} = \text{Corrected } (^{13}\text{C})\text{DPD-Q}$$

Correction type 2 is correction for (¹²C)DPD impurities in the (¹³C)DPD internal standard and was applied when the ratio of (¹²C)DPD-Q to (¹³C)DPD-Q signal was less than 0.2:

$$\text{Observed } (^{12}\text{C})\text{DPD-Q} - 0.008 \times \text{Observed } (^{13}\text{C})\text{DPD-Q} = \text{Corrected } (^{12}\text{C})\text{DPD-Q}$$

Using the known [(¹³C)DPD] added to the culture, following equation was then applied to calculate the [DPD]:

$$\frac{\text{Signal } (^{12}\text{C})\text{DPD-Q}}{\text{Signal } (^{13}\text{C})\text{DPD-Q}} \times [(^{13}\text{C})\text{DPD}] = [\text{DPD}]$$

Data Handling for the Calculation of [AHL(s)]

Data from the SRMs 202-104, 216-104, 216-104, 230-104 at a collision energy of 11 eV were selected and analyzed by manual integration of chromatographic peak area to obtain respective [AHL]. The SRMs 202-104, 216-104, 216-104, 230-104 correspond to the C6, 3OC6, C7, and C8 AHLs. Using the known [(D₂)AHL(s)] added to the culture, the following equation was applied to obtain [AHL]:

$$\frac{\text{Signal AHL}}{\text{Signal } (D_2)\text{AHL}} \times [(D_2)\text{AHL}] = [\text{AHL}]$$

No correction was necessary for the observed AHL signals due to the intentional incorporation of two deuteriums as previously discussed.

Measurement of Glucose Concentration by Colorimetric Glucose Oxidation Assay

At each time point, a 120 μL sample of culture was taken and placed into an empty microcentrifuge tube and centrifuged to remove cell particulates. The supernatants (90 μL) were then placed in a separate microcentrifuge tube and immediately stored at $-80\text{ }^{\circ}\text{C}$ for analysis for the glucose oxidation assay. To obtain glucose concentration at each time point ([glucose]), an external calibration curve was first constructed in a 96 well plate by diluting 2 μL of a 40% (w/v) glucose solution into 198 μL of DI water followed by two-fold serial dilutions. The set of calibration included 0.4, 0.2, 0.1, 0.05 % (w/v) glucose. This calibration curve was then diluted 1:10 into LB (10 μL into 90 μL LB) in order to accommodate all glucose concentrations in the linear range of the assay. If multiple plates were used, one calibration curve from the first was diluted into the second for consistency. The calibrations were then used to generate a calibration equation by least-squares linear regression of the data. This varied with each plate but ranged anywhere from 0.006 to 0.200 %:

$$A_{500} = m \times [\text{glucose}] + b$$

This equation was then used to calculate [glucose] at each time point in a given experiment. First 10 μL aliquot from each sample was diluted into 90 μL of LB on the same plate as the calibration curve. A 200 μL aliquot of a reagent⁵⁴ containing 0.30 M Tris, 0.36 M $\text{NaH}_2\text{PO}_4 \cdot 2\text{H}_2\text{O}$, 5.4 M glycerol, 1.0 mM *o*-dianisidine, 3 kU/L peroxidase and 1 kU/L glucose oxidase type X in water was added to both the wells that contained samples and the diluted calibration curve and the plate was incubated at $37\text{ }^{\circ}\text{C}$ for 15. At this time, the absorbance at 500 nm was measured, and the [glucose] was calculated using the equation generated as described.

***N*-Boc-(4,4-²H₂)homoserine- α -OtBu ester, 2**

To a stirring solution of Boc-Asp- α -OtBu, **1**, (5.64 g, 19.49 mmol) and triethylamine (1.97 g, 2.74 mL, 19.49 mmol) in 50 mL anhydrous THF, at $-5\text{ }^{\circ}\text{C}$, was added Ethyl chloroformate (2.11 g, 1.87 mL, 19.49 mmol) in 10 mL anhydrous THF via cannula. After stirring continuously at $-5\text{ }^{\circ}\text{C}$ for 45 min, a precipitate had formed. This precipitate was then filtered, and the filtrate added dropwise over 30 min to a stirring solution of NaBD_4 (1.63 g, 39.00 mmol) in 15 mL D_2O at $10\text{--}12\text{ }^{\circ}\text{C}$. The reaction was allowed to proceed at room temperature for 4 hours. At this time, the solution was acidified with 1 M HCl to pH 2-3. The product was extracted with diethyl ether (3 x

80 mL), dried, filtered and concentrated *in vacuo* to give a yellow oil. The crude product was purified by silica chromatography eluted with 7:3 hexanes:ethyl acetate. The purified product, **2**, (4.27 g, 15.40 mmol) was isolated in 85% yield as a clear oil.

$R_f = 0.49$ (1:1 hexanes:ethyl acetate); IR (neat) 3380, 2978, 2098, 1713, 1510, 1366, 1247, 1161 cm^{-1} ; ^1H NMR (300 MHz, CDCl_3) δ 5.35 (d, $J = 7.5$ Hz, 1H), 4.42-4.23 (m, 1H), 3.46 (s, 1H), 2.11 (dd, $J = 13.8, 3.1$ Hz, 1H), 1.56 - 1.48 (partially under protons at 1.46 ppm, m, 1H), 1.46 (s, 9H), 1.43 (s, 9H) ppm; ^{13}C NMR (126 MHz, CDCl_3) δ 172.00, 156.60, 82.28, 80.30, 59.16 - 55.74 (m), 50.86, 36.36, 28.25, 27.97 ppm; HRMS-DART (m/z): $[\text{M}+\text{H}]^+$ calculated for $\text{C}_{13}\text{H}_{24}^2\text{H}_2\text{NO}_5$, 278.19365; found, 278.19338.

N*-Boc-(4,4- $^2\text{H}_2$)homoserine- γ -OMs- α -OtBu ester, **3*

To a solution of **2** (0.902 g, 3.25 mmol), in anhydrous CH_2Cl_2 at 0 °C, was added triethylamine (0.658 g, 0.914 mL, 6.50 mmol) followed immediately by mesyl chloride (0.745 g, 0.507 mL, 6.50 mmol). After stirring at 0 °C for 2 h, the reaction was allowed to warm to room temperature and proceed for an additional 5 h. At this time, the reaction was concentrated *in vacuo* and immediately redissolved in CH_2Cl_2 . This solution was washed with water (3 x 20 mL), and the water layers extracted with CH_2Cl_2 (3 x 20 mL). All organic layers were combined, dried with MgSO_4 , filtered and concentrated *in vacuo* to give **3** (1.18 g, 3.32 mmol, quant., 80% purity) as a yellow oil. This crude product was carried through to the next reaction without purification. An analytical sample was purified twice via silica chromatography eluted first with 9:1, hexanes:ethyl acetate and second by 100% pentane for ~3 column volumes then 1:1 pentane:ethyl acetate. The purified product was isolated as a white solid.

$R_f = 0.32$ (7:3 hexanes:ethyl acetate); IR (neat) 3381, 2979, 1715, 1513, 1358, 1249, 1166 cm^{-1} ; ^1H NMR (300 MHz, CDCl_3) δ 5.16 (s, 1H), 4.28 (d, $J = 4.2$ Hz, 1H), 3.02 (s, 3H), 2.28 (dd, $J = 14, 2.6$ Hz, 1H), 2.03 (dd, $J = 14.5, 7.5$ Hz, 1H), 1.47 (s, 9H), 1.43 (s, 9H) ppm; ^{13}C NMR (126 MHz, CDCl_3) δ 170.77, 155.35, 82.75, 80.09, 66.51 - 64.29 (m), 50.89, 37.30, 32.02, 28.28, 27.95 ppm; MS-DART (m/z): $[\text{M}-\text{Boc}+\text{H}]^+$ found, 256.18048.

N*-Boc-(4,4-²H₂)methionine-OtBu ester, **4*

To a stirring solution of **3** (1.18g, 3.29 mmol) in 50 mL 95% ethanol was added a 15% aqueous solution of sodium thiomethoxide (2.86 mL, 6.58 mmol). The reaction was allowed to run for 8 h at room temperature. At this time, 50 mL of a saturated solution of NH₄Cl was added to the reaction mixture until a white precipitate formed. The product was extracted with ethyl acetate (3 x 75 mL), and the combined organic layers were dried, filtered and concentrated *in vacuo* to give **4** (0.721 g, 2.87 mmol) in 89% yield and 81% purity. The yellow oil was carried through crude to the next reaction. An analytical sample was purified via silica column chromatography eluted with 9:1 hexanes:ethyl acetate.

R_f = 0.68 (7:3 hexanes:ethyl acetate); IR (neat) 3354, 2976, 2928, 1795, 1508, 1541, 1364, 1248, 1192, 1048 cm⁻¹; ¹H NMR (300 MHz, CDCl₃) δ 5.12 (d, J = 7.9 Hz, 1H), 4.21 (dd, J = 12.5, 7.5 Hz, 1H), 2.10 - 1.95 (overlapping protons, m, 4H), 1.83 (dd, J = 13.9, 7.5 Hz, 1H), 1.42 (s, 9H), 1.39 (s, 9H) ppm; ¹³C NMR (101 MHz, CDCl₃) δ 171.35, 155.32, 82.08, 79.73, 53.41, 28.66 - 30.19 (m), 28.31, 28.00, 15.37; HRMS-DART (*m/z*): [M+H]⁺ calculated for C₁₄H₂₆²H₂NO₄S, 308.18646; found, 308.18597.

(4,4-²H₂)methionine, **5**

A 1:1 mixture of trifluoroacetic acid (TFA) and CH₂Cl₂ (14 mL), was added to a flask containing **4** (0.355 g, 1.15 mmol). After stirring for 5 h the TFA was removed *in vacuo* to give a brown oil. This oil was washed 4 times with CH₂Cl₂ to remove any additional TFA. Ethyl ether was then added to precipitate the product. The resulting white solid was then extracted with water (2 x 10 mL), and the water layers were washed with ethyl ether (2 x 20 mL). The combined water layers were then concentrated *in vacuo* to give the TFA salt of **5** (0.305 g, 1.15 mmol) in quantitative yield as a white solid. The product was carried through as the TFA salt in the next reaction. Trituration of the TFA salt of **5** in 95% ethanol solubilized the TFA and any impurities to give the pure sample after filtration for analytical analysis.

mp = 218 °C (decomp.); IR (KBr) 3440, 2952, 2762, 2659, 2106, 1583, 1414, 1338, 1259, 1156 cm⁻¹; ¹H NMR (300 MHz, D₂O) δ 3.79 (dd, J = 7.1, 5.4 Hz, 1H), 2.17 - 1.99 (overlapping protons, m, 5H); ¹³C NMR (126 MHz, D₂O) δ 174.13, 53.82, 29.41, 27.75 - 28.73 (m), 13.76; HRMS-DART (*m/z*): [M+H]⁺ calculated for C₅H₁₀²H₂NO₂S, 152.07143; found, 152.07072.

N-Fmoc-(4,4-²H₂)methionine, 6

To a stirring solution of the TFA salt of **5** (1.90 g, 7.16 mmol) was added sodium bicarbonate (1.20 g, 14.33 mmol) in 60 mL 1:1 acetone:water. After the reaction became homogeneous, Fmoc-OSu (*N*-(9-Fluorenylmethoxycarbonyloxy) succinimide) was added in one portion (2.42 g, 7.16 mmol). The reaction was allowed to run for 18 h before the acetone was removed by evaporation under reduced pressure. The solution was then acidified with 1 M HCl to pH 2. The product was extracted with ethyl acetate, and the combined organic layers were dried with MgSO₄, filtered, and concentrated *in vacuo* to give **6** (2.54 g, 6.80 mmol) as an off-white solid in 95% yield and 91% purity. The product could be coupled directly to the solid phase or purified via recrystallization from CH₂Cl₂:hexanes (77% recovery).

R_f = 0.166 (7:3 hexanes:ethyl acetate); mp = 144-146 °C; IR (neat) 3321, 3050, 1524, 1447, 1334, 1263, 1056, 746 cm⁻¹; ¹H NMR (500 MHz, CDCl₃) δ 7.77 (d, J = 7.5 Hz, 2H), 7.60 (s, 2H), 7.41 (t, J = 7.5 Hz, 2H), 7.32 (t, J = 7.5 Hz, 2H), 5.45 (d, J = 7.6 Hz, 1H), 4.64 - 4.49 (m, 1H), 4.45 (d, J = 6.7 Hz, 2H), 4.24 (t, J = 6.8 Hz, 1H), 2.22 (dd, J = 13.8, 4.0 Hz, 1H), 2.11 (s, 3H), 2.01 (dd, J = 14.0, 7.9 Hz, 1H) ppm; ¹³C NMR (101 MHz, CDCl₃) δ 176.02, 156.12, 143.69, 141.36, 127.78, 127.11, 125.02, 120.03, 67.19, 52.94, 47.17, 31.27, 15.32; HRMS-DART (*m/z*); [M+H]⁺ calculated for C₂₀H₂₀²H₂NO₄S, 374.13951; found, 374.13825.

Representative N-Fmoc-(4,4-²H₂)methionine resin loading protocol

Amino methyl polystyrene resin (0.100 g, 0.110 mmol) was placed into a 5 mL peptide vessel and washed with DMF, H₂O, EtOH, Acetone and CH₂Cl₂. Approximately 10 mL of each solvent was used for each washing, and the vessel was agitated for ~5 s for each washing to ensure removal of the prior solvent. To swell the resin after washing, 1 mL of CH₂Cl₂ was added to the vessel. In a vial, an activated solution of *N*-Fmoc-(4,4-²H₂)methionine, **6**, (0.163 g, 0.440 mmol), 1-hydroxybenzotriazole (HOBT), (0.017 g, 0.110 mmol), N,N-diisopropylcarbodiimide (DIC), (0.069 g, 0.440 mmol), and diisopropylethylamine (DIPEA), (0.095 g, 0.550 mmol) was prepared in 2 mL DMF. After the activated solution sat at room temperature for 15 min, it was added to the peptide vessel containing the resin. The resulting reaction mixture was then shaken for 2 h at room temperature. The resin was filtered and washed using the procedure described above. This material was then stored and used to synthesize various ²H₂ AHLs as needed.

Representative synthesis of (²H₂) AHLs, *N*-octanoyl-(4,4-²H₂) acylhomoserine lactone

In a standard peptide vessel containing the resin supported *N*-Fmoc-(4,4-²H₂)methionine, **6**, was added 4 mL of a 25% piperidine solution in DMF. This reaction mixture was allowed to shake at room temperature for 1 h. The resin was then filtered and washed using the washing procedure described above. A solution of octanoic acid (0.087 mL, 0.550 mmol), HOBT (0.017 g, 0.110 mmol), DIC (0.069 g, 0.440 mmol), and DIPEA (0.069 g, 0.550 mmol) was prepared in a separate flask in 3 mL DMF. This activated solution was allowed to sit for 15 min at room temperature. At this time, the activated coupling solution was added to the peptide vessel containing the now deprotected **6**. This reaction mixture was allowed to shake for 18 h at room temperature. At this time, the resin was filtered and washed as previously described for the resin loading protocol. The washed resin was then left on the filter to dry for 2 h before being transferred to a 20 mL where 1.67 mL of 1M CNBr in CHCl₃, 0.330 mL H₂O and 0.330 mL TFA were added. This reaction was allowed to stir at room temperature for 24 h, after which the resin was again filtered and washed with CHCl₃ (3 x 5 mL). The filtrate was then collected and concentrated *in vacuo* to give the crude *N*-octanoyl-(4,4-²H₂) acylhomoserine lactone as a yellow oil. The oil was then redissolved in 15 mL CH₂Cl₂ and washed with water (3 x 15 mL). The organic layer was then dried with MgSO₄ and concentrated *in vacuo* to give *N*-hexanoyl-(4,4-²H₂) acylhomoserine lactone, (²H₂)C8 AHL, (0.0109 g, 0.0475 mmol) as a white solid in 49% yield and >95% purity. All other AHLs can be synthesized using this procedure and the data for each of the other 7 (D₂)AHLs synthesized are listed below.

¹H NMR (300 MHz, CDCl₃) δ 6.09 (d, J = 4.9 Hz, 1H), 4.55 (ddd, J = 11.6, 8.6, 5.7 Hz, 1H), 2.83 (dd, J = 12.5, 8.6 Hz, 1H), 2.29 - 2.29 (m, 2H), 2.11 (t, 12.1 Hz, 1H), 1.71 - 1.56 (m, 2H), 1.28 (dt, J = 9.2, 4.6 Hz, 8H), 0.87 (t, J = 6.7 Hz, 3H); ¹³C NMR (101 MHz, CDCl₃) δ 175.57, 173.77, 67.34 - 63.46 (m), 49.24, 36.20, 31.64, 30.42, 29.16, 28.96, 25.43, 22.58, 14.04; HRMS-DART (*m/z*): [M+H]⁺ calculated for C₁₆H₂₈²H₂NO₃, 286.23512; found, 286.23441.

(D₂)C4

¹H NMR (500 MHz, CDCl₃) δ 5.99 (s, 1H), 4.56 (ddd, J = 11.6, 8.6, 5.7, Hz, 1H), 2.88 (dd, J = 12.5, 8.6 Hz, 1H), 2.25 (td, J = 7.4, 2.1 Hz, 2H), 2.13 (t, J = 12.1 Hz, 1H), 1.80 - 1.64 (m, 2H), 0.98 (t, J = 7.4 Hz, 3H); ¹³C NMR (126 MHz, CDCl₃) δ 175.48, 173.53, 66.86 - 64.22 (m), 49.27, 38.05, 30.50, 18.87, 13.68; HRMS-DART (*m/z*): [M+H]⁺ calculated for C₈H₁₄²H₂NO₃, 174.10992; found, 174.10910.

(D2)3OHC4

^1H NMR (300 MHz, D_2O) δ 4.66 (dd, $J = 20.4, 10.9$ Hz, 1H), 4.27 - 4.11 (m, 1H), 2.66 - 2.54 (m, 1H), 2.45 (d, $J = 6.6$ Hz, 2H), 2.32 (td, $J = 12.2, 5.1$ Hz, 1H), 1.21 (d, $J = 6.3$ Hz, 3H); ^{13}C NMR (126 MHz, D_2O) δ 178.47, 173.92, 64.78, 49.08, 44.38, 27.47, 21.76; HRMS-DART (m/z): $[\text{M}+\text{H}^+]$ calculated for $\text{C}_8\text{H}_{12}^2\text{H}_2\text{NO}_4$, 190.10484; found, 190.10444.

(D2)C6

^1H NMR (500 MHz, CDCl_3) δ 6.02 (s, 1H), 4.55 (ddd, $J = 11.6, 8.6, 5.8$ Hz, 1H), 2.86 (dd, $J = 12.5, 8.6$ Hz, 1H), 2.26 (td, $J = 7.4, 1.5$ Hz, 2H), 2.12 (t, $J = 12.0$ Hz, 1H), 1.66 (dt, $J = 15.1, 7.6$ Hz, 2H), 1.33 (dd, $J = 7.2, 3.8$ Hz, 4H), 0.91 (t, $J = 7.1$ Hz, 3H); ^{13}C NMR (75 MHz, CDCl_3) δ 175.48, 173.70, 49.27, 36.15, 31.34, 30.49, 25.09, 22.34, 13.88; HRMS-DART (m/z): $[\text{M}+\text{H}^+]$ calculated for $\text{C}_{10}\text{H}_{14}^2\text{H}_2\text{NO}_3$, 202.14122; found, 202.14083.

(D2)3OC6

^1H NMR (300 MHz, CDCl_3) δ 7.67 (s, 1H), 4.59 (ddd, $J = 11.5, 8.8, 6.6$ Hz, 1H), 3.46 (s, 2H), 2.74 (dd, $J = 12.5, 8.8$ Hz, 1H), 2.51 (t, $J = 7.3$ Hz, 2H), 2.22 (t, $J = 12.0$ Hz, 1H), 1.70 - 1.54 (m, 2H), 0.98 - 0.89 (m, 3H); ^{13}C NMR (126 MHz, CDCl_3) δ 206.42, 174.72, 166.26, 67.15 - 62.44 (m), 49.04, 48.04, 45.77, 29.65, 16.83, 13.50; HRMS-DART (m/z): $[\text{M}+\text{H}^+]$ calculated for $\text{C}_{10}\text{H}_{14}^2\text{H}_2\text{NO}_4$, 216.12049; found, 216.12074.

(D2)C7

^1H NMR (300 MHz, CDCl_3) δ 5.98 (s, 1H), 4.54 (ddd, $J = 11.6, 8.6, 5.7$ Hz, 1H), 2.85 (dd, $J = 12.5, 8.6$ Hz, 1H), 2.28 - 2.21 (m, 2H), 2.11 (t, $J = 12.1$ Hz, 1H), 1.64 (dt, $J = 15.2, 7.7$ Hz, 2H), 1.39 - 1.20 (m, 6H), 0.88 (dd, $J = 9.0, 4.6$ Hz, 3H); ^{13}C NMR (75 MHz, CDCl_3) δ 175.53, 173.73, 66.80 - 64.01 (m), 49.26, 36.19, 31.47, 30.48, 28.86, 25.38, 22.47, 14.02; HRMS-DART (m/z): $[\text{M}+\text{H}^+]$ calculated for $\text{C}_{11}\text{H}_{18}^2\text{H}_2\text{NO}_3$, 216.15687; found, 216.15664.

(D2)C12

^1H NMR (500 MHz, CDCl_3) δ 6.01 (d, $J = 4.3$ Hz, 1H), 4.55 (ddd, $J = 11.6, 8.6, 5.7$ Hz, 1H), 2.86 (dd, $J = 12.5, 8.6$ Hz, 1H), 2.25 (td, $J = 7.4, 1.5$ Hz, 1H), 1.65 (dt, $J = 15.0, 7.6$ Hz, 2H), 1.37 - 1.20 (m, 16H), 0.89 (t, $J = 7.0$ Hz, 3H); ^{13}C NMR (126 MHz, CDCl_3) δ 175.51, 173.73, 68.01 - 62.44 (m), 49.26, 36.20, 31.89, 30.48, 29.59, 29.44, 29.32, 29.30, 25.43, 22.67, 14.10; HRMS-DART (m/z): $[\text{M}+\text{H}^+]$ calculated for $\text{C}_{16}\text{H}_{28}^2\text{H}_2\text{NO}_3$, 286.23512; found, 186.23441.

(D2)C14

^1H NMR (500 MHz, CDCl_3) δ 6.03 (d, $J = 4.8$ Hz, 1H), 4.55 (ddd, $J = 11.6, 8.6, 5.8$ Hz, 1H), 2.86 (dd, $J = 12.5, 8.6$ Hz, 1H), 2.25 (td, $J = 7.3, 1.4$ Hz, 2H), 2.12 (t, $J = 12.1$ Hz, 1H), 1.65 (dt, 15.0, 7.6 Hz, 2H), 1.39 - 1.19 (M, 20H), 0.98 (t, $J = 7.0$ Hz, 3H); ^{13}C NMR (126 MHz, CDCl_3) δ 175.53, 173.74, 68.60 - 63.18 (m), 49.25, 36.20, 31.91, 30.45, 29.66, 29.63, 29.45, 29.31, 29.21, 25.43, 22.68, 14.11; HRMS-DART (m/z): $[\text{M}+\text{H}^+]$ calculated for $\text{C}_{18}\text{H}_{32}^2\text{H}_2\text{NO}_3$, 314.26642; found, 314.26532.

Chapter II

Determining Metabolic Profiles of Rat Insulinoma Cells

A version of this chapter was originally published by J. Jason Collier, Susan J. Burke, Mary E. Eisenhauer, Danhong Lu, Renee C. Sapp, Carlie J. Frydman, and Shawn R. Campagna:

Collier JJ, Burke SJ, Eisenhauer ME, Lu D, Sapp RC, et al. (2011) Pancreatic β -Cell Death in Response to Pro-Inflammatory Cytokines Is Distinct from Genuine Apoptosis. PLoS ONE 6(7): e22485. doi:10.1371/journal.pone.0022485

The results and discussion, and methods and materials sections of the following chapter can be found in the stated publication with no revisions as the author has been credited as a writer, researcher, and analyzer for these sections. Results that were obtained by credited co-researchers are clearly defined within the text.

Abstract

Type 1 Diabetes mellitus (T1DM) occurs in response to the autoimmune destruction of insulin producing β -cells of the pancreas. It has been proposed that the method of β -cell death proceeds by one of two mechanisms, necrosis or apoptosis, and that these mechanisms are independent of each other and that one will prevail over the other preferentially. Until now, T1DM has been studied mainly by genomic and proteomics techniques. While these techniques are the standard in this field of research, a chemical approach, particularly at the level of metabolism provides a better representation of what is happening in a system in real time. The technological platform that addresses the metabolism of a given system is called metabolomics. Often, metabolism will change in response to toxins or disease; the study of these systems in response to a stimulus is one useful application of metabolomics. Here, a targeted metabolomics mass spectrometry approach was employed to measure the metabolome of rat islet β -cells that were exposed to inducers of cell death. This method was then used to determine a metabolic profile for the two proposed mechanisms of β -cell death. Approximately 90 metabolites were observed that demonstrated statistically reliable and valid changes when compared to a control group. In the profiles generated, several key differences were noted that corresponded with supporting or previous findings. As a result, these findings provided evidence that these stimuli not only resulted in a reduction in cell viability, but the metabolic profiles were additionally distinct from one another.

Background and Significance

In the past 10 years, systems biology has grown in regards to technological platforms in which systems can be explored and the data interpreted on the molecular level, with the emergence of metabolomics being the newest of these platforms.⁵⁵ The ability to accurately detect, identify and quantitate the metabolites present in living organisms can provide a wealth of information that complements other technologies such as genomics and proteomics in a variety of biologically relevant applications.⁵⁶⁻⁵⁸ The analysis of molecular metabolism can be an effective method to evaluate the state of a system. In the “omics” cascade, metabolism represents what is actually happening in an organism after genes have been regulated, expressed as phenotypes and finally modified post-transcriptionally. Further, it can be probed in systems where stress of various forms has been applied. This chapter focuses on one of those applications. T1DM is known to be caused by the reduction of insulin producing β -cells in the Langerhans of the pancreas due to the death of these cells.⁵⁹ Insulin deficiency then causes increased blood glucose along with a multitude of symptoms that must be treated. Currently, treatments of the disease usually include insulin injections, as there is no known cure for T1DM. While it is known that β -cell death is a hallmark for T1DM, how these cells die, as well as why they are specifically selected for destruction, remains largely unknown. Two mechanisms of cell death have been proposed, although these have been debated. Conceivably, clarification as to which mechanism, if either, is responsible for β -cell death will advance discussions of possible treatments or cures for T1DM. Here, a mass spectrometry based metabolomics approach was used to determine metabolic profiles for rat insulinoma cells treated with cell death inducers, in an effort to explore mechanisms of cell death on a chemical level.

Metabolomics Background

Biologists rely on a number of analytical techniques to study the often complex systems of living organisms. Starting at the genotypic level, there is what is described as the “omics” cascade that consists of all the technology from which systems biology research is conducted. The newest discipline to emerge is also closest to the phenotypic level and deals with the metabolome.⁵⁸ The metabolome refers to the set of all small molecule metabolites found in a biological sample, and the technological platform has been termed metabolomics. Currently, there is no single platform for the complete analysis of all the metabolites present in a single

system; however, over the past 10 years there have been an increasing number of papers published that use metabolomics as a bioanalytical technique, demonstrating its usefulness as a bioanalytical tool.^{60, 61} One possible reason that metabolomics has lagged behind other techniques such as genomics and proteomics is that the metabolome is often dynamic and complex. There are an estimated 2,000 major metabolites in mammalian organisms and up to ~200,000 in the plant kingdom, and these compounds represent a broad variety of chemical classes with different chemical properties.⁶⁰ Metabolite pools can change on the order of seconds, and even slight environmental changes, such as a minor temperature change, can result in changes in the metabolome. Despite the challenges associated with metabolomics, one can easily recognize its benefits. Metabolism gives an accurate and timely view of the state of the system and is often associated with the overall well-being of the organism or cell.

Metabolic Profiling vs. Metabolic Fingerprinting

The two major approaches to metabolomics include metabolic profiling and metabolic fingerprinting. In most cases, metabolic profiling refers to the analysis of a certain group of metabolites that is usually hypothesis driven and quantitative, also called a targeted analysis. An example would be the analysis of fatty acids in a mammalian tissue. An even more specific application is the selection of specific compounds for identification that may serve as biomarkers of a disease or toxin exposure. This type of targeted analysis can be useful in supporting the data collected from other technical “omics” platforms. Conversely, metabolic fingerprinting is the global analysis of samples with the intent to obtain a characteristic metabolite pattern or “fingerprint” and therefore, inherently an untargeted approach. This application is useful in showing the overall change in metabolism in response to a treatment or alteration such as genetic manipulations. Regardless of the sample or application, the steps leading to a metabolomics data set are the same: sample collection, extraction, chemical analysis, and data analysis.

Sample Type

Clinical applications of metabolomics have been useful in the field of human biology, where fluids, such as serums and urine, can be quickly analyzed for changes in metabolic profiles in response to disease, diet, toxins etc.⁶² This application, however, only provides information on

the metabolism of the organism as a whole, which usually provides no quantitative information, and can also result in the introduction of additional variables. When dealing with individual cell types, variables such as gender, environmental exposures, and contributions from different tissues, essentially become non-existent due to the fact that the sample is often derived from a controllable cell line as opposed to a human or animal model.⁶⁰

Sampling and Extracting

The sampling in a metabolomics experiment should be determined by the experimental design and type. In any case, the best results are obtained when the following are taken into consideration: replication and quality control. Inter-day and multiple-day replications should be taken in order to reduce biological variability. Additionally, the appropriate use of control samples and/or internal standards can greatly enhance the statistical validity of the data set. Once an experiment has been designed and the samples have been acquired, they must be handled with extreme care as to not cause any disturbances in the existing metabolome. Often this requires the use of cold temperatures to suspend metabolism. Some techniques used include flash freezing, freeze clamping or immediate quenching. In cases where the metabolome is not immediately extracted, the sample should be kept cold and the length of time before extraction should be kept constant between all samples. The extraction technique will vary with the experiment, but careful measures should be taken to ensure that all parameters of a given experiment remain the same for all samples to be analyzed once an extraction technique has been validated. Usually, the metabolome is extracted in order to separate the metabolites from the complex biological matrices in which they are found, however direct injection is one method of sample preparation. The extraction solvent should be suitable for the type of sample. For example, a cold methanolic solution is usually used for mammalian tissue, whereas more complex solvents, such as acidic acetonitrile mixtures, are typically used for bacterial cultures.⁶³ Here, the use of an internal standard spike can provide another means by which the data set can be validated. It should be noted that in no experiment will the whole metabolome remain intact. The very nature of the sample preparation step will guarantee that some metabolites will be lost due to the fact that not all metabolites can be extracted by one method.

Analytical Methods

After the sample has been collected and extracted, the final stages in a metabolomics experiment are the analyses of the metabolites which include: separation, detection, and if possible, quantification. Some of the requirements for obtaining scientifically relevant metabolomics data are that the instruments used for analysis have excellent sensitivity and resolution for a wide range of molecules, the ability to work with a variable range of metabolite concentrations, relatively short analysis times, and reasonable reproducibility. Currently, the two most widely used methods for metabolic analysis are nuclear magnetic resonance (NMR), and mass spectrometry (MS). Both have their own particular advantages and disadvantages. With NMR, samples require minimal preparation which preserves the sample.^{64, 65} NMR also offers the ability to directly quantitate the relative abundance of metabolites in a sample, which can be difficult to do with MS.

Mass Spectrometry Based Metabolomics

MS has come to the forefront of metabolomics research since becoming a successful tool in drug metabolite analysis.⁶¹ The application of modern MS to cell culture metabolism is particularly useful because of its high sensitivity and possibility for metabolite quantitation. Several variations of MS have been implemented to study metabolism.^{61, 66, 67} One of the simplest, direct injection has been useful for samples with sufficient metabolite content and concentrations, such as urine. The major drawback of this method is that the biological matrix in which the sample is located will usually reduce signal quality. Another problem associated with direct injection is the difficulty when attempting to distinguish between analytes of the same mass-to-charge ratio (m/z). When working with cell cultures, additional steps, such as the incorporation of chromatography, are typically required for the analysis of global metabolism. Variations such as gas chromatography mass spectrometry (GC-MS) and liquid chromatography mass spectrometry (LC-MS) are often used in order to increase the number of metabolites seen, however because of the complexity often involved with sample preparation in GC-MS, LC-MS has taken a leading role in most MS metabolomics research.⁶⁸ Considerations when choosing a LC-MS method include 1) separation of the metabolites from the biological matrix, 2) separation using chromatography, 3) analyte ionization, 4) detection of the fragment and 5) identification. Again, separation of the metabolome from the matrix as well as using chromatography is important for the overall signal quality. Reduction of the number of analytes

at a given time reduces the occurrence of ion suppression, and provides another level of specificity. The ionization method most widely used for metabolomics has been electrospray ionization (ESI). ESI is a soft ionization technique that ionizes liquid samples directly into the gas phase, which is well suited for LC-MS. The number of metabolites measured increases when both positive and negative ion modes are used. Metabolites such as amines will ionize best in positive ion mode while acidic metabolites such as phosphates will ionize better in negative mode. The two most common mass analyzers used in metabolomics directed research are time-of-flight (TOF) and quadrupole analyzers.⁶⁷ As mentioned in the previous chapter, the preferred MS method used by our lab is detection by selected reaction monitoring (SRM) on a triple quadrupole mass spectrometer. Coupled with separation by high performance liquid chromatography (HPLC), this method has the sensitivity and selectivity required to detect up to ~350 polar metabolites as developed by Rabinowitz and co-workers. The target experiments that will use this method will require that both the parent and product mass be known however, a library of the ~350 metabolites was also created by Rabinowitz using chemical standards that will be used in the studies presented in this chapter.

Data Analysis

The data sets generated by MS metabolomics techniques are often large and complex. The first challenge encountered after data collection is the organization of these data into similar classes by correctly identifying each individual metabolite.⁶⁹ Often, the differences in metabolite pools are of interest so it is imperative that metabolites are identified correctly. The use of chemical standards and databases can greatly enhance identification, although these tools are still in the beginning stages of development.^{70, 71 72} Software for the identification and selection of chromatographic peaks has been important for evaluation of untargeted metabolomics data sets.⁶⁷ Once the metabolite has been identified, certain normalization factors will often be applied to the raw data in order to correct for variability in the experiment. Once these have been applied, the final task is to assemble the data for visualization.

Pancreatic β -cell Death

T1DM is an autoimmune disease that is characterized as the loss of the beta-cell mass of the islets of the Langerhans in the pancreas that results in insulin deficiency.⁵⁹ Pro-inflammatory

cytokines, such as interleukin-1 β (IL-1 β) and gamma-interferon (γ -IFN), induce the expression of genes that produce inflammatory mediators, such as nitric oxide synthase (iNOS), and the production and accumulation of nitric oxide (NO) inside the cell will inevitably decrease β -cell viability.^{73, 74} While it is known that the secretion of pro-inflammatory cytokines play a role in β -cell death, the initial cause and the precise method by which β -cells are destroyed are not fully understood. Two mechanisms of cell death that are generally accepted, yet debated, are an apoptotic pathway^{75, 76} and/or a necrotic pathway.^{77, 78} Pro-inflammatory cytokines could induce either of these pathways through a common bcl-2 inhibitory pathway, which makes discerning the direct cause of β -cell death problematic.⁷⁹ Apoptosis is a programmed form of cell death that causes morphological changes in the cell which lead to irreversible damage.⁸⁰ It is known to be activated by a cascade of different caspases. With regards to β -cell death, initiation of the apoptotic cascade results in targeted degradation of intracellular proteins that lead to cellular death. When cleaved, one of these caspases, Caspase 3 (CASP3), is responsible for the targeted destruction of intracellular proteins that lead to cell death.⁸¹ CASP3 activity is a known marker for apoptosis mediated cell death. The pathways of non-apoptosis forms of cell death, such as necrosis are even less understood.

There are several different models in which T1DM has been studied. The first animal model for diabetes research was the non-obese diabetic (NOD) mouse model. Developed in 1970, this strain spontaneously develops the autoimmune disease, similar to human T1DM.⁸² Even with this model, the exact cellular mechanism behind β -cell death is unknown; the complexity of the pathways involved in several different rat modeling systems has added confusion as to which, if any of these pathways is actually involved in human T1DM.

Pancreatic β -cell Death is likely the Result of a Non-Apoptotic Mechanism

In a series of studies, pro- and anti-apoptotic proteins were subject to manipulation in order to test the hypothesis that if apoptosis is indeed the primary pathway involved in β -cell death, then exposure to cytokines known to be involved in a non-apoptotic method of cell death should be protected the cell from damage.⁷⁷ Several methods were implemented in order to first show that apoptosis was not occurring in cells exposed to pro-inflammatory cytokines. First, the effects of cytokines interleukin-1 β (IL-1 β) and gamma-interferon (γ -IFN) were compared with the effects of a known apoptosis inducer, camptothecin, in both a normal cytokine sensitive cell line

(832/13) and a cell line selected for cytokine resistance (833/15).⁸³ Results indicated a 40% decrease in viability in the 832/13 cell line when exposed to cytokines, and an identical 80% decrease in viability in both cell lines with exposure to camptothecin. This showed that selectivity for cytokine resistance protected against death by exposure to the cytokines, but offered no protection against exposure to apoptosis induced cell death. Next the 832/13 cell line was subjected to overexpression of the anti-apoptotic protein kinase Akt1. This provided protection against cell death when the cells were treated with camptothecin, but not with cytokines. Additionally, siRNA mediated suppression of the proapoptotic protein Bax enhanced cell viability in those treated with apoptosis inducers, but provided no protection in cells treated with cytokines. In apoptosis, CASP3 activity can be measured via radioimmunoassay, and it was verified that camptothecin induced CASP3 cleavage in both cell lines as well as isolated primary cells. In contrast, NO is known to prevent caspase activity⁸⁴; this was consistent with the finding that no increase in CASP3 activity occurred in these cell lines treated with pro-inflammatory cytokines. Another marker of apoptotic cell death, annexin V staining, was used, and results again showed that camptothecin and not IL-1 β and γ -IFN caused increases in staining. Finally, intracellular ATP levels were examined. It has been suggested that ATP levels could be an important biomarker for a switch from necrosis to apoptosis. Caspase activity requires energy, and so it is presumed that intracellular ATP will be higher if apoptosis is occurring while ATP levels will drop if a switch to a non-apoptosis pathway has occurred.⁸⁵ Results in these studies indeed showed that ATP levels increased in both sensitive and resistant cell lines treated with camptothecin, while IL-1 β and γ -IFN decreased ATP levels in the sensitive cell line 832/13 and had no effect on the intracellular levels of ATP in the cytokine resistant cell line 833/15. Taken together, these studies clearly support the idea that pro-inflammatory cytokine mediated β -cell death proceeds by a mechanism independent and distinct from those known to occur in apoptotic mediated pathways. It should be noted that previous reports with contradictory results failed to employ a control for apoptosis such as a genuine apoptosis inducer.^{86, 87} Several biomarkers are proven to be useful when attempting to distinguish between the two proposed pathways. Therefore, we intended to study the metabolome of rat insulinoma cells which had been exposed to either pro-inflammatory cytokines or known apoptosis inducers. If the information obtained from the metabolome were consistent with the previous findings, then cell lines treated with known apoptotic inducers should show differences in metabolites when contrasted with cell lines treated with pro-inflammatory cytokines.

Results and Discussion

The unique intersection of the strategies previously employed by the Collier lab and mass spectrometry based metabolomics developed by our lab aimed to further support the findings that a non-apoptosis pathway is predominate in rat islet cells. The initial goal was to develop an extraction method to analyze the metabolome of rat islet cells from two different cell lines. Given that this type of analysis has never been initiated in any islet cell line, it was unknown as to whether this method would ultimately provide any metabolic information. A preliminary extraction was done using a typical mammalian tissue protocol⁶³, and the supernatants analyzed via liquid chromatography tandem mass spectrometry (LC-MS/MS) in SRM mode. Results indicated the extraction performed and method of analysis was suitable for the islet cells, so a series of studies was conducted on islet cells of various treatments. The treatments used were specifically selected in order to compare the metabolic differences in islet cells where apoptosis was induced versus cytokine exposure. This preliminary hypothesis presumes that these two cellular mechanisms are independent and involve discretely separate metabolic pathways, and therefore metabolic profiling of cells undergoing these two different mechanisms of cell death will reveal differences in metabolite pools.

Distinction between Cell Death via Exposure to Pro-inflammatory Cytokines versus Genuine Apoptosis Inducers

In a second series of studies conducted by the Collier lab, the hypothesis that pro-inflammatory cytokines and apoptosis inducers differed in the mechanism by which cell death occurs was further explored. In an effort to prove that the cytokine sensitive cell line 832/13 used in these and past studies was just as sensitive to cytokine and apoptosis mediated killing as other cell lines used in contradictory studies,⁸⁸ an INS-1E derived cell line was first tested for viability when exposed to both. It was found that both cell lines were equally sensitive to both inducers. In order to further support the hypothesis that cytokine mediated cell death proceeds by a different mechanism than apoptosis, key components from known pathways of each mechanism were manipulated and tested for viability in response to both IL-1 β and γ -IFN and camptothecin. Manipulation of apoptosome by siRNA-mediated suppression of APAF-1 or a dominant-negative form of capsase-9, protected against killing by camptothecin but not IL-1 β and γ -IFN. Inhibition of IKK β , a known component of the NF-kB signaling pathway, by pharmacological inhibitor

TPCA or overexpression of an I κ B α super repressor, blunted cytokine inducer NO production and provided protection against losses in β -cell viability. No protection against camptothecin mediated apoptosis was observed with either method.

Metabolic Profiling by Tandem Mass Spectrometry

From here, the metabolome of 832/13 rat islet cells treated separately with either proinflammatory cytokines (IL-1 β and γ -IFN), or an apoptosis inducer (camptothecin) was first extracted, and then analyzed using the previously validated LC-MS/MS technique.^{89, 90} Again, stemming from the previous findings, it was hypothesized that the metabolic profiling of the differently treated cell lines would reveal differences in some metabolite pools and no differences in others because the two different methods of β -cell death would be using different metabolic pathways; cytokines induce cell death by increasing levels of intracellular NO into the μ M range, while apoptosis induces DNA damage through the caspase cascade. To show these differences, fold changes in both treatments relative to a non-treated 832/13 cell sample were considered. Figure 14 is a representative heatmap that displays these fold changes. Approximately 130 metabolites were measured in positive mode and 175 were measured in negative mode. Of these, 90 metabolites were verified to have changed with respect to the control samples. Additionally, a table of p-values was constructed in order to determine the probability that the differences seen in the treated cells relative to the non-treated cells were indeed due to addition of the treatment (Tables 30 and 31, Appendix). In both cases, distinct metabolic profiles were seen. However, it should be noted that although the concentration of most metabolites in both the IL-1 β and γ -IFN and camptothecin treated cells increase, this does not necessarily indicate that these cells are more metabolically active than the control cells. Metabolism changes can both be the result of a build-up of a metabolite or an increased use of a metabolite, and it is impossible to distinguish between the causes of these changes in pool size measurements, unless flux experiments are conducted. Regardless, obvious differences in the metabolic response to the two different treatments were observed. One of the most notable changes was the 400-fold increase in citrulline in cells treated with IL-1 β and γ -IFN. Citrulline is an end product of the iNOS reaction, and these results support the previous findings that NO levels increase in cells treated with IL-1 β and γ -IFN.

IL-1 β + γ -IFN : camptothecin

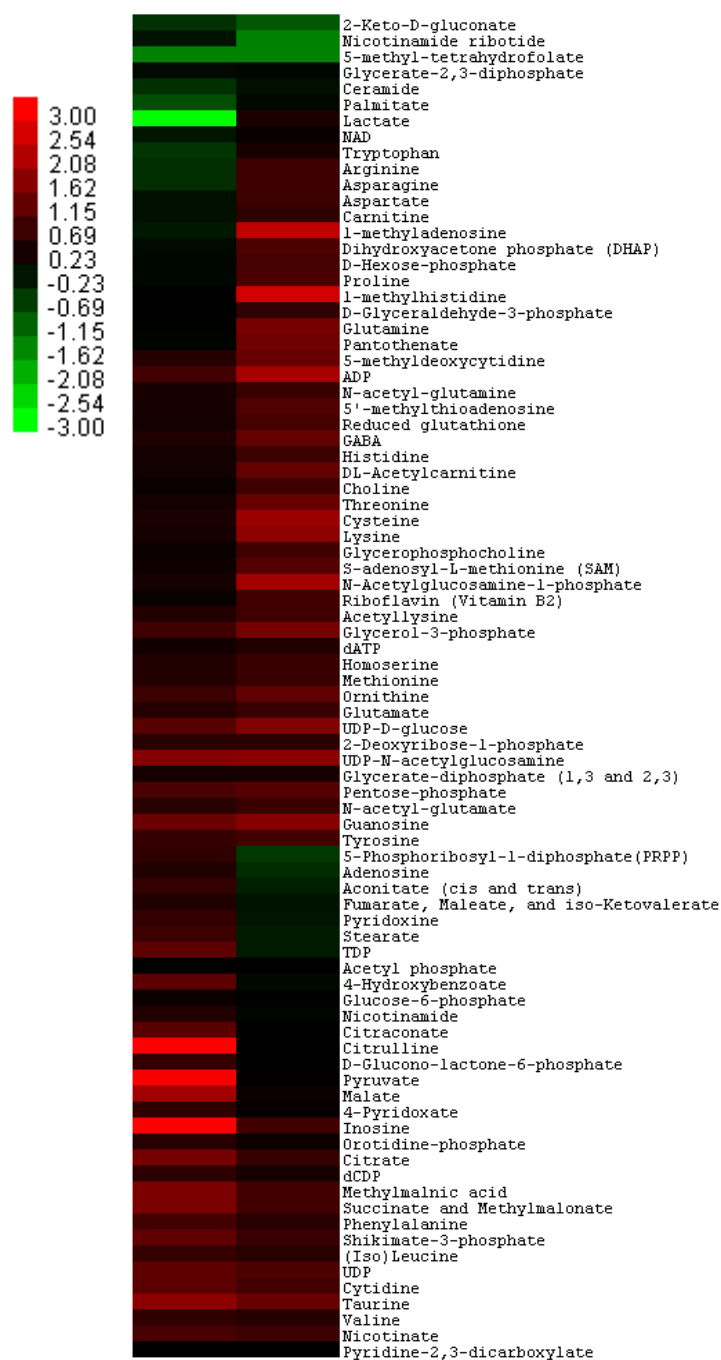


Figure 14: Representative heatmap displaying metabolite fold changes relative to a control. Values are given in \log_2 , so that “3.00” is a minimum of an 8-fold increase, while “-3.00” is a minimum of an 8-fold decrease. Red indicates a metabolite increase in the treatment condition relative to an untreated control, while green represents a decrease relative to control.

Methods and Materials

General Methods

The LC-MS/MS system used for detection of metabolites consisted of a Thermo Electron Surveyor Autosampler Plus, a Surveyor MS Pump Plus, and a TSQ Quantum Discovery Max triple quadrupole MS. All MS spectra were collected and analyzed using the Xcalibur MS v 2.0.7 software package (Thermo Electron Corporation). HPLC separations performed in positive mode used a Luna NH₂ HILIC column (5µm pore size, 100 Å particle size, 250 x 2.00 mm) supplied by Phenomenex. HPLC separations performed in negative mode used a Synergi Hydro-RP C₁₈ column (4 µm pore size, 80 Å particle size, 150 x 2.00 mm) supplied by Phenomenex.

Cell Extraction Procedure

832/13 cells were grown to confluence in 15 cm dishes and treated as indicated in the figure legends. At the end of the treatment period, cells were washed twice with ice cold phosphate buffered saline, scraped and pelleted at 500 x g; the aspirated dry cell pellets were immediately flash frozen using liquid N₂. Four individual experiments were performed in duplicate on each of 3 days. Prior to extraction, the collected cell pellets were weighed, and 30-50 mg of each was placed into a microcentrifuge tube at -78 °C. A solution of cold methanol and water (8:2 v/v, 1.5 mL) kept at -80 °C was then added to the tube to extract the metabolome from the cells. The contents were mixed by vortexing and allowed to sit at the extraction temperature for 20 min. Particulates were then removed from the samples by centrifugation, and the supernatants were transferred to autosampler vials for further analysis by the LC-MS/MS methods described below.

Chromatographic Details

High performance liquid chromatographic separations of metabolites were performed via a slight modification of previously reported methods.⁹¹ Due to slight changes, methods are also reported below. In total, two HPLC runs are necessary to fully characterize the metabolome for each sample since separate detection for positively ionizing and negatively ionizing compounds is required. For all samples, 10 µL was injected onto the column via an autosampler. A

quaternary pump was used to generate the following gradient for the elution of compounds from the stationary phase:

Positive Mode

The mobile phase flow rate was 150 $\mu\text{L}/\text{min}$, and a gradient of two solvents was used for elution. Solvent A was a mixture composed of 95% 20 mM ammonium acetate and 20 mM ammonium hydroxide in HPLC grade water buffered at pH = 9.4 with 5% HPLC grade acetonitrile. Solvent B was pure HPLC grade acetonitrile. These were used to construct the following 40 min gradient elution profile: $t = 0$ min, 15% solvent A, 85% solvent B; $t = 15$ min, 100% solvent A, 0% solvent B; $t = 28$ min, 100% solvent A, 0% solvent B; $t = 30$, 15% solvent A, 85% solvent B; $t = 40$, 15% solvent A, 85% solvent B. Separations were performed with the column temperature set at 10 $^{\circ}\text{C}$.

Negative Mode

The mobile phase flow rate was 200 $\mu\text{L}/\text{min}$, and a gradient of two solvents was again used for elution. Solvent A consisted of a mixture containing 97% 11 mM tributylamine and 15 mM acetic acid in HPLC grade water and 3% HPLC grade methanol. Solvent B was pure HPLC grade methanol. These were used to construct the following 50 min gradient elution profile: $t = 0$ min, 100% solvent A, 0% solvent B; $t = 5$ min, 100% solvent A, 0% solvent B; $t = 10$ min, 80% solvent A, 20% solvent B; $t = 15$, 80% solvent A, 20% solvent B; $t = 30$, 35% solvent A, 65% solvent B; $t = 33$, 5% solvent A, 95% solvent B; $t = 37$, 5% solvent A, 95% solvent B; $t = 38$, 100% solvent A, 0% solvent B; $t = 50$, 100% solvent A, 0% solvent B. Separations were performed with the column temperature maintained at 25 $^{\circ}\text{C}$.

Mass Spectrometric Detection Parameters

Samples were introduced into the electrospray ionization (ESI) chamber through a 0.1 mm internal diameter fused silica capillary after delivery by HPLC as described above. The spray voltage for the ESI source was set to 4500 V, if detection occurred in positive ion mode. If detection occurred in negative mode, the spray voltage for the ESI source was set to 3000 V. Nitrogen was used as the sheath gas (40 psi), and the inlet capillary temperature was 290 $^{\circ}\text{C}$. Argon was used as the collision gas at a pressure of 1.5 mTorr. Samples were analyzed using selected reaction monitoring (SRM) with the scan time for each SRM set to 0.05 s and a scan

width of 1 m/z . Full selected reaction monitoring (SRM) detection parameters for most compounds have been previously reported by Rabinowitz and coworkers.⁹¹

Data Handling and Statistical Analysis

The peak for each detected metabolite was manually integrated to determine the peak area using the Quan Browser function of Xcalibur. The integration values were then directly entered into an Excel spreadsheet where they were normalized to the mass of tissue extracted. Since inter-day variability in the ion counts for metabolites was observed due to MS sampling variation, the treated samples were compared only to the control samples run on the same day. This comparison consisted of averaging the ion counts for the duplicate measurements of a metabolite from a treated sample on a given day and then dividing this number by the average of the duplicate measurements of the same metabolite from the control sample obtained on the same day to generate the fold change for the compound. The fold changes for the metabolite from each of the three days were then averaged and clustered and displayed in heat map format using the freely available Cluster 3.0 (www.falw.vu/~huik/cluster.htm) and Java Treeview⁹² data analysis packages. The p-value for each metabolite fold change was obtained by performing an F-test using the data analysis tool pack in Microsoft Excel. The variance in the fold changes for the metabolites in the treatment group was compared to a set of standardized fold changes for the metabolites from the control group that was generated by taking the intra-day ratio of the ion counts from the duplicate measurements of the control.

Conclusion

The tools available to a chemist or biologist can greatly impact the scope and quality of research conducted. Here, a chemical approach conducted with analytical techniques was applied to the study of two biological systems. Quantitation of both systems, absolute for quorum sensing molecules, and relative for the metabolic profiling of rat insulinoma cells, were ultimately achieved using LC-MS/MS methods, providing novel results as well as further questions.

The synthesis of stable isotopically labeled AHLs allowed for the quantitation of the naturally occurring molecules in four strains of *Vibrio fischeri*. This synthesis proved to be exceptionally valuable for AHL studies in any bacterial system, as it was able to produce any AHL necessary with minimal purification. Additionally, the AI-2 mediated quorum sensing systems of *Yersinia enterocolitica* and *Edwardsiella tarda* were analyzed. Results from these studies contribute to the growing amount of information about quorum sensing systems, and have been useful in efforts to better understand these systems.

The application of known LC-MS/MS methods to the study of rat insulinoma cells provided visibly distinctive metabolic profiles for two proposed mechanisms of β -cell death. Taken together with results from the Collier lab, we were able to conclude that β -cell death in response to pro-inflammatory cytokines is unlikely to proceed through an apoptotic mechanism. Further studies are currently underway to continue probing these mechanisms metabolically, with the ultimate goal of determining the exact cause of pancreatic β -cell death and eventually, T1DM.

References

1. Fuqua, C., Parsek, M. R., and Greenberg, E. P. (2001) Regulation of gene expression by cell-to-cell communication: Acyl-homoserine lactone quorum sensing, *Annual Review of Genetics* 35, 439-468.
2. Miller, M. B., and Bassler, B. L. (2001) Quorum sensing in bacteria, *Annual Review of Microbiology* 55, 165-199.
3. Waters, C. M. (2005) Quorum sensing: Cell-to-cell communication in bacteria, In *Annual Review of Cell and Developmental Biology*, pp 319-346.
4. Fuqua, W. C., Winans, S. C., and Greenberg, E. P. (1994) Quorum Sensing in Bacteria - The LuxR-LuxI Family of Density-Responsive Transcriptional Regulators, *Journal of Bacteriology* 176, 269-275.
5. Hall-Stoodley, L., Costerton, J. W., and Stoodley, P. (2004) Bacterial biofilms: From the natural environment to infectious diseases, *Nature Reviews Microbiology* 2, 95-108.
6. Dickschat, J. S. (2010) Quorum sensing and bacterial biofilms, *Natural Product Reports* 27, 343-369.
7. Donlan, R. M. (2002) Biofilms: Microbial life on surfaces, *Emerging Infectious Diseases* 8, 881-890.
8. Rickard, A. H., Colacino, K. R., Manton, K. M., Morton, R. I., Pulcini, E., Pfeil, J., Rhoads, D., Wolcott, R. D., and James, G. (2010) Production of cell-cell signalling molecules by bacteria isolated from human chronic wounds, *Journal of Applied Microbiology* 108, 1509-1522.
9. Singh, P. K., Schaefer, A. L., Parsek, M. R., Moninger, T. O., Welsh, M. J., and Greenberg, E. P. (2000) Quorum-sensing signals indicate that cystic fibrosis lungs are infected with bacterial biofilms, *Nature* 407, 762-764.
10. Lyczak, J. B., Cannon, C. L., and Pier, G. B. (2002) Lung infections associated with cystic fibrosis, *Clinical Microbiology Reviews* 15, 194.
11. Bjarnsholt, T., and Givskov, M. (2007) Quorum-sensing blockade as a strategy for enhancing host defences against bacterial pathogens, *Philosophical Transactions of the Royal Society B-Biological Sciences* 362, 1213-1222.
12. Kaufmann, G. F., Park, J., and Janda, K. D. (2008) Bacterial quorum sensing: a new target for anti-infective immunotherapy, *Expert Opinion on Biological Therapy* 8, 719-724.
13. Boyer, M., and Wisniewski-Dye, F. (2009) Cell-cell signalling in bacteria: not simply a matter of quorum, *Fems Microbiology Ecology* 70, 1-19.
14. Platt, T. G., and Fuqua, C. (2010) What's in a name? The semantics of quorum sensing, *Trends in Microbiology* 18, 383-387.
15. Xavier, K. B., and Bassler, B. L. (2003) LuxS quorum sensing: more than just a numbers game, *Current Opinion in Microbiology* 6, 191-197.
16. Bassler, B. L. (1999) How bacteria talk to each other: regulation of gene expression by quorum sensing, *Current Opinion in Microbiology* 2, 582-587.

17. Lupp, C., Urbanowski, M., Greenberg, E. P., and Ruby, E. G. (2003) The *Vibrio fischeri* quorum-sensing systems *ain* and *lux* sequentially induce luminescence gene expression and are important for persistence in the squid host, *Molecular Microbiology* 50, 319-331.
18. Passador, L., Cook, J. M., Gambello, M. J., Rust, L., and Iglewski, B. H. (1993) Expression of *Pseudomonas aeruginosa* virulence genes requires cell-to-cell communication, *Science* 260, 1127-1130.
19. Jaques, S., and McCarter, L. L. (2006) Three new regulators of swarming in *Vibrio parahaemolyticus*, *Journal of Bacteriology* 188, 2625-2635.
20. Kleerebezem, M., Quadri, L. E. N., Kuipers, O. P., and Devos, W. M. (1997) Quorum sensing by peptide pheromones and two-component signal-transduction systems in Gram-positive bacteria, *Molecular Microbiology* 24, 895-904.
21. Surette, M. G., Miller, M. B., and Bassler, B. L. (1999) Quorum sensing in *Escherichia coli*, *Salmonella typhimurium*, and *Vibrio harveyi*: A new family of genes responsible for autoinducer production, *Proceedings of the National Academy of Sciences of the United States of America* 96, 1639-1644.
22. Bassler, B. L., Wright, M., Showalter, R. E., and Silverman, M. R. (1993) Intercellular Signaling in *Vibrio harveyi* - sequence and Function of Genes Regulating Expression of Luminescence, *Molecular Microbiology* 9, 773-786.
23. Chen, X., Schauder, S., Potier, N., Van Dorsselaer, A., Pelczer, I., Bassler, B. L., and Hughson, F. M. (2002) Structural identification of a bacterial quorum-sensing signal containing boron, *Nature* 415, 545-549.
24. Schauder, S., Shokat, K., Surette, M. G., and Bassler, B. L. (2001) The LuxS family of bacterial autoinducers: biosynthesis of a novel quorum-sensing signal molecule, *Molecular Microbiology* 41, 463-476.
25. Miller, C. H., and Duerre, J. A. (1968) S-ribosylhomocysteinase cleavage enzyme from *Escherichia coli*, *Journal of Biological Chemistry* 243, 92-&.
26. Visick, K. L., Foster, J., Doino, J., Mcfall-Ngai, M., and Ruby, E. G. (2000) *Vibrio fischeri lux* genes play an important role in colonization and development of the host light organ, *Journal of Bacteriology* 182, 4578-4586.
27. Whitehead, N. A., Barnard, A. M. L., Slater, H., Simpson, N. J. L., and Salmond, G. P. C. (2001) Quorum-sensing in gram-negative bacteria, *Fems Microbiology Reviews* 25, 365-404.
28. Fuqua, C., and Greenberg, E. P. (2002) Listening in on bacteria: Acyl-homoserine lactone signalling, *Nature Reviews Molecular Cell Biology* 3, 685-695.
29. Fuqua, C., Winans, S. C., and Greenberg, E. P. (1996) Census and consensus in bacterial ecosystems: The LuxR-LuxI family of quorum-sensing transcriptional regulators, *Annual Review of Microbiology* 50, 727-751.
30. Halliday, N. M., Hardie, K. R., Williams, P., Winzer, K., and Barrett, D. A. (2010) Quantitative liquid chromatography-tandem mass spectrometry profiling of activated methyl cycle metabolites involved in LuxS-dependent quorum sensing in *Escherichia coli*, *Analytical Biochemistry* 403, 20-29.

31. Waters, C. M., and Bassler, B. L. (2006) The *Vibrio harveyi* quorum-sensing system uses shared regulatory components to discriminate between multiple autoinducers, *Genes & Development* 20, 2754-2767.
32. Xavier, K. B., and Bassler, B. L. (2005) Regulation of uptake and processing of the quorum-sensing autoinducer AI-2 in *Escherichia coli*, *Journal of Bacteriology* 187, 238-248.
33. Gooding, J. R., May, A. L., Hilliard, K. R., and Campagna, S. R. (2010) Establishing a Quantitative Definition of Quorum Sensing Provides Insight into the Information Content of the Autoinducer Signals in *Vibrio harveyi* and *Escherichia coli*, *Biochemistry* 49, 5621-5623.
34. Piper, K. R., Vonbodman, S. B., and Farrand, S. K. (1993) Conjugation factor of *Agrobacterium tumefaciens* regulates TI-plasmid transfer by autoinduction, *Nature* 362, 448-450.
35. Shaw, P. D., Ping, G., Daly, S. L., Cha, C., Cronan, J. E., Rinehart, K. L., and Farrand, S. K. (1997) Detecting and characterizing *N*-acyl-homoserine lactone signal molecules by thin-layer chromatography, *Proceedings of the National Academy of Sciences of the United States of America* 94, 6036-6041.
36. Blosser-Middleton, R. S., and Gray, K. M. (2001) Multiple *N*-acyl homoserine lactone signals of *Rhizobium leguminosarum* are synthesized in a distinct temporal pattern, *Journal of Bacteriology* 183, 6771-6777.
37. Charlton, T. S., De Nys, R., Netting, A., Kumar, N., Hentzer, M., Givskov, M., and Kjelleberg, S. (2000) A novel and sensitive method for the quantification of *N*-3-oxoacyl homoserine lactones using gas chromatography-mass spectrometry: application to a model bacterial biofilm, *Environmental Microbiology* 2, 530-541.
38. Thiel, V., Kunze, B., Verma, P., Wagner-Dobler, I., and Schulz, S. (2009) New Structural Variants of Homoserine Lactones in Bacteria, *Chembiochem* 10, 1861-1868.
39. Morin, D., Grasland, B., Vallee-Rehel, K., Dufau, C., and Haras, D. (2003) On-line high-performance liquid chromatography-mass spectrometric detection and quantification of *N*-acylhomoserine lactones, quorum sensing signal molecules, in the presence of biological matrices, *Journal of Chromatography A* 1002, 79-92.
40. Ortori, C. A., Atkinson, S., Chhabra, S. R., Camara, M., Williams, P., and Barrett, D. A. (2007) Comprehensive profiling of *N*-acylhomoserine lactones produced by *Yersinia pseudotuberculosis* using liquid chromatography coupled to hybrid quadrupole-linear ion trap mass spectrometry, *Analytical and Bioanalytical Chemistry* 387, 497-511.
41. Campagna, S. R., Gooding, J. R., and May, A. L. (2009) Direct Quantitation of the Quorum Sensing Signal, Autoinducer-2, in Clinically Relevant Samples by Liquid Chromatography-Tandem Mass Spectrometry, *Analytical Chemistry* 81, 6374-6381.
42. Semmelhack, M. F., Campagna, S. R., Federle, M. J., and Bassler, B. L. (2005) An expeditious synthesis of DPD and boron binding studies, *Organic Letters* 7, 569-572.
43. Gould, T. A., Herman, J., Krank, J., Murphy, R. C., and Churchill, M. E. A. (2006) Specificity of acyl-homoserine lactone synthases examined by mass spectrometry, *Journal of Bacteriology* 188, 773-783.

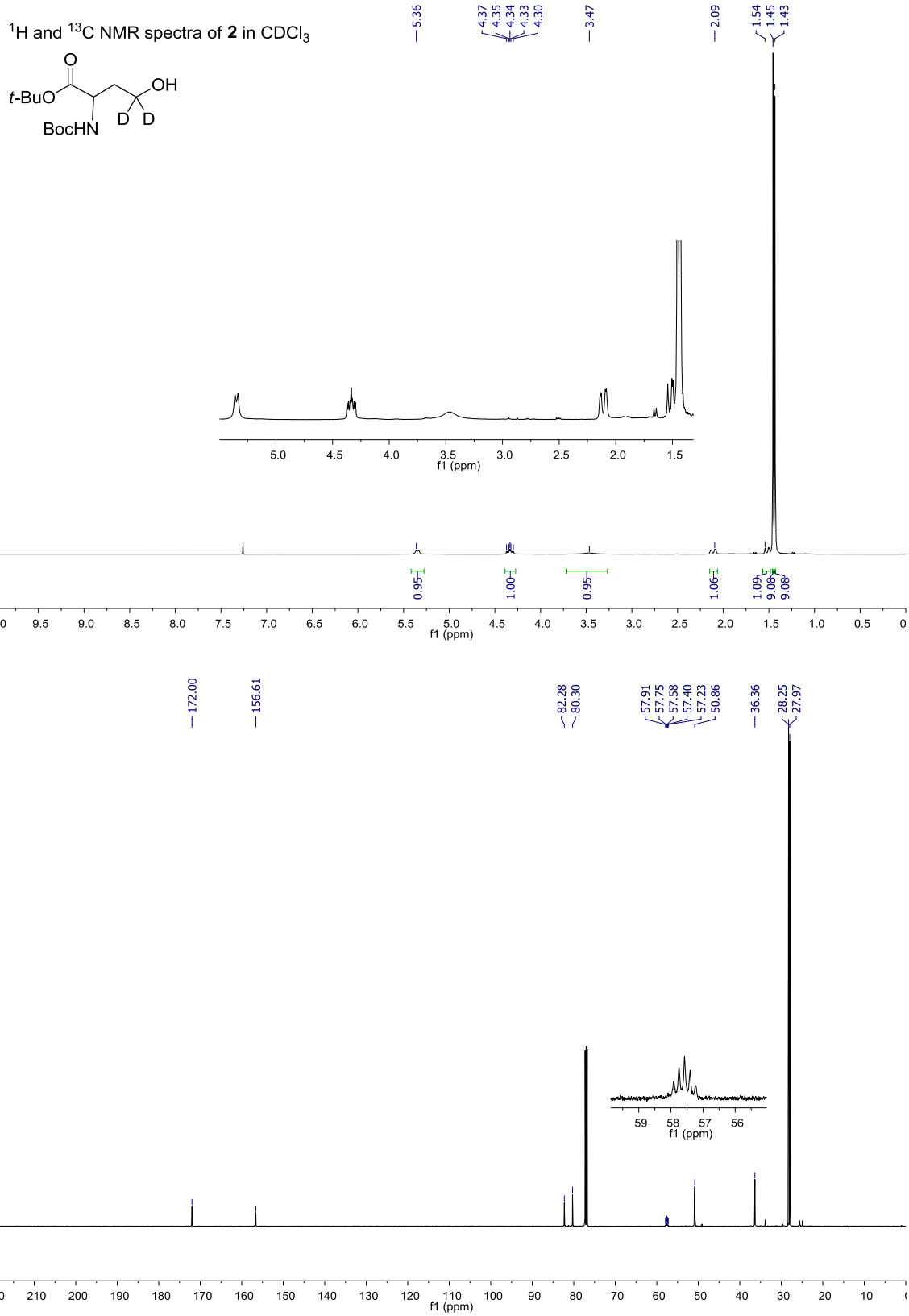
44. Kai, K., Tani, A., and Hayashi, H. (2010) Facile preparation of deuterium-labeled *N*-acylhomoserine lactones as internal standards for isotope dilution mass spectrometry, *Bioorganic & Medicinal Chemistry* 18, 3776-3782.
45. Yang, C. C., and Merrifield, R. B. (1976) Beta-phenacyl ester as a temporary protecting group to minimize cyclic imide formation during subsequent treatment of aspartyl peptides with HF, *Journal of Organic Chemistry* 41, 1032-1041.
46. Ramalingam, K., and Woodard, R. W. (1988) Synthesis of Stereospecific Deuterium-Labeled Homoserines and Homoserine Lactones, *Journal of Organic Chemistry* 53, 1900-1903.
47. Kumari, A., Pasini, P., and Daunert, S. (2008) Detection of bacterial quorum sensing *N*-acyl homoserine lactones in clinical samples, *Analytical and Bioanalytical Chemistry* 391, 1619-1627.
48. Ortori, C. A., Dubern, J.-F., Chhabra, S. R., Camara, M., Hardie, K., Williams, P., and Barrett, D. A. (2011) Simultaneous quantitative profiling of *N*-acyl-L-homoserine lactone and 2-alkyl-4(1H)-quinolone families of quorum-sensing signaling molecules using LC-MS/MS, *Analytical and Bioanalytical Chemistry* 399, 839-850.
49. Wang, F., Zhang, M., Hu, Y. H., Zhang, W. W., and Sun, L. (2009) Regulation of the *Edwardsiella tarda* Hemolysin Gene and LuxS by EthR, *Journal of Microbiology and Biotechnology* 19, 765-773.
50. Zhang, M., Jiao, X. D., Hu, Y. H., and Sun, L. (2009) Attenuation of *Edwardsiella tarda* Virulence by Small Peptides That Interfere with LuxS/Autoinducer Type 2 Quorum Sensing, *Applied and Environmental Microbiology* 75, 3882-3890.
51. Heermann, R., and Fuchs, T. M. (2008) Comparative analysis of the *Photobacterium luminescens* and the *Yersinia enterocolitica* genomes: uncovering candidate genes involved in insect pathogenicity, *Bmc Genomics* 9.
52. Sezonov, G., Joseleau-Petit, D., and D'ari, R. (2007) *Escherichia coli* physiology in Luria-Bertani broth, *Journal of Bacteriology* 189, 8746-8749.
53. Dalsgaard, I. (2001) Selection of media for antimicrobial susceptibility testing of fish pathogenic bacteria, *Aquaculture* 196, 267-275.
54. Lloyd, J. B., and Whelan, W. J. (1969) An Improved Method for Enzymatic Determination of Glucose in Presence of Maltose, *Analytical Biochemistry* 30, 467.
55. Weckwerth, W. (2003) Metabolomics in systems biology, *Annual Review of Plant Biology* 54, 669-689.
56. Bino, R. J., Hall, R. D., Fiehn, O., Kopka, J., Saito, K., Draper, J., Nikolau, B. J., Mendes, P., Roessner-Tunali, U., Beale, M. H., Trethewey, R. N., Lange, B. M., Wurtele, E. S., and Sumner, L. W. (2004) Potential of metabolomics as a functional genomics tool, *Trends in Plant Science* 9, 418-425.
57. Fiehn, O. (2001) Combining genomics, metabolome analysis, and biochemical modelling to understand metabolic networks, *Comparative and Functional Genomics* 2, 155-168.
58. Fiehn, O. (2002) Metabolomics - the link between genotypes and phenotypes, *Plant Molecular Biology* 48, 155-171.

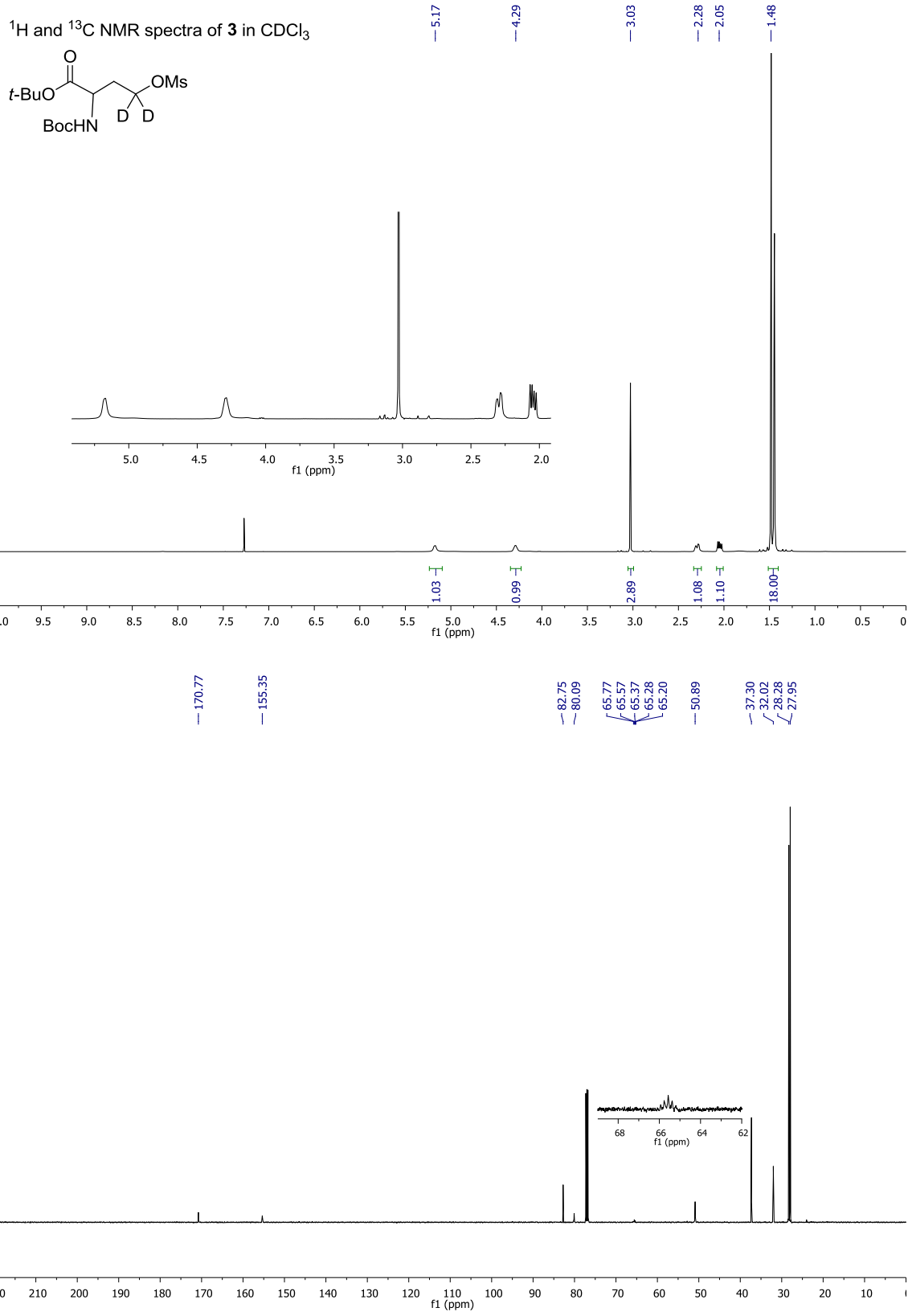
59. Mathis, D., Vence, L., and Benoist, C. (2001) Beta-cell death during progression to diabetes, *Nature* 414, 792-798.
60. Cuperlovic-Culf, M., Barnett, D. A., Culf, A. S., and Chute, I. (2010) Cell culture metabolomics: applications and future directions, *Drug Discovery Today* 15, 610-621.
61. Dettmer, K., Aronov, P. A., and Hammock, B. D. (2007) Mass spectrometry-based metabolomics, *Mass Spectrometry Reviews* 26, 51-78.
62. Hirai, M. Y., Yano, M., Goodenowe, D. B., Kanaya, S., Kimura, T., Awazuhara, M., Arita, M., Fujiwara, T., and Saito, K. (2004) Integration of transcriptomics and metabolomics for understanding of global responses to nutritional stresses in *Arabidopsis thaliana*, *Proceedings of the National Academy of Sciences of the United States of America* 101, 10205-10210.
63. Yuan, J., Bennett, B. D., and Rabinowitz, J. D. (2008) Kinetic flux profiling for quantitation of cellular metabolic fluxes, *Nature Protocols* 3, 1328-1340.
64. Dunn, W. B., and Ellis, D. I. (2005) Metabolomics: Current analytical platforms and methodologies, *Trac-Trends in Analytical Chemistry* 24, 285-294.
65. Viant, M. R., Rosenblum, E. S., and Tjeerdema, R. S. (2003) NMR-based metabolomics: A powerful approach for characterizing the effects of environmental stressors on organism health, *Environmental Science & Technology* 37, 4982-4989.
66. Dunn, W. B., Bailey, N. J. C., and Johnson, H. E. (2005) Measuring the metabolome: current analytical technologies, *Analyst* 130, 606-625.
67. Want, E. J., Nordstrom, A., Morita, H., and Siuzdak, G. (2007) From exogenous to endogenous: The inevitable imprint of mass spectrometry in metabolomics, *Journal of Proteome Research* 6, 459-468.
68. Wilson, I. D., Plumb, R., Granger, J., Major, H., Williams, R., and Lenz, E. A. (2005) HPLC-MS-based methods for the study of metabolomics, *Journal of Chromatography B-Analytical Technologies in the Biomedical and Life Sciences* 817, 67-76.
69. Kell, D. B. (2004) Metabolomics and systems biology: making sense of the soup, *Current Opinion in Microbiology* 7, 296-307.
70. Katajamaa, M., and Oresic, M. (2005) Processing methods for differential analysis of LC/MS profile data, *Bmc Bioinformatics* 6.
71. Wishart, D. S., Tzur, D., Knox, C., Eisner, R., Guo, A. C., Young, N., Cheng, D., Jewell, K., Arndt, D., Sawhney, S., Fung, C., Nikolai, L., Lewis, M., Coutouly, M. A., Forsythe, I., Tang, P., Shrivastava, S., Jeroncic, K., Stothard, P., Amegbey, G., Block, D., Hau, D. D., Wagner, J., Miniaci, J., Clements, M., Gebremedhin, M., Guo, N., Zhang, Y., Duggan, G. E., Macinnis, G. D., Weljie, A. M., Dowlatabadi, R., Bamforth, F., Clive, D., Greiner, R., Li, L., Marrie, T., Sykes, B. D., Vogel, H. J., and Querengesser, L. (2007) HMDB: the human metabolome database, *Nucleic Acids Research* 35, D521-D526.
72. Schauer, N., Steinhauser, D., Strelkov, S., Schomburg, D., Allison, G., Moritz, T., Lundgren, K., Roessner-Tunali, U., Forbes, M. G., Willmitzer, L., Fernie, A. R., and Kopka, J. (2005) GC-MS libraries for the rapid identification of metabolites in complex biological samples, *Febs Letters* 579, 1332-1337.

73. Corbett, J. A., and Mcdaniel, M. L. (1992) Does Nitric Oxide Mediate Autoimmune Destruction of Beta-Cells - Possible Therapeutic Interventions in IDDM, *Diabetes* 41, 897-903.
74. Mandruppoulsen, T., Spinass, G. A., Prowse, S. J., Hansen, B. S., Jorgensen, D. W., Bendtzen, K., Nielsen, J. H., and Nerup, J. (1987) Islet cytotoxicity of interleukin-1 - Influence of culture conditions and islet donor characteristics, *Diabetes* 36, 641-647.
75. Grunnet, L. G., Aikin, R., Tonnesen, M. F., Paraskevas, S., Blaabjerg, L., Storling, J., Rosenberg, L., Billestrup, N., Maysinger, D., and Mandrup-Poulsen, T. (2009) Proinflammatory Cytokines Activate the Intrinsic Apoptotic Pathway in beta-Cells, *Diabetes* 58, 1807-1815.
76. Gurzov, E. N., Germano, C. M., Cunha, D. A., Ortis, F., Vanderwinden, J.-M., Marchetti, P., Zhang, L., and Eizirik, D. L. (2010) p53 Up-regulated Modulator of Apoptosis (PUMA) Activation Contributes to Pancreatic beta-Cell Apoptosis Induced by Proinflammatory Cytokines and Endoplasmic Reticulum Stress, *Journal of Biological Chemistry* 285, 19910-19920.
77. Collier, J. J., Fueger, P. T., Hohmeier, H. E., and Newgard, C. B. (2006) Pro- and antiapoptotic proteins regulate apoptosis but do not protect against cytokine-mediated cytotoxicity in rat islets and beta-cell lines, *Diabetes* 55, 1398-1406.
78. Fehsel, K., Kolb-Bachofen, V., and Kroncke, K. D. (2003) Necrosis is the predominant type of islet cell death during development of insulin-dependent diabetes mellitus in BB rats, *Laboratory Investigation* 83, 549-559.
79. Saldeen, J. (2000) Cytokines induce both necrosis and apoptosis via a common bcl-2-inhibitable pathway in rat insulin-producing cells, *Endocrinology* 141, 2003-2010.
80. Kerr, J. F. R., Wyllie, A. H., and Currie, A. R. (1972) Apoptosis - Basic Biological Phenomenon with Wide-Ranging Implications in Tissue Kinetics, *British Journal of Cancer* 26, 239.
81. Taylor, R. C., Cullen, S. P., and Martin, S. J. (2008) Apoptosis: controlled demolition at the cellular level, *Nature Reviews Molecular Cell Biology* 9, 231-241.
82. Reddy, S., Bradley, J., and Ross, J. M. (2003) Immunolocalization of caspase-3 in pancreatic islets of NOD mice during cyclophosphamide-accelerated diabetes, In *Immunology of Diabetes II: Pathogenesis from Mouse to Man* (Sanjeevi, C. B., and Eisenbarth, G. S., Eds.), pp 192-195.
83. Chen, G. X., Hohmeier, H. E., Gasa, R., Tran, V. V., and Newgard, C. B. (2000) Selection of insulinoma cell lines with resistance to interleukin-1 beta- and gamma-interferon-induced cytotoxicity, *Diabetes* 49, 562-570.
84. Zech, B., Kohl, R., Von Knethen, A., and Brune, B. (2003) Nitric oxide donors inhibit formation of the Apaf-1/caspase-9 apoptosome and activation of caspases, *Biochemical Journal* 371, 1055-1064.
85. Nicotera, P., and Merlino, G. (2004) Regulation of the apoptosis-necrosis switch, *Oncogene* 23, 2757-2765.
86. Li, L., El-Kholy, W., Rhodes, C. J., and Brubaker, P. L. (2005) Glucagon-like peptide-1 protects beta cells from cytokine-induced apoptosis and necrosis: role of protein kinase B, *Diabetologia* 48, 1339-1349.

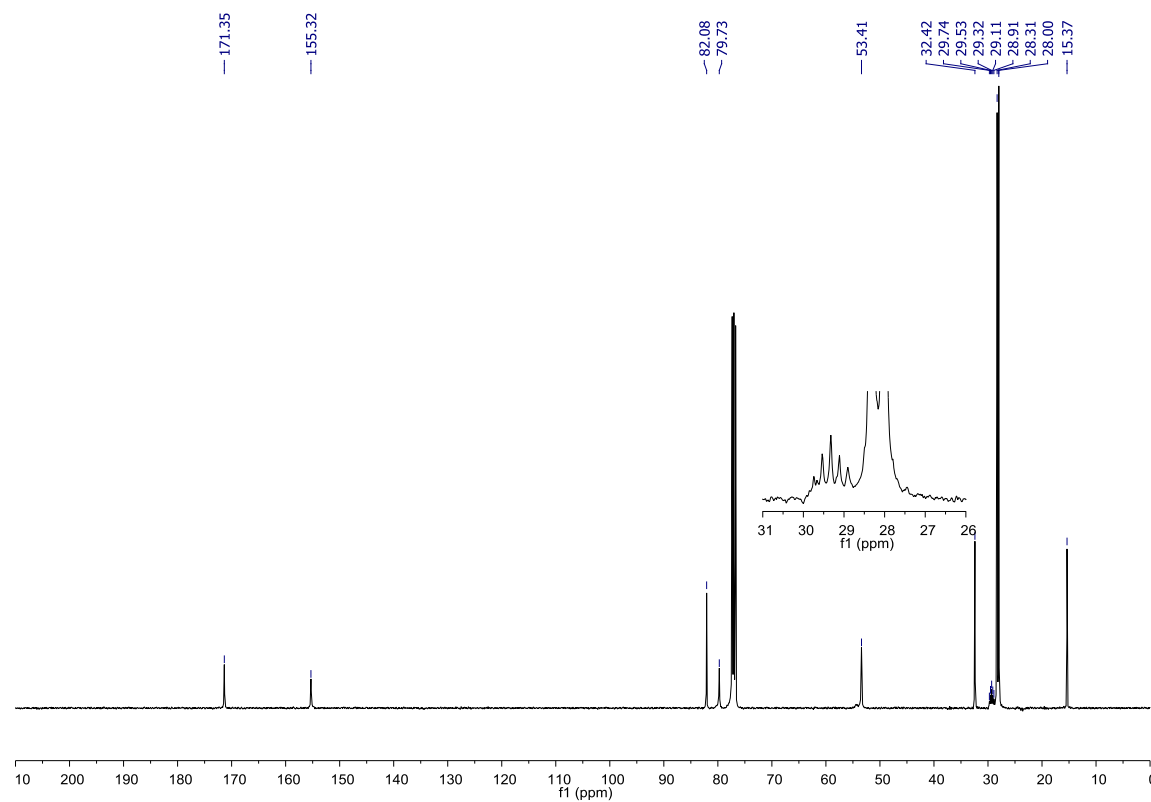
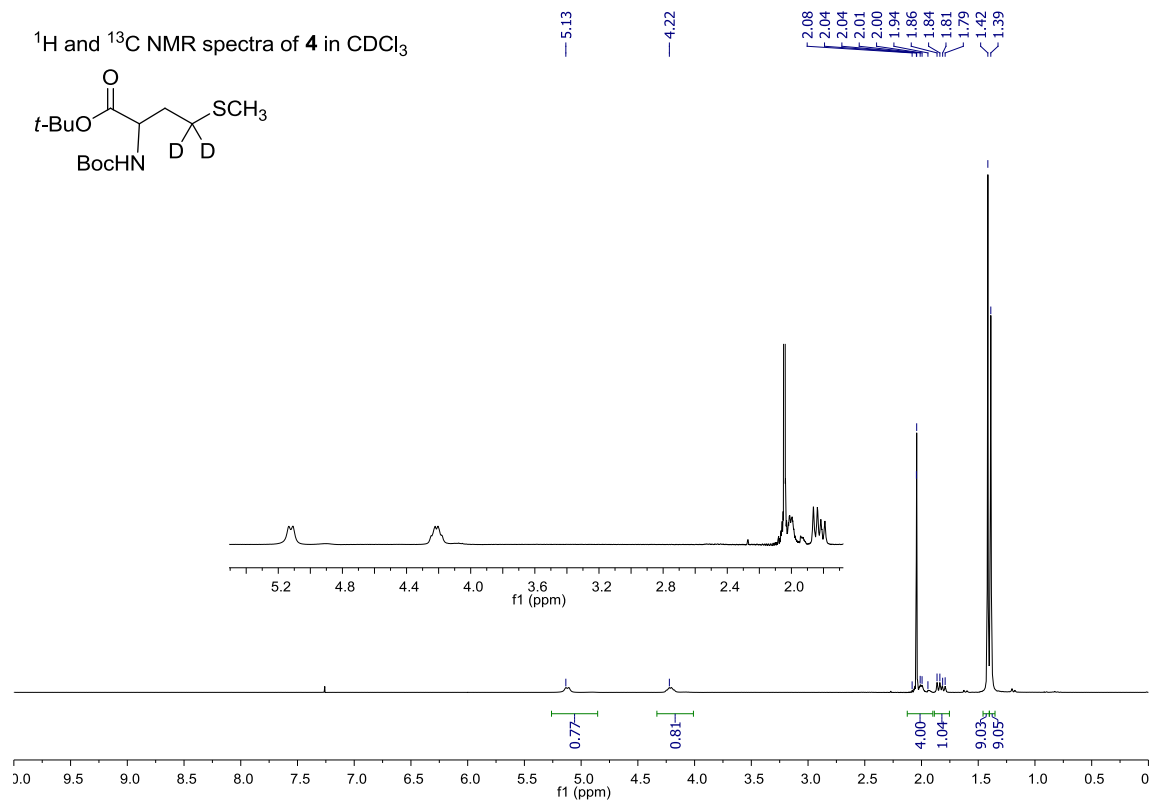
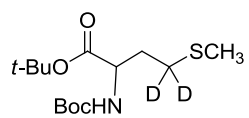
87. Rakatzi, I., Mueller, H., Ritzeler, O., Tennagels, N., and Eckel, J. (2004) Adiponectin counteracts cytokine- and fatty acid-induced apoptosis in the pancreatic beta-cell line INS-1, *Diabetologia* 47, 249-258.
88. Heitmeier, M. R., Scarim, A. L., and Corbett, J. A. (1999) Prolonged STAT1 activation is associated with interferon-gamma priming for interleukin-1-induced inducible nitric-oxide synthase expression by islets of Langerhans, *Journal of Biological Chemistry* 274, 29266-29273.
89. Waters, C. A., Lu, W., Rabinowitz, J. D., and Bassler, B. L. (2008) Quorum sensing controls biofilm formation in *Vibrio cholerae* through modulation of cyclic Di-GMP levels and repression of vpsT, *Journal of Bacteriology* 190, 2527-2536.
90. Lu, W., Bennett, B. D., and Rabinowitz, J. D. (2008) Analytical strategies for LC-MS-based targeted metabolomics, *Journal of Chromatography B-Analytical Technologies in the Biomedical and Life Sciences* 871, 236-242.
91. Bajad, S. U., Lu, W., Kimball, E. H., Yuan, J., Peterson, C., and Rabinowitz, J. D. (2006) Separation and quantitation of water soluble cellular metabolites by hydrophilic interaction chromatography-tandem mass spectrometry, *Journal of Chromatography A* 1125, 76-88.
92. Saldanha, A. J. (2004) Java Treeview-extensible visualization of microarray data, *Bioinformatics* 20, 3246-3248.

Appendix

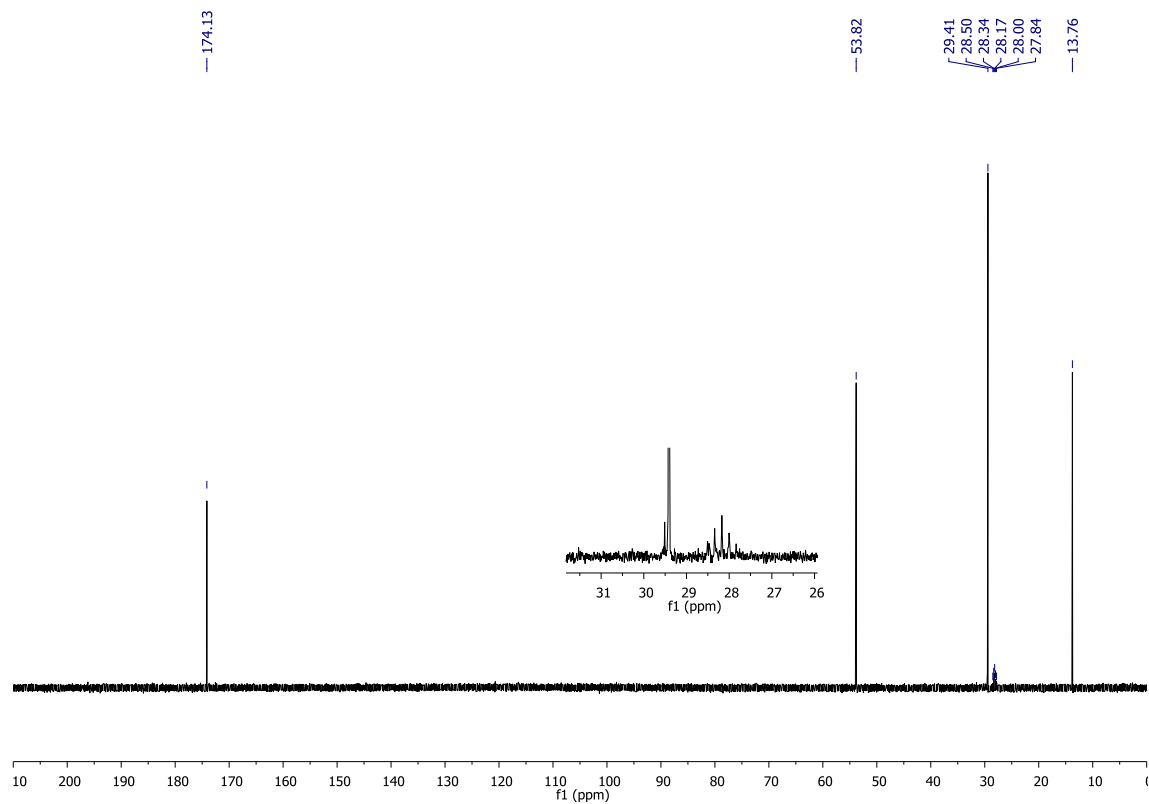
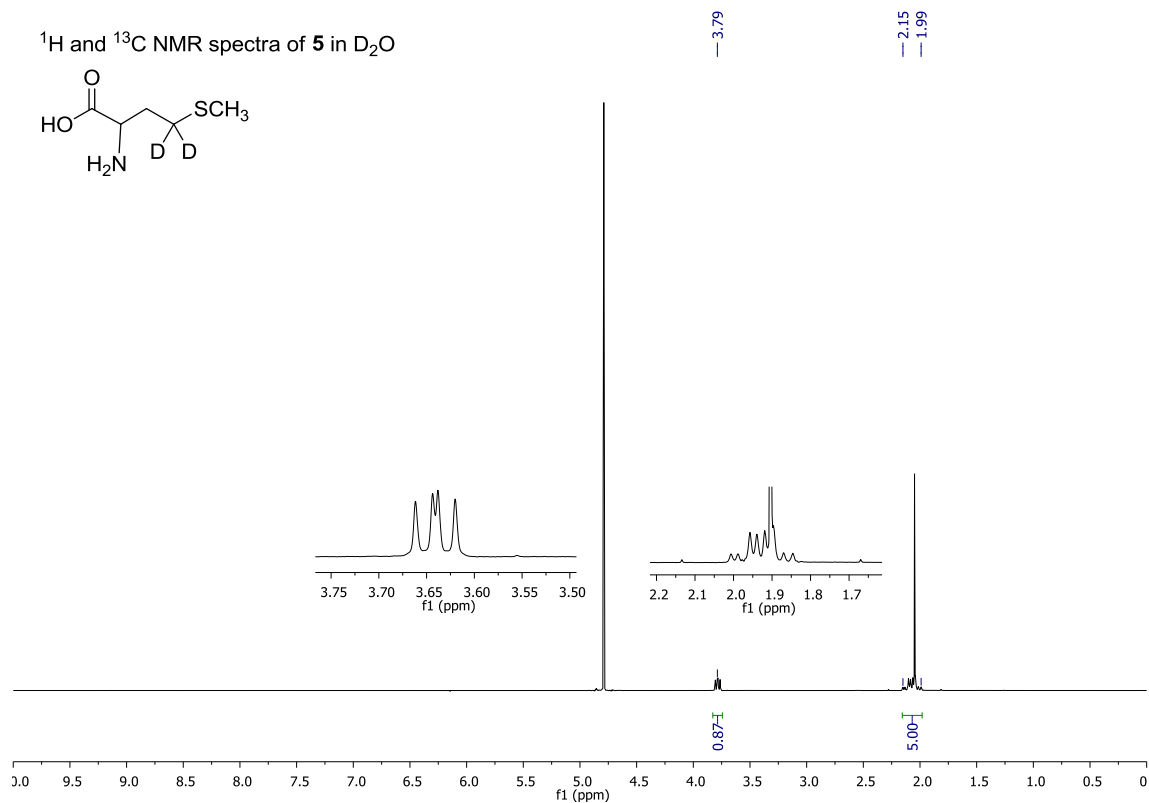
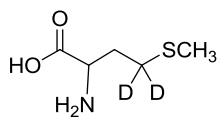


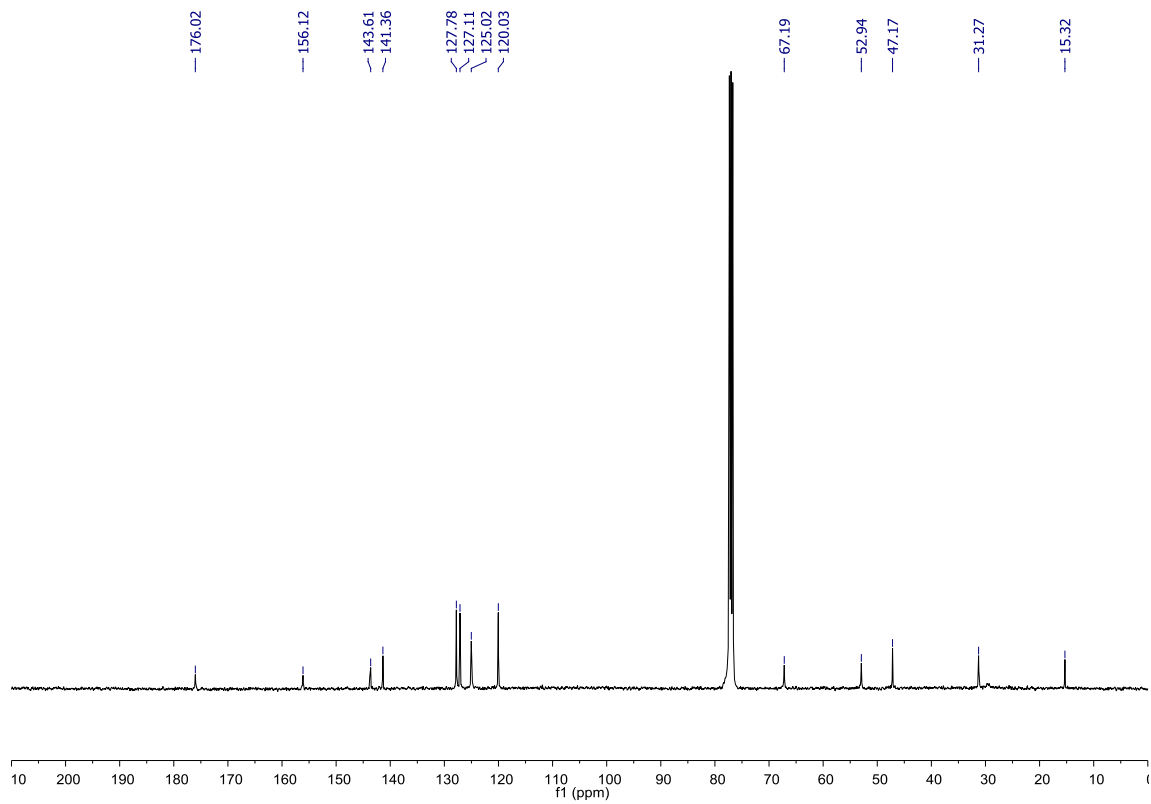
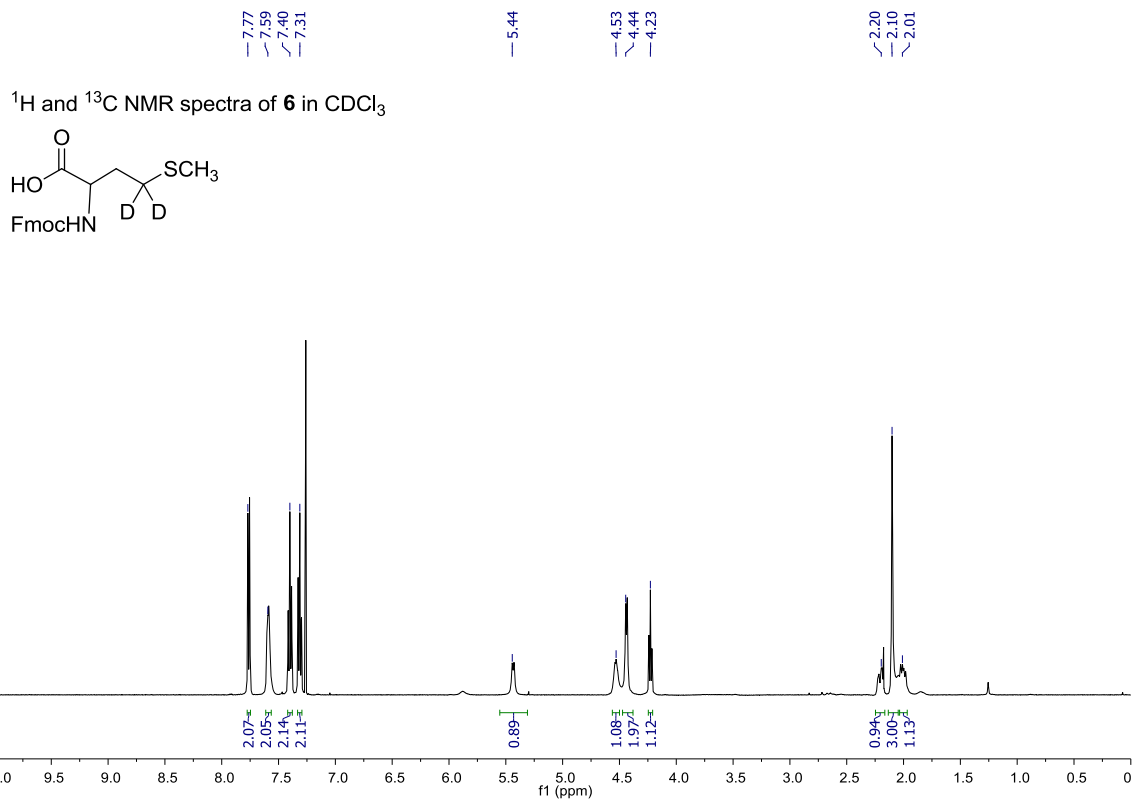


^1H and ^{13}C NMR spectra of **4** in CDCl_3

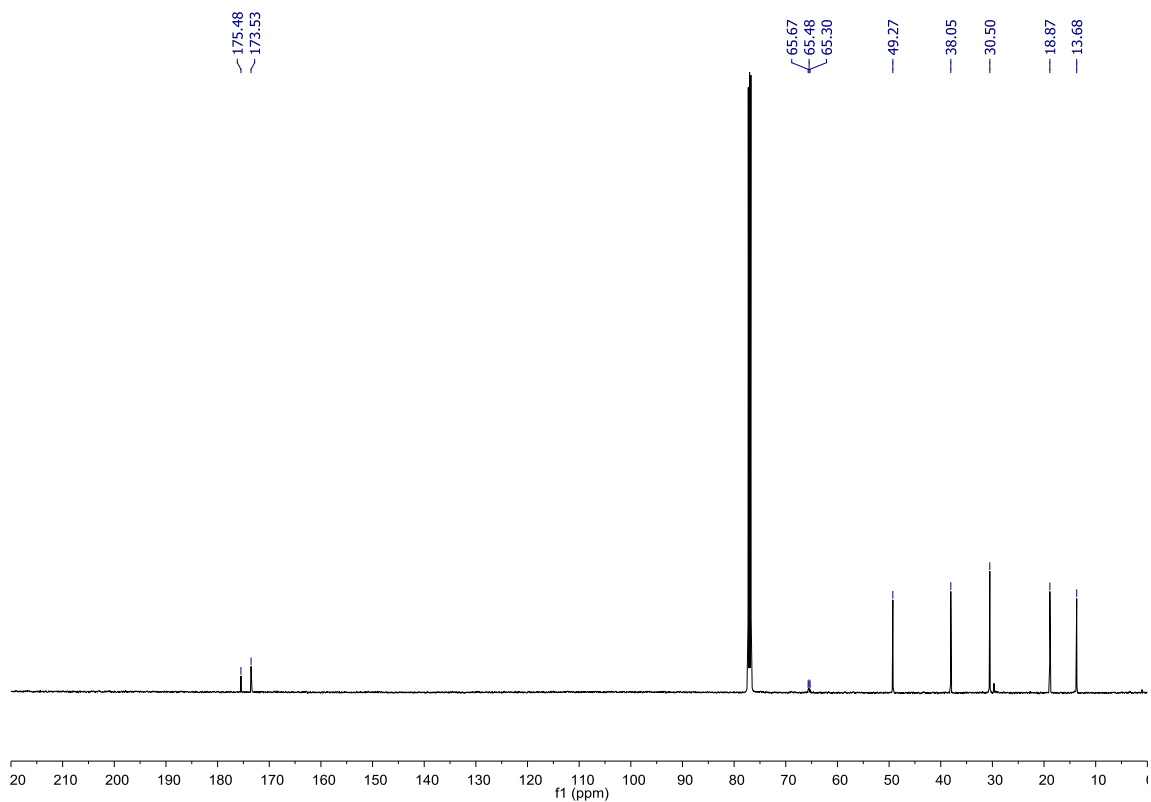
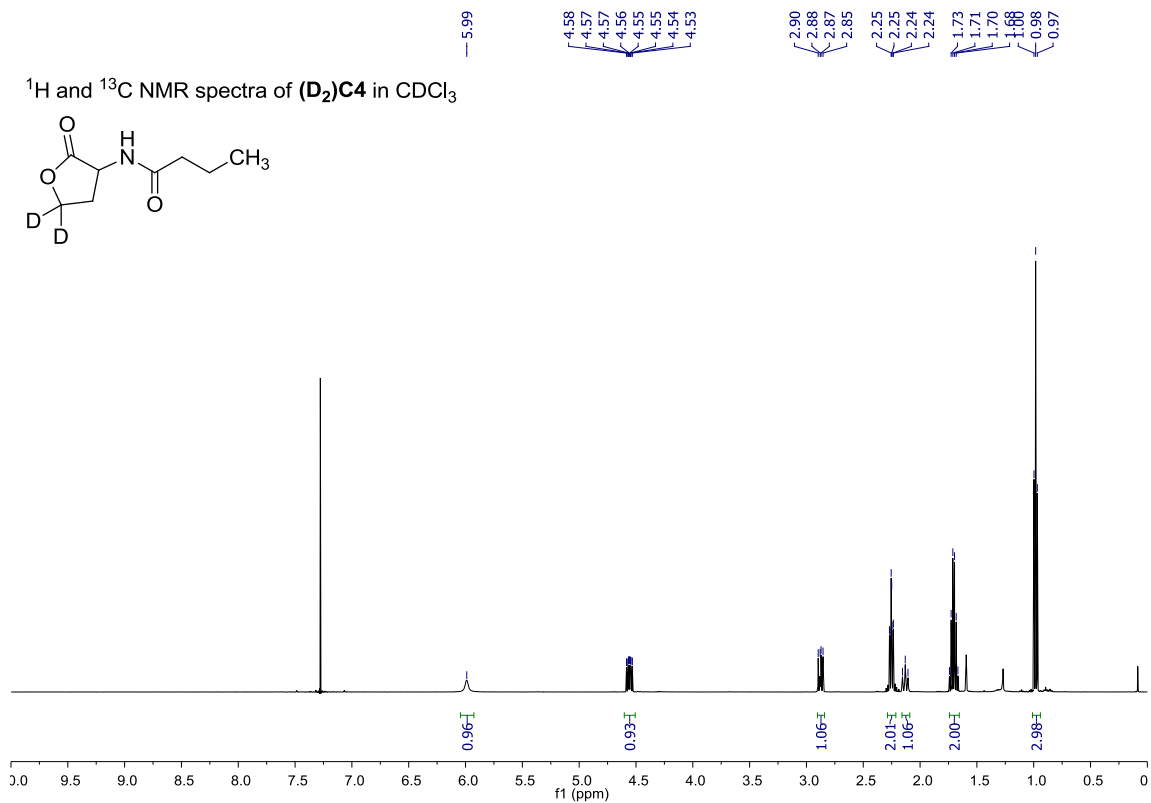
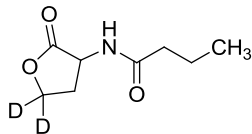


^1H and ^{13}C NMR spectra of **5** in D_2O

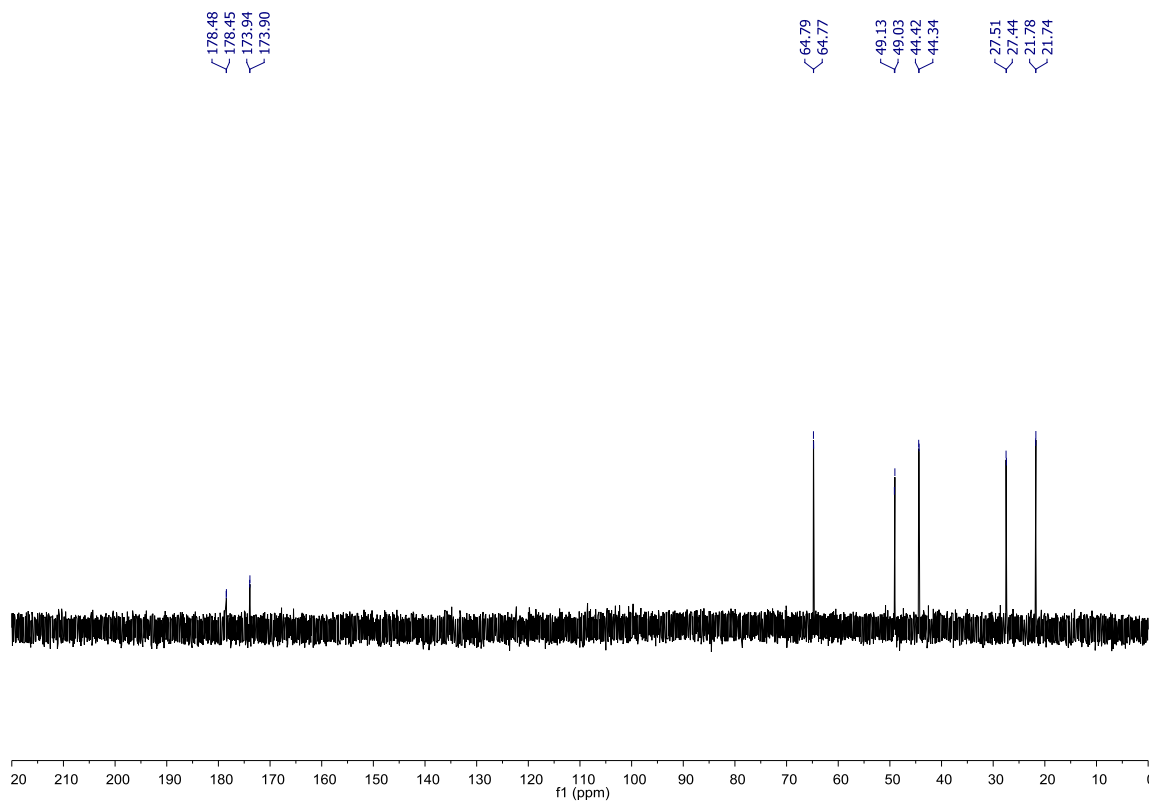
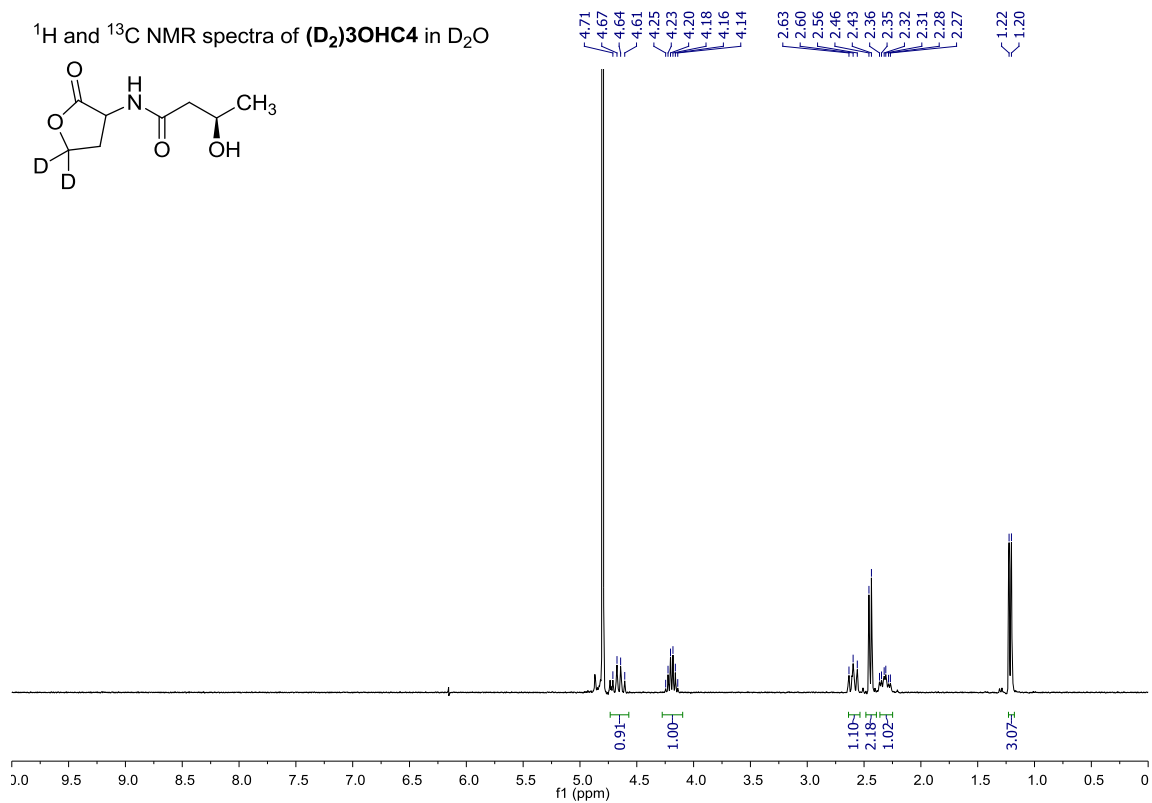
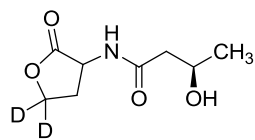




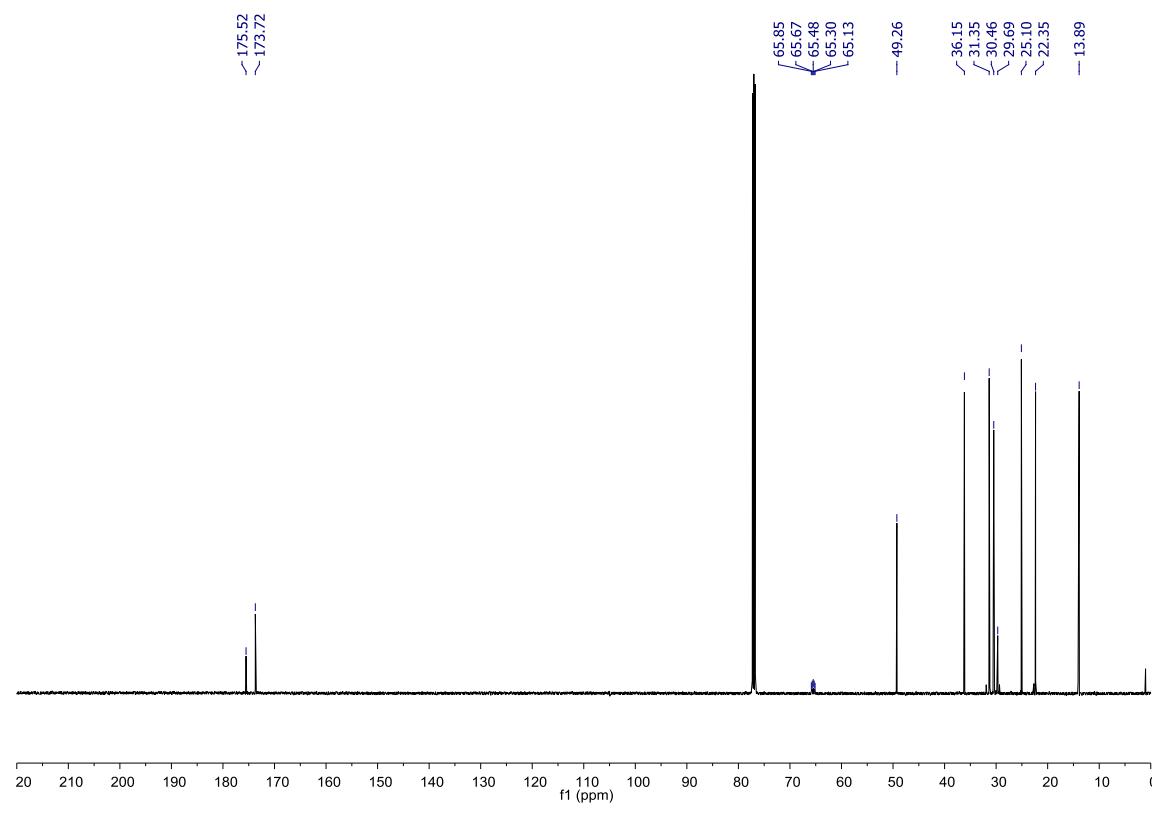
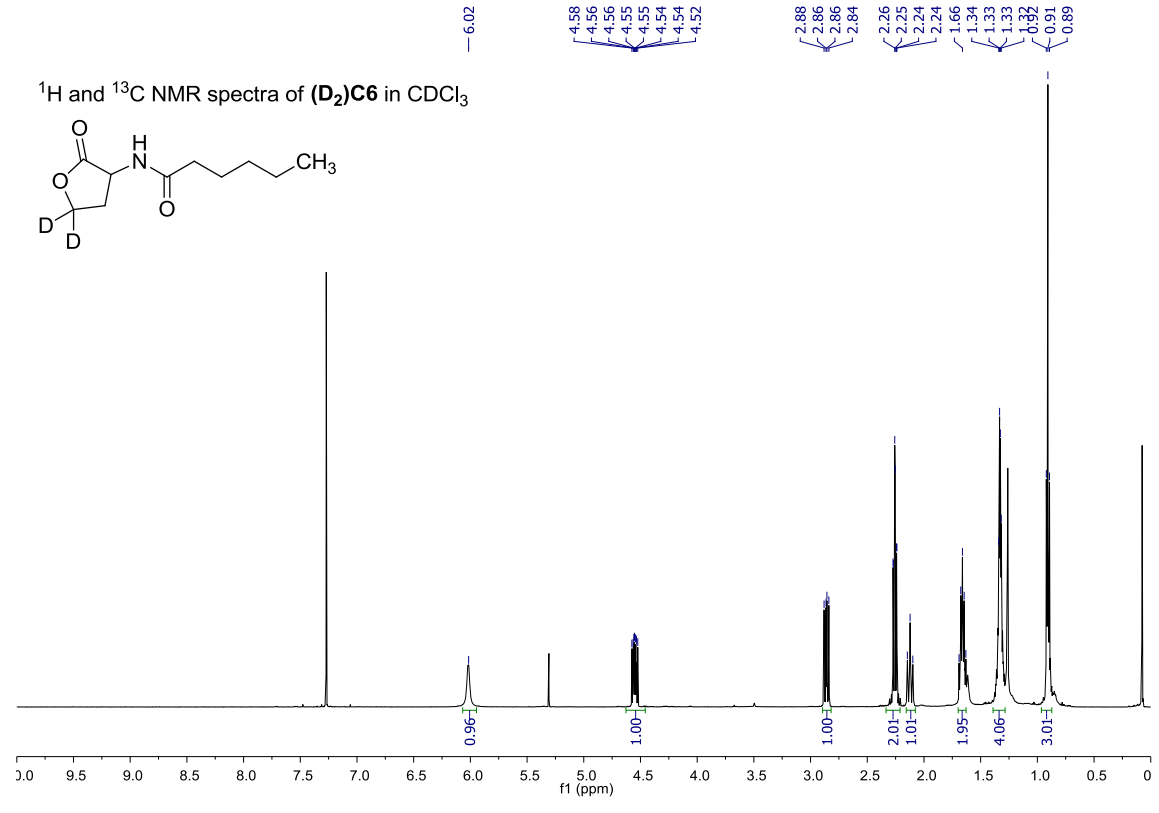
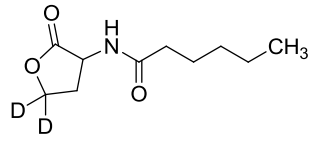
^1H and ^{13}C NMR spectra of $(\text{D}_2)\text{C4}$ in CDCl_3



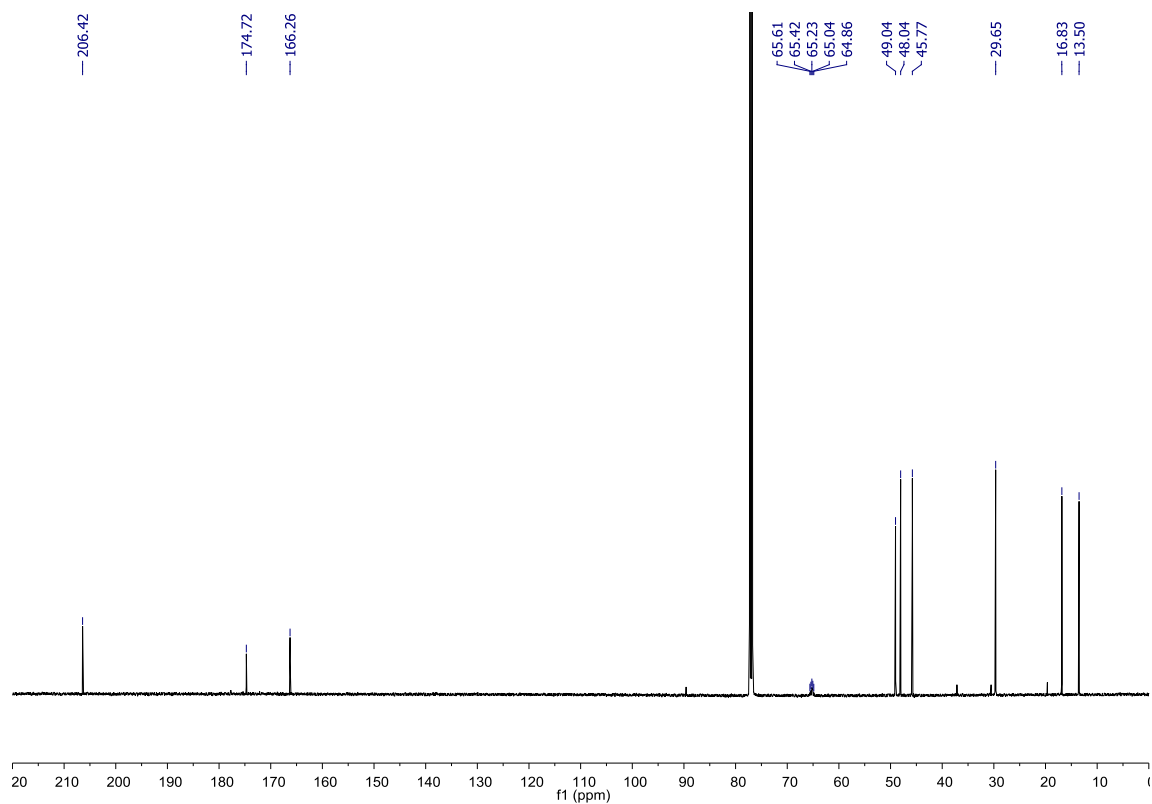
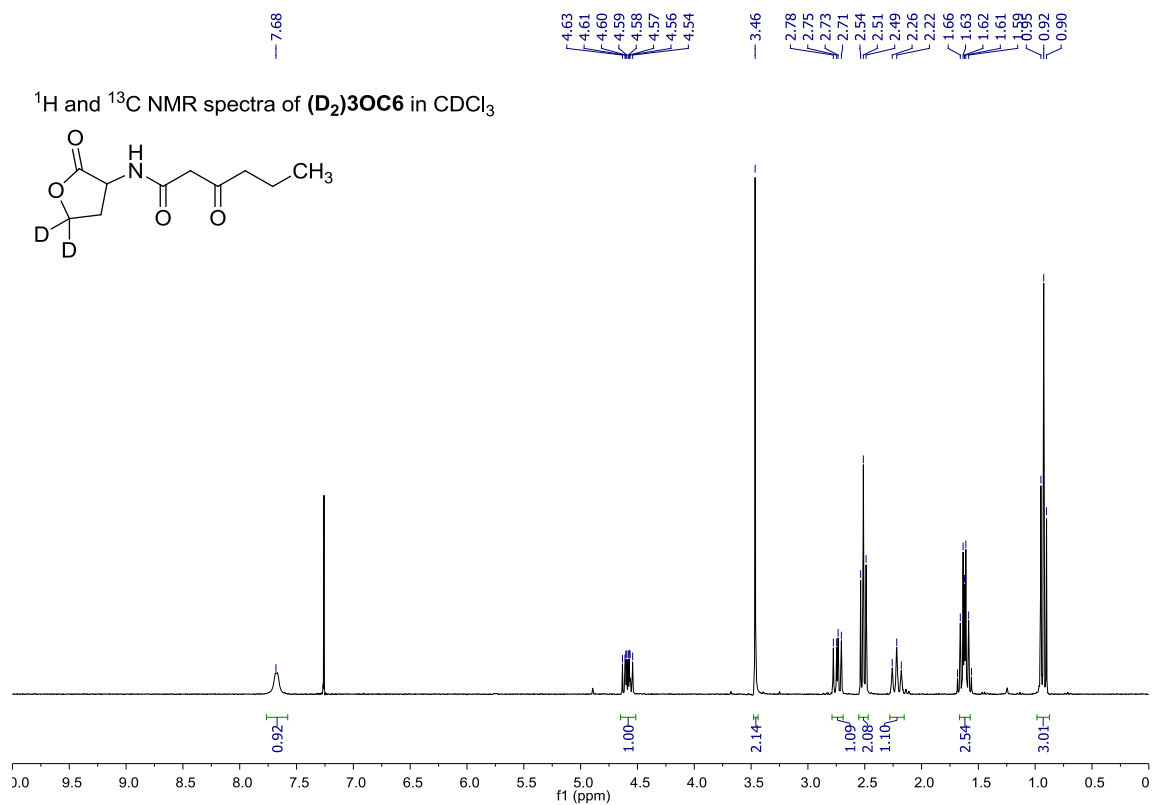
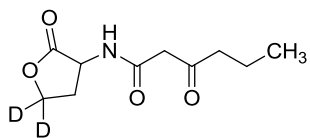
^1H and ^{13}C NMR spectra of (D_2)3OHC4 in D_2O



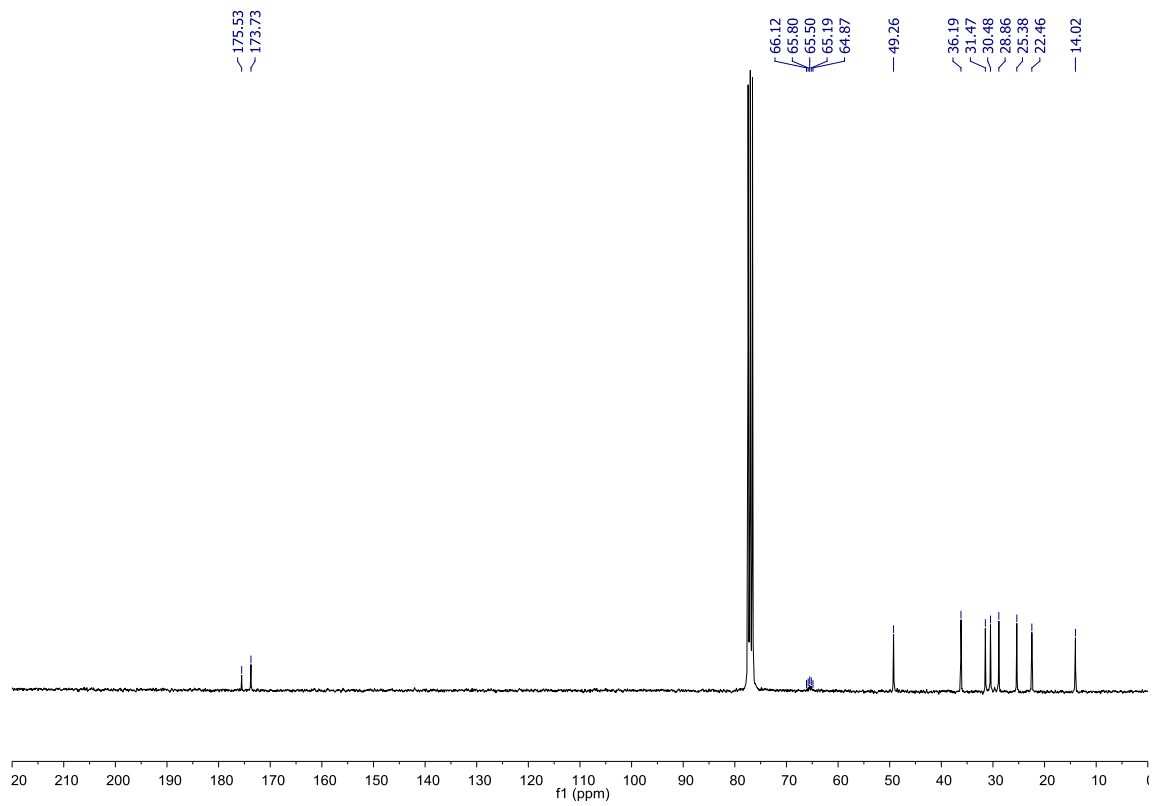
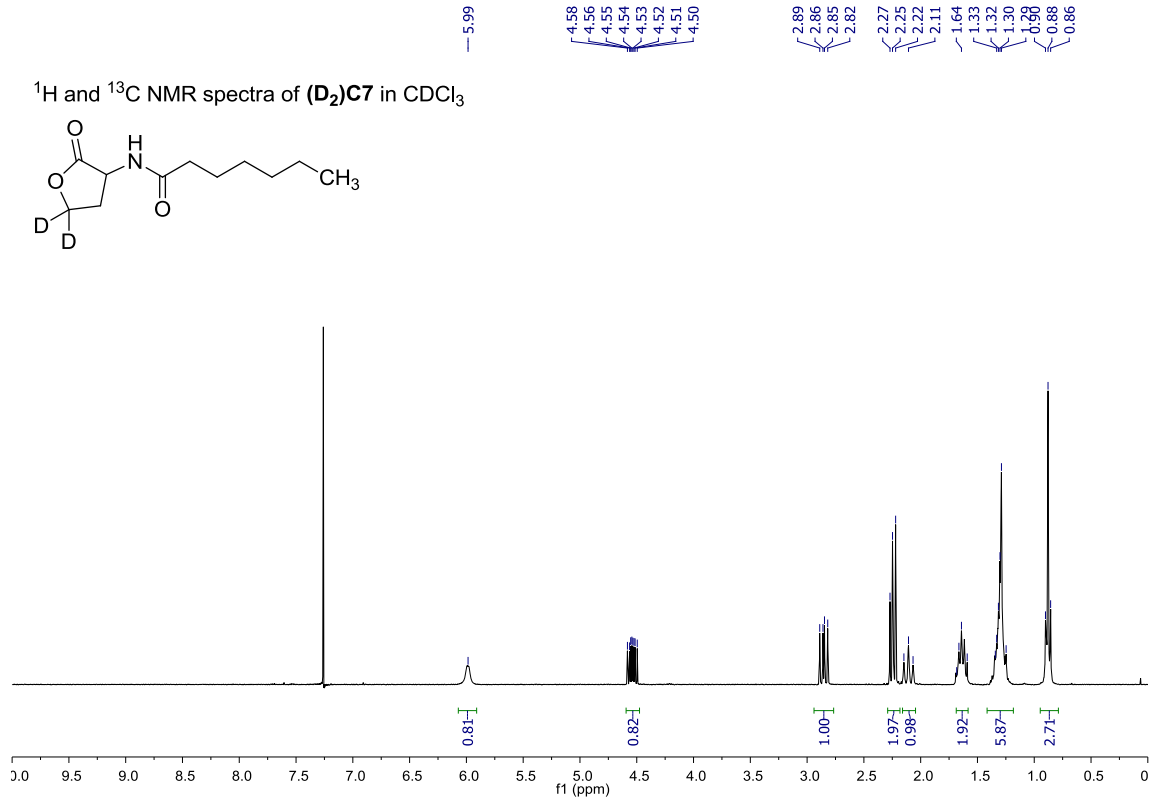
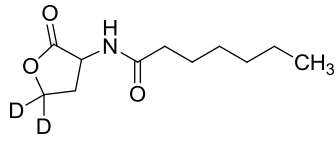
^1H and ^{13}C NMR spectra of (D_2)**C6** in CDCl_3



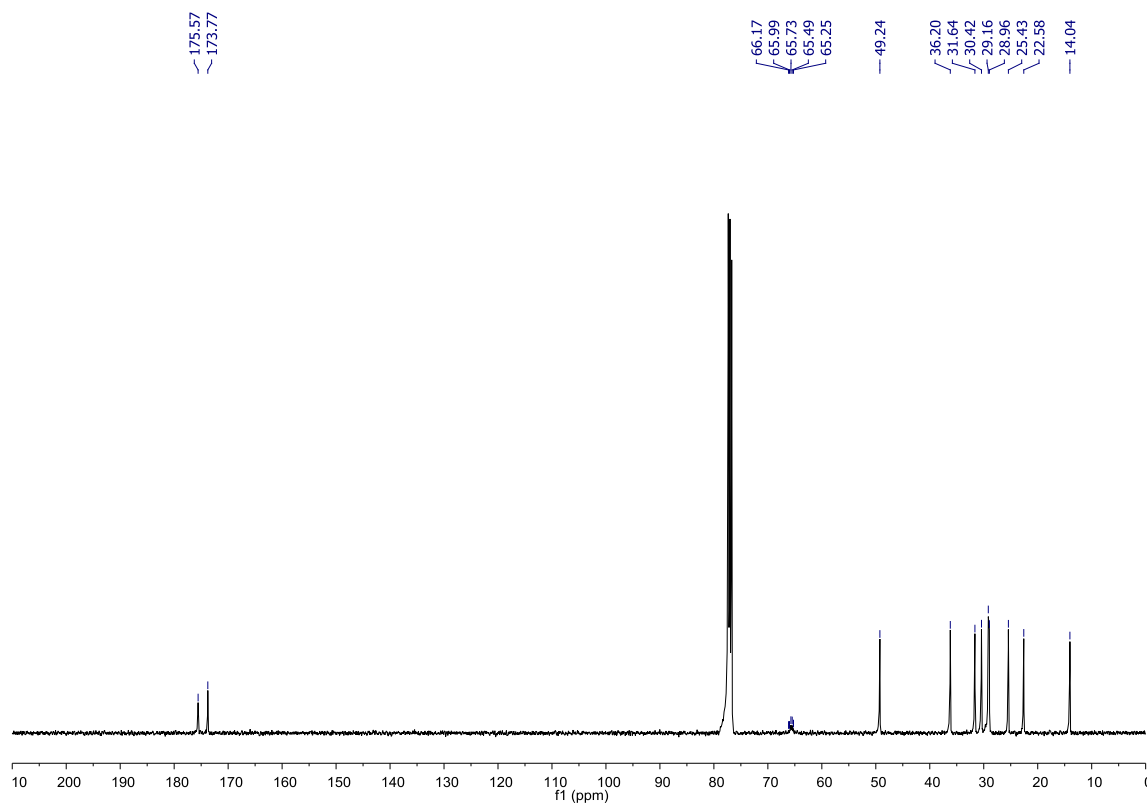
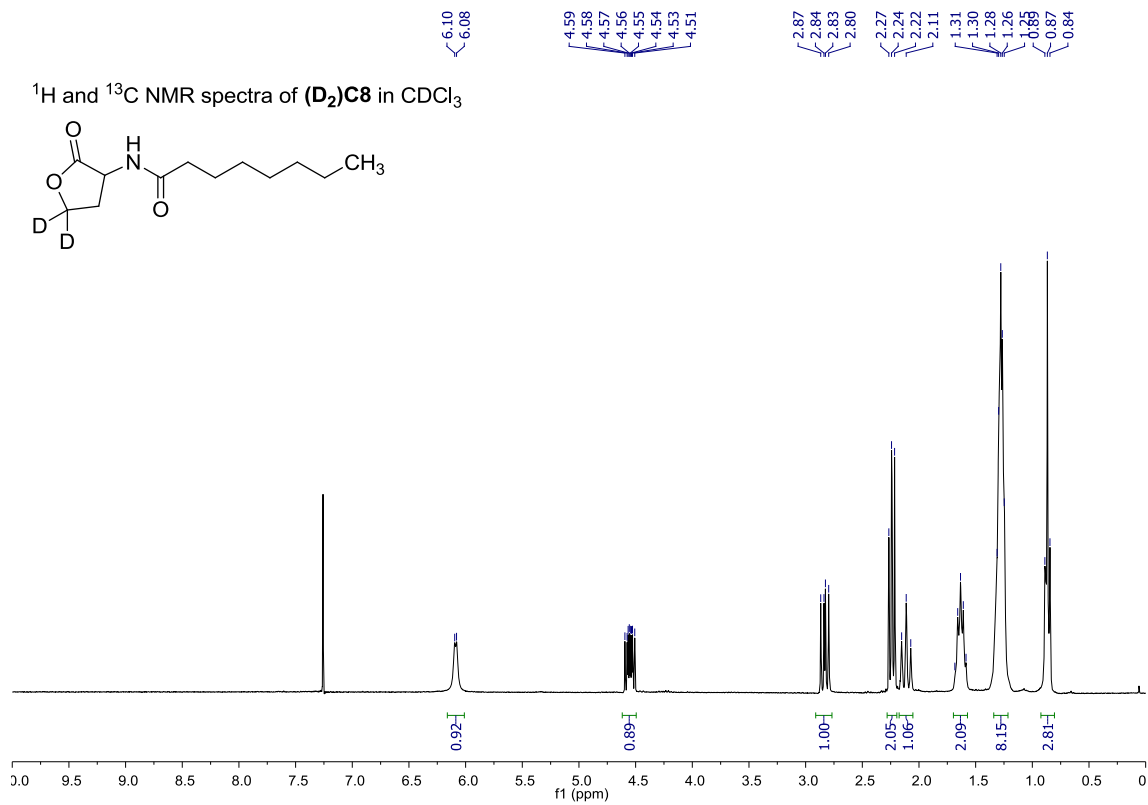
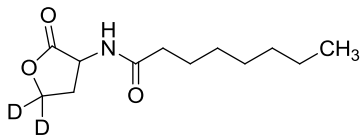
^1H and ^{13}C NMR spectra of $(\text{D}_2)\text{3OC6}$ in CDCl_3

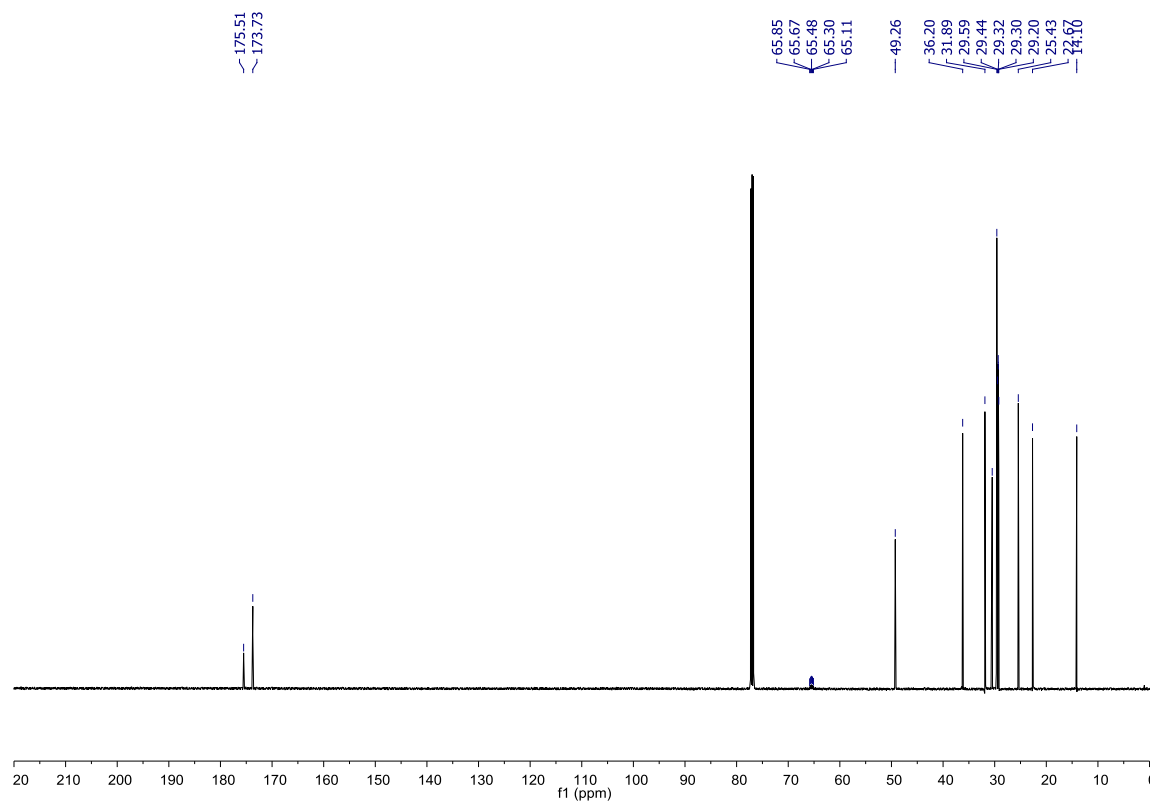
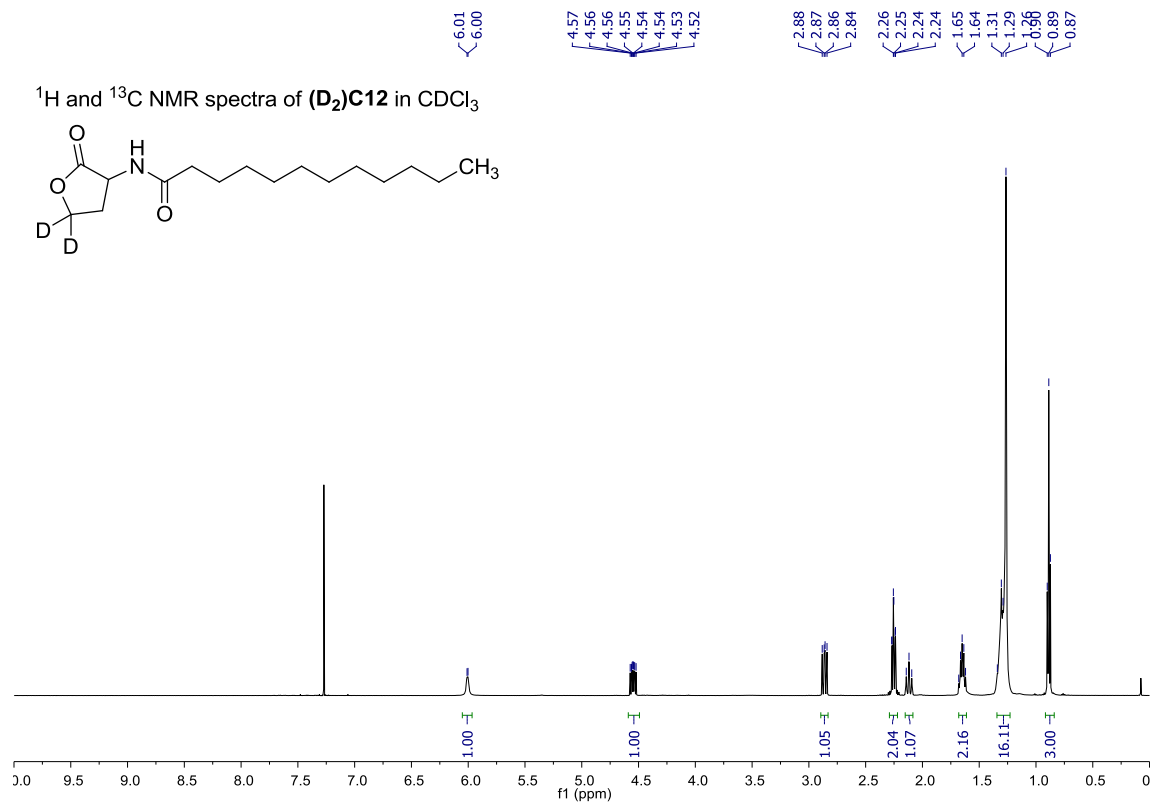


^1H and ^{13}C NMR spectra of (D_2)C7 in CDCl_3



^1H and ^{13}C NMR spectra of (D_2)**C8** in CDCl_3





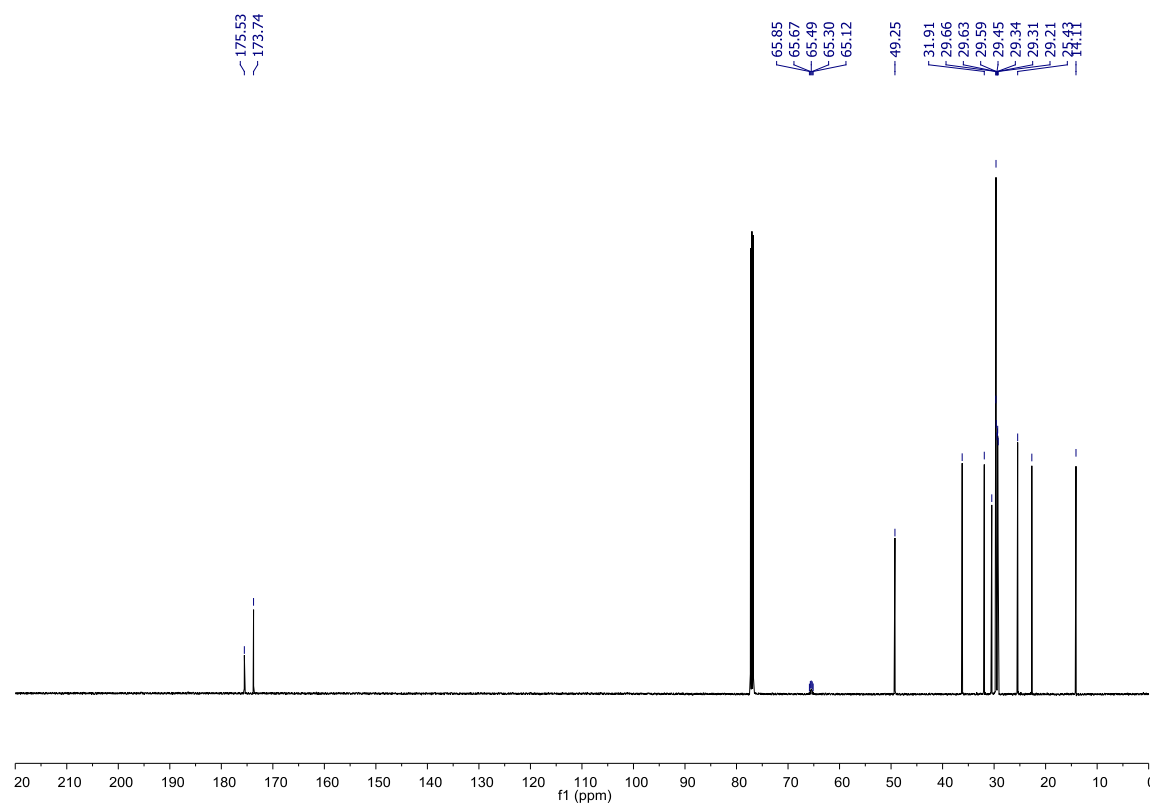
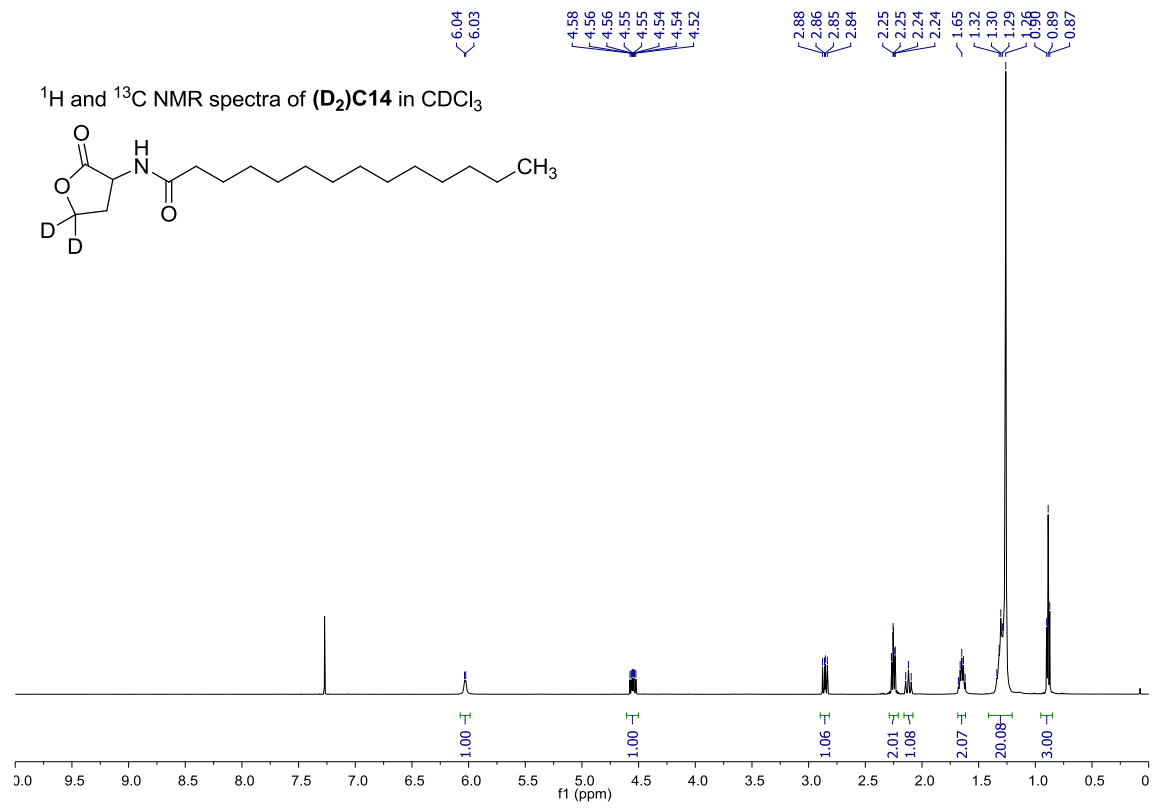


Table 3: *V. fischeri* strain ES114 [AHLs] Used in Figure 6A and 7B

Time (h)	C6		3OC6		C7 AHL		C8	
	[AHL] Average (μM)	Range	[AHL] Average (μM)	Range	[AHL] Average (μM)	Range	[AHL] Average (μM)	Range
0	0.000	± 0.000	0.000	± 0.000	0.000	± 0.000	0.007	± 0.001
1	0.000	± 0.000	0.000	± 0.000	0.000	± 0.000	0.016	± 0.001
2	0.000	± 0.000	0.000	± 0.000	0.000	± 0.000	0.082	± 0.063
3	0.000	± 0.000	0.000	± 0.000	0.000	± 0.000	0.023	± 0.003
4	0.000	± 0.000	0.000	± 0.000	0.000	± 0.000	0.049	± 0.002
5	0.000	± 0.000	0.000	± 0.000	0.000	± 0.000	0.116	± 0.006
6	0.011	± 0.003	0.000	± 0.000	0.000	± 0.000	0.251	± 0.010
7	0.021	± 0.003	0.000	± 0.000	0.000	± 0.000	0.487	± 0.021
8	0.040	± 0.009	0.000	± 0.000	0.000	± 0.000	0.744	± 0.039
9	0.073	± 0.010	0.000	± 0.000	0.002	± 0.002	1.175	± 0.038
10	0.089	± 0.002	0.000	± 0.000	0.000	± 0.000	1.579	± 0.068
11	0.123	± 0.016	0.000	± 0.000	0.000	± 0.000	1.924	± 0.191
12	0.147	± 0.006	0.000	± 0.000	0.004	± 0.004	2.134	± 0.019
13	0.159	± 0.001	0.000	± 0.000	0.002	± 0.002	2.341	± 0.178
14	0.138	± 0.004	0.000	± 0.000	0.024	± 0.024	2.475	± 0.211
15	0.132	± 0.011	0.000	± 0.000	0.098	± 0.004	2.394	± 0.002
16	0.123	± 0.001	0.000	± 0.000	0.113	± 0.019	2.264	± 0.081
17	0.094	± 0.002	0.000	± 0.000	0.118	± 0.013	1.729	± 0.151
18	0.136	± 0.010	0.000	± 0.000	0.102	± 0.025	1.764	± 0.057
19	0.104	± 0.005	0.000	± 0.000	0.082	± 0.000	1.526	± 0.120
20	0.104	± 0.000	0.000	± 0.000	0.065	± 0.002	1.382	± 0.086
21	0.081	± 0.012	0.000	± 0.000	0.046	± 0.001	1.166	± 0.091
22	0.058	± 0.002	0.000	± 0.000	0.046	± 0.001	1.003	± 0.120
23	0.060	± 0.002	0.000	± 0.000	0.040	± 0.008	0.978	± 0.096
24	0.052	± 0.004	0.000	± 0.000	0.009	± 0.009	0.640	± 0.019

Table 4: *V. fischeri* strain MJ-1 [AHLs] Used in Figure 6B and 7A

Time (h)	C6		3OC6		C7 AHL		C8	
	[AHL] Average (μM)	Range	[AHL] Average (μM)	Range	[AHL] Average (μM)	Range	[AHL] Average (μM)	Range
0	0.000	± 0.000	0.005	± 0.005	0.000	± 0.000	0.000	± 0.000
1	0.000	± 0.000	0.012	± 0.002	0.000	± 0.000	0.000	± 0.000
2	0.000	± 0.000	0.022	± 0.005	0.000	± 0.000	0.000	± 0.000
3	0.000	± 0.000	0.015	± 0.003	0.000	± 0.000	0.001	± 0.001
4	0.000	± 0.000	0.018	± 0.009	0.000	± 0.000	0.004	± 0.000
5	0.000	± 0.000	0.029	± 0.002	0.000	± 0.000	0.017	± 0.004
6	0.000	± 0.000	0.067	± 0.006	0.000	± 0.000	0.041	± 0.004
7	0.000	± 0.000	0.091	± 0.011	0.000	± 0.000	0.073	± 0.010
8	0.011	± 0.003	0.125	± 0.046	0.000	± 0.000	0.121	± 0.003
9	0.015	± 0.007	0.158	± 0.035	0.000	± 0.000	0.139	± 0.006
10	0.026	± 0.003	0.253	± 0.058	0.000	± 0.000	0.193	± 0.031
11	0.037	± 0.001	0.184	± 0.063	0.000	± 0.000	0.186	± 0.000
12	0.028	± 0.004	0.287	± 0.041	0.000	± 0.000	0.199	± 0.008
13	0.047	± 0.007	0.209	± 0.014	0.000	± 0.000	0.213	± 0.002
14	0.027	± 0.002	0.223	± 0.013	0.000	± 0.000	0.250	± 0.010
15	0.038	± 0.010	0.150	± 0.028	0.000	± 0.000	0.230	± 0.017
16	0.026	± 0.003	0.160	± 0.027	0.021	± 0.000	0.209	± 0.011
17	0.024	± 0.002	0.115	± 0.024	0.034	± 0.005	0.161	± 0.010
18	0.032	± 0.001	0.095	± 0.008	0.034	± 0.003	0.147	± 0.020
19	0.019	± 0.001	0.073	± 0.013	0.026	± 0.001	0.159	± 0.007
20	0.022	± 0.010	0.044	± 0.010	0.022	± 0.005	0.118	± 0.014
21	0.019	± 0.001	0.040	± 0.005	0.015	± 0.002	0.098	± 0.003
22	0.016	± 0.005	0.028	± 0.003	0.026	± 0.004	0.071	± 0.006
23	0.004	± 0.004	0.013	± 0.000	0.005	± 0.005	0.073	± 0.012
24	0.000	± 0.000	0.009	± 0.009	0.000	± 0.000	0.058	± 0.009

Table 5: *V. fischeri* strain CL21 [AHLs] Used in Figure 6C

Time (h)	C6		3OC6		C7 AHL		C8	
	[AHL] Average (μM)	Range	[AHL] Average (μM)	Range	[AHL] Average (μM)	Range	[AHL] Average (μM)	Range
0	0.000	± 0.000	0.000	± 0.000	0.000	± 0.000	0.000	± 0.000
1	0.000	± 0.000	0.000	± 0.000	0.000	± 0.000	0.000	± 0.000
2	0.000	± 0.000	0.000	± 0.000	0.000	± 0.000	0.000	± 0.000
3	0.000	± 0.000	0.000	± 0.000	0.000	± 0.000	0.000	± 0.000
4	0.000	± 0.000	0.000	± 0.000	0.000	± 0.000	0.000	± 0.000
5	0.000	± 0.000	0.000	± 0.000	0.000	± 0.000	0.000	± 0.000
6	0.000	± 0.000	0.000	± 0.000	0.000	± 0.000	0.000	± 0.000
7	0.000	± 0.000	0.000	± 0.000	0.000	± 0.000	0.000	± 0.000
8	0.000	± 0.000	0.000	± 0.000	0.000	± 0.000	0.000	± 0.000
9	0.000	± 0.000	0.000	± 0.000	0.000	± 0.000	0.000	± 0.000
10	0.000	± 0.000	0.000	± 0.000	0.000	± 0.000	0.000	± 0.000
11	0.000	± 0.000	0.000	± 0.000	0.000	± 0.000	0.000	± 0.000
12	0.000	± 0.000	0.000	± 0.000	0.000	± 0.000	0.000	± 0.000
13	0.000	± 0.000	0.000	± 0.000	0.000	± 0.000	0.000	± 0.000
14	0.000	± 0.000	0.000	± 0.000	0.000	± 0.000	0.000	± 0.000
15	0.000	± 0.000	0.000	± 0.000	0.000	± 0.000	0.000	± 0.000
16	0.000	± 0.000	0.000	± 0.000	0.000	± 0.000	0.000	± 0.000
17	0.000	± 0.000	0.000	± 0.000	0.000	± 0.000	0.000	± 0.000
18	0.000	± 0.000	0.000	± 0.000	0.000	± 0.000	0.000	± 0.000
19	0.000	± 0.000	0.000	± 0.000	0.000	± 0.000	0.000	± 0.000
20	0.000	± 0.000	0.000	± 0.000	0.000	± 0.000	0.000	± 0.000
21	0.000	± 0.000	0.000	± 0.000	0.000	± 0.000	0.000	± 0.000
22	0.000	± 0.000	0.000	± 0.000	0.000	± 0.000	0.000	± 0.000
23	0.000	± 0.000	0.000	± 0.000	0.000	± 0.000	0.000	± 0.000
24	0.000	± 0.000	0.000	± 0.000	0.000	± 0.000	0.000	± 0.000

Table 6: *V. fischeri* strain VCW2G7 [AHLs] Used in Figure 6D

Time (h)	C6		3OC6		C7 AHL		C8	
	[AHL] Average (μM)	Range	[AHL] Average (μM)	Range	[AHL] Average (μM)	Range	[AHL] Average (μM)	Range
0	0.000	± 0.000	0.000	± 0.000	0.000	± 0.000	0.000	± 0.000
1	0.000	± 0.000	0.000	± 0.000	0.000	± 0.000	0.003	± 0.001
2	0.000	± 0.000	0.000	± 0.000	0.000	± 0.000	0.004	± 0.001
3	0.000	± 0.000	0.000	± 0.000	0.000	± 0.000	0.010	± 0.001
4	0.000	± 0.000	0.000	± 0.000	0.000	± 0.000	0.054	± 0.004
5	0.008	± 0.008	0.000	± 0.000	0.000	± 0.000	0.232	± 0.009
6	0.017	± 0.004	0.000	± 0.000	0.000	± 0.000	0.456	± 0.006
7	0.033	± 0.016	0.000	± 0.000	0.000	± 0.000	0.807	± 0.060
8	0.038	± 0.003	0.000	± 0.000	0.000	± 0.000	1.116	± 0.039
9	0.062	± 0.001	0.000	± 0.000	0.000	± 0.000	1.627	± 0.160
10	0.088	± 0.006	0.000	± 0.000	0.000	± 0.000	1.866	± 0.146
11	0.130	± 0.020	0.000	± 0.000	0.000	± 0.000	2.073	± 0.241
12	0.112	± 0.003	0.000	± 0.000	0.000	± 0.000	2.251	± 0.097
13	0.117	± 0.003	0.000	± 0.000	0.000	± 0.000	2.100	± 0.141
14	0.125	± 0.018	0.000	± 0.000	0.001	± 0.001	2.051	± 0.187
15	0.123	± 0.004	0.000	± 0.000	0.005	± 0.005	2.078	± 0.141
16	0.109	± 0.000	0.000	± 0.000	0.083	± 0.014	1.834	± 0.080
17	0.116	± 0.008	0.000	± 0.000	0.128	± 0.009	1.540	± 0.007
18	0.092	± 0.001	0.000	± 0.000	0.103	± 0.015	1.474	± 0.074
19	0.096	± 0.013	0.000	± 0.000	0.101	± 0.001	1.276	± 0.087
20	0.071	± 0.003	0.000	± 0.000	0.088	± 0.012	1.053	± 0.091
21	0.063	± 0.004	0.000	± 0.000	0.103	± 0.018	0.922	± 0.045
22	0.049	± 0.007	0.000	± 0.000	0.049	± 0.004	0.685	± 0.091
23	0.039	± 0.008	0.000	± 0.000	0.036	± 0.009	0.615	± 0.109
24	0.020	± 0.008	0.000	± 0.000	0.032	± 0.005	0.489	± 0.084

Table 7: *V. fischeri* Cell Densities Used in Figure 6E

Time (h)	ES114		MJ-1		CL21		VCW2G7	
	Cell Density Average (OD ₆₀₀)	Range	Cell Density Average (OD ₆₀₀)	Range	Cell Density Average (OD ₆₀₀)	Range	Cell Density Average (OD ₆₀₀)	Range
0	0.00	± 0.00	0.00	± 0.00	0.04	± 0.00	0.04	± 0.00
1	0.08	± 0.00	0.05	± 0.00	0.08	± 0.00	0.10	± 0.00
2	0.31	± 0.00	0.30	± 0.00	0.30	± 0.00	0.36	± 0.01
3	0.54	± 0.00	0.73	± 0.01	0.64	± 0.00	0.80	± 0.02
4	0.68	± 0.00	1.10	± 0.00	0.98	± 0.00	1.22	± 0.01
5	1.03	± 0.01	1.45	± 0.00	1.43	± 0.01	1.88	± 0.05
6	1.58	± 0.01	1.83	± 0.11	1.80	± 0.02	2.42	± 0.05
7	2.17	± 0.15	2.30	± 0.05	2.27	± 0.04	2.88	± 0.07
8	2.62	± 0.06	2.72	± 0.13	2.63	± 0.07	3.27	± 0.08
9	3.09	± 0.09	3.16	± 0.13	3.30	± 0.10	3.68	± 0.01
10	3.40	± 0.10	3.51	± 0.09	3.41	± 0.01	3.94	± 0.07
11	3.86	± 0.04	3.77	± 0.16	3.86	± 0.20	4.28	± 0.02
12	4.08	± 0.06	4.19	± 0.09	4.16	± 0.14	4.74	± 0.02
13	4.23	± 0.02	4.31	± 0.06	4.24	± 0.13	4.86	± 0.03
14	4.41	± 0.03	4.52	± 0.07	4.61	± 0.00	5.15	± 0.13
15	4.62	± 0.00	4.82	± 0.16	4.76	± 0.06	5.52	± 0.02
16	4.52	± 0.02	5.00	± 0.05	5.16	± 0.14	5.86	± 0.05
17	4.60	± 0.07	5.20	± 0.01	5.32	± 0.15	5.93	± 0.03
18	4.67	± 0.02	5.24	± 0.03	5.50	± 0.09	6.18	± 0.12
19	4.66	± 0.00	5.10	± 0.04	5.92	± 0.04	6.37	± 0.07
20	4.63	± 0.06	5.13	± 0.03	5.60	± 0.04	5.99	± 0.07
21	4.65	± 0.04	5.28	± 0.00	5.52	± 0.06	5.96	± 0.08
22	4.72	± 0.14	5.36	± 0.06	5.69	± 0.07	5.89	± 0.02
23	4.65	± 0.02	5.21	± 0.02	5.63	± 0.11	5.94	± 0.08
24	4.65	± 0.08	5.25	± 0.01	5.91	± 0.07	5.84	± 0.04

Table 8: *V. fischeri* strains MJ-1 and ES114 [DPD] Used in Figure 7

Time (h)	MJ-1		ES114	
	[DPD] (μM)	Range	[DPD] (μM)	Range
0	0.25	± 0.04	0.34	± 0.01
1	0.30	± 0.02	0.32	± 0.02
2	0.51	± 0.04	0.53	± 0.03
3	1.33	± 0.00	1.33	± 0.00
4	1.88	± 0.00	1.88	± 0.00
5	1.52	± 0.00	1.52	± 0.00
6	0.70	± 0.05	1.28	± 0.00
7	0.71	± 0.00	1.21	± 0.00
8	0.69	± 0.14	1.03	± 0.08
9	0.59	± 0.10	0.78	± 0.05
10	0.66	± 0.01	0.64	± 0.00
11	0.72	± 0.00	0.67	± 0.09
12	0.53	± 0.09	0.45	± 0.08
13	0.35	± 0.09	0.44	± 0.10
14	0.32	± 0.00	0.39	± 0.10
15	0.33	± 0.08	0.33	± 0.01
16	0.47	± 0.05	0.42	± 0.02
17	0.25	± 0.04	0.36	± 0.01
18	0.24	± 0.02	0.26	± 0.02
19	0.30	± 0.08	0.26	± 0.09
20	0.32	± 0.07	0.24	± 0.06
21	0.26	± 0.01	0.32	± 0.13
22	0.25	± 0.03	0.30	± 0.05
23	0.25	± 0.06	0.22	± 0.13
24	0.17	± 0.04	0.18	± 0.00

Table 9: *E. tarda* No Added Glucose and 0.14% Glucose Cell Density and [DPD] Figure 8

Time (h)	No Added Glucose		0.14% Glucose	
	Cell Density (OD ₆₀₀)	[DPD] (μM)	Cell Density (OD ₆₀₀)	[DPD] (μM)
0	0.01	0.30	0.01	0.32
1	0.04	0.49	0.04	0.39
2	0.08	0.58	0.09	0.59
3	0.23	1.06	0.25	1.05
4	0.50	2.24	0.56	2.44
5	0.74	3.38	1.25	6.10
6	1.04	6.00	2.30	10.58
7	1.49	9.15	3.04	23.15
8	1.60	11.82	3.50	40.82
9	1.90	15.37	3.62	56.01
10	2.20	20.15	3.69	68.49
11	2.56	23.82	3.68	76.08
12	2.94	31.62	3.91	87.48
13	2.91	27.92	3.77	89.63
14	3.12	9.82	3.99	99.66
15	3.30	0.06	4.03	98.99
16	3.59	0.05	4.00	107.71
17	3.77	0.06	4.42	112.09
18	4.12	0.05	4.66	103.73
19	4.14	0.05	4.84	89.27
20	4.42	0.53	5.05	40.18
21	4.45	0.83	5.51	0.96
22	4.50	0.73	5.60	0.69
23	4.56	0.78	5.98	0.73
24	4.52	0.71	6.17	0.43

Table 10: *Y. enterocolitica* No Added Glucose Cell Density and [DPD]/OD Used in Figure 9

Time (h)	Cell Density Average (OD ₆₀₀)	Range	[DPD]/OD Average (μM/OD ₆₀₀)	Range
1	0.03	± 0.00	25.13	± 0.66
2	0.07	± 0.00	13.78	± 0.22
3	0.14	± 0.00	7.44	± 0.21
4	0.31	± 0.00	4.72	± 0.10
5	0.52	± 0.02	4.41	± 0.11
6	0.95	± 0.01	4.82	± 0.02
7	1.68	± 0.03	6.06	± 0.09
8	2.25	± 0.06	11.43	± 0.31
9	2.40	± 0.15	22.45	± 0.93
10	2.94	± 0.05	26.75	± 0.54
11	3.26	± 0.13	20.44	± 1.22
12	3.46	± 0.14	8.53	± 0.18
13	3.69	± 0.10	0.17	± 0.14
14	3.79	± 0.11	0.13	± 0.11
15	4.05	± 0.05	0.09	± 0.08
16	4.05	± 0.05	0.08	± 0.07

Table 11: *Y. enterocolitica* 0.08% Glucose Cell Density and [DPD]/OD Used in Figure 9

Time (h)	Cell Density Average (OD ₆₀₀)	Range	[DPD]/OD Average (μM/OD ₆₀₀)	Range
1	0.03	± 0.00	26.48	± 0.05
2	0.07	± 0.00	13.75	± 0.32
3	0.14	± 0.00	7.49	± 0.17
4	0.31	± 0.01	4.74	± 0.07
5	0.51	± 0.01	4.34	± 0.17
6	0.90	± 0.02	4.80	± 0.05
7	1.53	± 0.05	6.22	± 0.03
8	2.00	± 0.04	11.68	± 0.39
9	2.19	± 0.06	24.32	± 0.02
10	2.63	± 0.15	34.15	± 0.47
11	2.99	± 0.08	36.54	± 0.39
12	3.50	± 0.14	24.61	± 1.38
13	3.73	± 0.01	8.49	± 0.19
14	4.02	± 0.02	0.34	± 0.01
15	4.22	± 0.02	0.24	± 0.00
16	4.22	± 0.02	0.22	± 0.04

Table 12: *Y. enterocolitica* 0.14% Glucose Cell Density and [DPD]/OD Used in Figure 9

Time (h)	Cell Density Average (OD ₆₀₀)	Range	[DPD]/OD Average (μM/OD ₆₀₀)	Range
1	0.03	± 0.00	45.97	± 6.89
2	0.05	± 0.00	22.07	± 2.99
3	0.11	± 0.00	10.97	± 0.35
4	0.25	± 0.01	5.80	± 0.10
5	0.46	± 0.01	4.71	± 0.05
6	0.86	± 0.01	4.80	± 0.11
7	1.71	± 0.00	5.48	± 0.28
8	2.19	± 0.04	10.10	± 0.73
9	2.69	± 0.03	18.53	± 1.00
10	3.13	± 0.03	27.53	± 1.21
11	3.52	± 0.04	31.50	± 0.39
12	3.88	± 0.01	20.17	± 0.85
13	4.20	± 0.07	2.76	± 1.05
14	4.37	± 0.03	0.51	± 0.04
15	4.63	± 0.05	0.31	± 0.03
16	4.89	± 0.06	0.32	± 0.05

Table 13: *Y. enterocolitica* 0.20% Glucose Cell Density and [DPD]/OD Used in Figure 9

Time (h)	Cell Density Average (OD ₆₀₀)	Range	[DPD]/OD Average (μM/OD ₆₀₀)	Range
1	0.03	± 0.00	38.42	± 1.50
2	0.05	± 0.00	19.17	± 0.49
3	0.12	± 0.00	10.17	± 0.16
4	0.25	± 0.00	5.86	± 0.11
5	0.47	± 0.00	4.83	± 0.03
6	0.87	± 0.01	4.96	± 0.01
7	1.73	± 0.03	5.72	± 0.02
8	2.20	± 0.00	10.18	± 0.14
9	2.67	± 0.02	20.07	± 0.44
10	3.11	± 0.02	27.86	± 0.21
11	3.60	± 0.05	31.98	± 1.56
12	3.96	± 0.05	24.58	± 0.74
13	4.30	± 0.05	5.89	± 0.66
14	4.47	± 0.02	0.45	± 0.00
15	4.72	± 0.04	0.34	± 0.00
16	5.03	± 0.02	0.24	± 0.01

Table 14: *Y. enterocolitica* No Added Glucose [DPD] and % Glucose Used in Figure 10A

Time (h)	[DPD] Average (μ M)	Range	% Glucose Average (% (w/v))	Range
0	0.78	± 0.02	0.15	± 0.01
1	0.84	± 0.02	0.14	± 0.01
2	0.91	± 0.01	0.12	± 0.00
3	1.05	± 0.00	0.11	± 0.00
4	1.47	± 0.01	0.10	± 0.00
5	2.31	± 0.01	0.08	± 0.00
6	4.56	± 0.04	0.08	± 0.00
7	10.18	± 0.07	0.07	± 0.01
8	25.71	± 0.02	0.02	± 0.00
9	53.69	± 1.19	-0.01	± 0.00
10	78.62	± 0.24	-0.01	± 0.00
11	66.37	± 1.31	-0.01	± 0.00
12	29.48	± 0.59	-0.01	± 0.00
13	0.63	± 0.51	-0.01	± 0.00
14	0.47	± 0.39	-0.01	± 0.00
15	0.37	± 0.31	0.00	± 0.00
16	0.33	± 0.27	-0.01	± 0.00

$$A_{500} = 6.808 \times [\text{glucose}] + 0.4399; R^2 = 0.9938$$

Table 15: *Y. enterocolitica* 0.08% Glucose [DPD] and % Glucose Used in Figure 10B

Time (h)	[DPD] Average (μ M)	Range	% Glucose Average (% (w/v))	Range
0	0.78	± 0.01	0.12	± 0.01
1	0.81	± 0.01	0.10	± 0.01
2	0.91	± 0.01	0.10	± 0.01
3	1.02	± 0.04	0.10	± 0.02
4	1.45	± 0.00	0.10	± 0.01
5	2.20	± 0.13	0.10	± 0.02
6	4.32	± 0.13	0.10	± 0.01
7	9.48	± 0.24	0.11	± 0.01
8	23.31	± 1.24	0.08	± 0.02
9	53.13	± 1.29	0.04	± 0.02
10	89.75	± 3.89	0.00	± 0.01
11	109.14	± 1.66	0.01	± 0.02
12	85.84	± 1.51	0.00	± 0.02
13	31.63	± 0.68	0.00	± 0.01
14	1.37	± 0.03	0.00	± 0.01
15	0.99	± 0.00	0.00	± 0.01
16	0.93	± 0.15	0.00	± 0.01

$$A_{500} = 5.869 \times [\text{glucose}] + 0.2882; R^2 = 0.9849$$

Table 16: *Y. enterocolitica* 0.14% Glucose [DPD] and % Glucose Used in Figure 10C

Time (h)	[DPD] Average (μM)	Range	% Glucose Average (% (w/v))	Range
0	0.77	± 0.02	0.12	± 0.02
1	1.15	± 0.17	0.16	± 0.01
2	1.12	± 0.11	0.15	± 0.03
3	1.24	± 0.07	0.17	± 0.04
4	1.46	± 0.03	0.15	± 0.03
5	2.15	± 0.02	0.15	± 0.01
6	4.11	± 0.15	0.16	± 0.01
7	9.35	± 0.48	0.14	± 0.01
8	22.04	± 1.25	0.14	± 0.02
9	49.77	± 2.18	0.06	± 0.01
10	86.00	± 2.95	0.00	± 0.01
11	110.93	± 0.04	-0.01	± 0.02
12	78.33	± 3.43	-0.01	± 0.02
13	11.65	± 4.58	0.00	± 0.02
14	2.24	± 0.21	-0.01	± 0.02
15	1.45	± 0.15	-0.01	± 0.02
16	1.58	± 0.28	-0.01	± 0.02

$$A_{500} = 5.869 \times [\text{glucose}] + 0.2882; R^2 = 0.9849$$

Table 17: *Y. enterocolitica* 0.20% Glucose [DPD] and % Glucose Used in Figure 10D

Time (h)	[DPD] Average (μM)	Range	% Glucose Average (% (w/v))	Range
0	0.86	± 0.01	0.14	± 0.04
1	1.00	± 0.00	0.17	± 0.01
2	1.03	± 0.01	0.17	± 0.02
3	1.18	± 0.04	0.18	± 0.01
4	1.49	± 0.03	0.19	± 0.01
5	2.26	± 0.01	0.20	± 0.00
6	4.29	± 0.06	0.22	± 0.00
7	9.87	± 0.14	0.19	± 0.02
8	22.37	± 0.29	0.17	± 0.03
9	53.50	± 1.57	0.09	± 0.02
10	86.51	± 0.04	0.04	± 0.02
11	115.12	± 4.10	-0.01	± 0.02
12	97.29	± 1.72	-0.01	± 0.02
13	25.27	± 2.56	0.00	± 0.02
14	2.00	± 0.03	-0.01	± 0.01
15	1.58	± 0.00	0.00	± 0.02
16	1.19	± 0.02	0.00	± 0.02

$$A_{500} = 5.869 \times [\text{glucose}] + 0.2882; R^2 = 0.9849$$

Table 18: *Y. enterocolitica* No Added Glucose Cell Density and [DPD]/OD Used in Figure 11

Time (h)	Cell Density Average (OD ₆₀₀)	Range	[DPD]/OD Average (μM/OD ₆₀₀)	Range
1	0.02	± 0.00	18.35	± 0.87
2	0.04	± 0.00	10.41	± 0.41
3	0.11	± 0.00	5.48	± 0.05
4	0.24	± 0.02	4.16	± 0.38
5	0.52	± 0.01	4.14	± 0.13
6	0.82	± 0.05	5.84	± 0.22
7	1.50	± 0.04	6.00	± 0.35
8	1.73	± 0.06	6.39	± 0.38
9	1.92	± 0.09	4.95	± 0.16
10	2.25	± 0.11	1.62	± 0.20
11	2.54	± 0.09	0.27	± 0.00
12	2.84	± 0.09	0.20	± 0.00
13	3.11	± 0.10	0.18	± 0.01
14	3.48	± 0.07	0.17	± 0.01
15	3.72	± 0.16	0.14	± 0.01
16	4.03	± 0.10	0.12	± 0.00

Table 19: *Y. enterocolitica* 0.08% Glucose Cell Density and [DPD]/OD Used in Figure 11

Time (h)	Cell Density Average (OD ₆₀₀)	Range	[DPD]/OD Average (μM/OD ₆₀₀)	Range
1	0.02	± 0.00	16.84	± 0.19
2	0.05	± 0.00	9.90	± 0.52
3	0.12	± 0.00	5.38	± 0.01
4	0.27	± 0.00	3.79	± 0.04
5	0.59	± 0.01	4.62	± 0.10
6	0.88	± 0.01	8.76	± 0.05
7	1.44	± 0.10	13.38	± 0.62
8	1.70	± 0.05	19.39	± 0.36
9	2.01	± 0.08	25.11	± 2.20
10	2.38	± 0.12	24.64	± 1.41
11	2.81	± 0.15	15.52	± 1.57
12	2.97	± 0.07	3.47	± 1.77
13	3.19	± 0.05	0.23	± 0.01
14	3.43	± 0.04	0.19	± 0.01
15	3.73	± 0.06	0.14	± 0.01
16	4.06	± 0.03	0.12	± 0.00

Table 20: *Y. enterocolitica* 0.14% Glucose Cell Density and [DPD]/OD Used in Figure 11

Time (h)	Cell Density Average (OD ₆₀₀)	Range	[DPD]/OD Average (μM/OD ₆₀₀)	Range
1	0.02	± 0.00	23.59	± 0.95
2	0.05	± 0.00	11.45	± 0.04
3	0.13	± 0.00	5.11	± 0.15
4	0.32	± 0.01	3.86	± 0.05
5	0.66	± 0.02	4.83	± 0.05
6	1.08	± 0.01	7.51	± 0.14
7	1.70	± 0.00	11.26	± 0.25
8	1.95	± 0.08	18.71	± 0.68
9	2.32	± 0.03	25.04	± 1.06
10	2.62	± 0.04	28.56	± 0.07
11	3.02	± 0.05	25.34	± 0.96
12	3.29	± 0.04	16.24	± 0.57
13	3.38	± 0.01	6.97	± 0.43
14	3.42	± 0.01	0.27	± 0.01
15	3.64	± 0.00	0.21	± 0.02
16	3.92	± 0.06	0.18	± 0.01

Table 21: *Y. enterocolitica* 0.20% Glucose Cell Density and [DPD]/OD Used in Figure 11

Time (h)	Cell Density Average (OD ₆₀₀)	Range	[DPD]/OD Average (μM/OD ₆₀₀)	Range
1	0.02	± 0.00	24.32	± 0.39
2	0.05	± 0.00	10.33	± 0.04
3	0.13	± 0.00	5.51	± 0.08
4	0.31	± 0.01	3.86	± 0.16
5	0.67	± 0.00	4.60	± 0.04
6	1.10	± 0.02	7.79	± 0.33
7	1.68	± 0.00	11.81	± 0.32
8	1.98	± 0.02	18.58	± 0.58
9	2.38	± 0.02	26.89	± 0.08
10	2.62	± 0.07	32.92	± 0.37
11	3.01	± 0.08	32.36	± 1.12
12	3.31	± 0.06	26.24	± 1.07
13	3.49	± 0.13	18.55	± 2.00
14	3.55	± 0.11	7.56	± 1.65
15	3.47	± 0.41	0.29	± 0.01
16	4.03	± 0.19	0.21	± 0.00

Table 22: *Y. enterocolitica* 0.30% Glucose Cell Density and [DPD]/OD Used in Figure 11

Time (h)	Cell Density Average (OD ₆₀₀)	Range	[DPD]/OD Average (μM/OD ₆₀₀)	Range
1	0.03	± 0.00	19.61	± 1.59
2	0.07	± 0.01	9.25	± 1.26
3	0.18	± 0.00	4.99	± 0.22
4	0.48	± 0.00	4.82	± 0.86
5	0.99	± 0.00	5.16	± 0.07
6	1.79	± 0.03	9.78	± 0.34
7	2.27	± 0.17	17.49	± 0.54
8	2.35	± 0.06	26.68	± 0.34
9	2.48	± 0.05	30.74	± 0.48
10	2.89	± 0.11	31.52	± 0.04
11	3.10	± 0.03	33.89	± 0.43
12	3.21	± 0.06	33.48	± 1.25
13	3.48	± 0.04	29.77	± 0.17
14	3.69	± 0.06	25.94	± 0.80
15	3.96	± 0.07	24.58	± 1.61
16	4.30	± 0.12	18.27	± 1.33

Table 23: *Y. enterocolitica* 0.50% Glucose Cell Density and [DPD]/OD Used in Figure 11

Time (h)	Cell Density Average (OD ₆₀₀)	Range	[DPD]/OD Average (μM/OD ₆₀₀)	Range
1	0.02	± 0.00	21.41	± 0.17
2	0.07	± 0.01	8.84	± 0.87
3	0.18	± 0.00	4.89	± 0.12
4	0.49	± 0.00	3.96	± 0.01
5	0.98	± 0.00	5.58	± 0.06
6	1.83	± 0.03	10.33	± 0.32
7	2.33	± 0.01	17.64	± 0.71
8	2.35	± 0.02	26.04	± 0.22
9	2.59	± 0.02	29.33	± 0.45
10	2.83	± 0.05	33.39	± 0.76
11	3.09	± 0.04	32.82	± 2.39
12	3.28	± 0.02	34.26	± 0.10
13	3.59	± 0.02	30.18	± 0.13
14	3.72	± 0.05	33.29	± 0.91
15	3.62	± 0.22	34.40	± 3.15
16	4.00	± 0.02	27.45	± 1.60

Table 24: *Y. enterocolitica* No Added Glucose [DPD] and % Glucose Used in Figure 12A

Time (h)	[DPD] Average (μM)	Range	% Glucose Average (% (w/v))	Range
0	0.39	± 0.00	-0.01	± 0.00
1	0.41	± 0.01	-0.01	± 0.00
2	0.45	± 0.00	-0.01	± 0.00
3	0.59	± 0.02	0.00	± 0.00
4	0.98	± 0.01	-0.01	± 0.00
5	2.15	± 0.10	-0.01	± 0.00
6	4.78	± 0.10	-0.01	± 0.00
7	9.01	± 0.30	-0.01	± 0.01
8	11.03	± 0.27	-0.03	± 0.01
9	9.50	± 0.14	-0.02	± 0.00
10	3.62	± 0.28	-0.01	± 0.00
11	0.68	± 0.03	-0.01	± 0.00
12	0.57	± 0.01	-0.01	± 0.00
13	0.57	± 0.01	-0.01	± 0.00
14	0.58	± 0.03	-0.01	± 0.00
15	0.51	± 0.01	-0.01	± 0.01
16	0.49	± 0.01	-0.02	± 0.00

$$A_{500} = 4.197 \times [\text{glucose}] + 0.4597; R^2 = 0.9966$$

Table 25: *Y. enterocolitica* 0.08% Glucose [DPD] and % Glucose Used in Figure 12B

Time (h)	[DPD] Average (μM)	Range	% Glucose Average (% (w/v))	Range
0	0.34	± 0.00	0.12	± 0.01
1	0.40	± 0.00	0.11	± 0.03
2	0.47	± 0.01	0.12	± 0.03
3	0.62	± 0.01	0.13	± 0.03
4	1.04	± 0.02	0.15	± 0.01
5	2.74	± 0.01	0.11	± 0.01
6	7.72	± 0.11	0.07	± 0.00
7	19.14	± 0.38	-0.01	± 0.00
8	32.94	± 0.45	-0.02	± 0.00
9	50.34	± 2.36	-0.02	± 0.00
10	58.54	± 0.46	-0.01	± 0.01
11	43.39	± 2.17	-0.01	± 0.00
12	10.17	± 5.03	-0.01	± 0.00
13	0.73	± 0.03	-0.01	± 0.00
14	0.63	± 0.02	-0.01	± 0.00
15	0.52	± 0.01	-0.01	± 0.01
16	0.48	± 0.02	-0.03	± 0.00

$$A_{500} = 4.197 \times [\text{glucose}] + 0.4597; R^2 = 0.9966$$

Table 26: *Y. enterocolitica* 0.14% Glucose [DPD] and % Glucose Used in Figure 12C

Time (h)	[DPD] Average (μM)	Range	% Glucose Average (%(w/v))	Range
0	0.31	± 0.00	0.17	± 0.01
1	0.38	± 0.02	0.14	± 0.01
2	0.52	± 0.02	0.16	± 0.03
3	0.66	± 0.03	0.19	± 0.02
4	1.24	± 0.04	0.18	± 0.02
5	3.18	± 0.08	0.17	± 0.01
6	8.10	± 0.19	0.14	± 0.02
7	19.08	± 0.42	0.08	± 0.01
8	36.33	± 0.07	0.01	± 0.01
9	58.01	± 1.64	-0.02	± 0.00
10	74.70	± 1.47	-0.01	± 0.01
11	76.43	± 1.68	-0.01	± 0.00
12	53.46	± 1.27	0.00	± 0.00
13	23.57	± 1.49	-0.01	± 0.00
14	0.92	± 0.02	0.00	± 0.00
15	0.78	± 0.07	-0.01	± 0.00
16	0.69	± 0.04	-0.02	± 0.00

$$A_{500} = 4.197 \times [\text{glucose}] + 0.4597; R^2 = 0.9966$$

Table 27: *Y. enterocolitica* 0.20% Glucose [DPD] and % Glucose Used in Figure 12D

Time (h)	[DPD] Average (μM)	Range	% Glucose Average (% (w/v))	Range
0	0.31	± 0.01	0.15	± 0.02
1	0.39	± 0.01	0.16	± 0.00
2	0.48	± 0.01	0.16	± 0.00
3	0.71	± 0.01	0.15	± 0.03
4	1.20	± 0.01	0.15	± 0.00
5	3.07	± 0.03	0.16	± 0.01
6	8.57	± 0.18	0.12	± 0.01
7	19.81	± 0.50	0.12	± 0.01
8	36.77	± 0.69	0.07	± 0.01
9	64.01	± 0.87	0.00	± 0.01
10	86.12	± 3.27	-0.01	± 0.00
11	97.31	± 0.77	-0.01	± 0.00
12	86.73	± 2.05	-0.01	± 0.01
13	64.49	± 4.67	-0.01	± 0.01
14	26.68	± 5.05	-0.01	± 0.00
15	1.01	± 0.08	-0.01	± 0.00
16	0.83	± 0.05	-0.02	± 0.00

$$A_{500} = 6.034 \times [\text{glucose}] + 0.4786; R^2 = 0.9997$$

Table 28: *Y. enterocolitica* 0.30% Glucose [DPD] and % Glucose Used in Figure 12E

Time (h)	[DPD] Average (μM)	Range	% Glucose Average (% (w/v))	Range
0	0.47	± 0.02	0.19	± 0.01
1	0.49	± 0.02	0.16	± 0.03
2	0.64	± 0.00	0.16	± 0.01
3	0.88	± 0.03	0.19	± 0.02
4	2.29	± 0.41	0.17	± 0.02
5	5.13	± 0.06	0.17	± 0.03
6	17.52	± 0.34	0.16	± 0.01
7	39.60	± 1.65	0.14	± 0.01
8	62.79	± 2.33	0.10	± 0.00
9	76.33	± 2.82	0.06	± 0.00
10	91.00	± 3.42	0.03	± 0.01
11	105.07	± 2.36	-0.02	± 0.00
12	107.39	± 2.17	-0.02	± 0.00
13	103.53	± 1.72	-0.01	± 0.00
14	95.55	± 1.25	-0.02	± 0.00
15	97.24	± 4.77	-0.02	± 0.00
16	78.45	± 3.48	-0.02	± 0.00

$$A_{500} = 6.034 \times [\text{glucose}] + 0.4786; R^2 = 0.9997$$

Table 29: *Y. enterocolitica* 0.50% Glucose [DPD] and % Glucose Used in Figure 12F

Time (h)	[DPD] Average (μ M)	Range	% Glucose Average (% (w/v))	Range
0	0.48	± 0.01	0.21	± 0.01
1	0.51	± 0.02	0.22	± 0.00
2	0.61	± 0.01	0.22	± 0.01
3	0.86	± 0.01	0.20	± 0.01
4	1.92	± 0.00	0.20	± 0.01
5	5.50	± 0.04	0.20	± 0.00
6	18.85	± 0.28	0.20	± 0.00
7	41.14	± 1.80	0.20	± 0.02
8	61.26	± 0.06	0.17	± 0.00
9	75.80	± 0.57	0.18	± 0.01
10	94.46	± 0.48	0.17	± 0.01
11	101.32	± 6.23	0.15	± 0.01
12	112.46	± 0.43	0.11	± 0.01
13	108.18	± 1.09	0.03	± 0.01
14	123.63	± 1.72	-0.01	± 0.00
15	123.86	± 3.73	-0.01	± 0.00
16	109.69	± 5.93	-0.02	± 0.00

$$A_{500} = 6.034 \times [\text{glucose}] + 0.4786; R^2 = 0.9997$$

Table 30: Metabolites Measured

Metabolite	Fold change in cells treated with IL-1 β + γ -IFN Relative to NT	p-value
Citrulline	431.17	2.65 x 10 ⁻²⁵
Inosine	11.70	3.60 x 10 ⁻⁷
Pyruvate	7.58	2.03 x 10 ⁻⁶
TDP	2.14	8.55 x 10 ⁻⁶
Lactate	-8.15	4.42 x 10 ⁻⁵
Shikimate-3-phosphate	2.20	7.20 x 10 ⁻⁵
Malate	3.78	1.38 x 10 ⁻⁵
Taurine	3.18	1.75 x 10 ⁻⁴
UDP-N-acetylglucosamine	2.98	2.12 x 10 ⁻⁴
Methylmalnic acid	2.78	3.95 x 10 ⁻⁴
4-Hydroxybenzoate	2.10	4.16 x 10 ⁻⁴
Succinate and Methylmalonate	2.75	4.48 x 10 ⁻⁴
Citrate	2.65	5.49 x 10 ⁻⁴
Citraconate	2.06	6.52 x 10 ⁻⁴
N-Acetylglucosamine-1-phosphate	1.21	1.28 x 10 ⁻³
D-Glyceraldehyde-3-phosphate	1.00	1.65 x 10 ⁻³
UDP-D-glucose	2.05	2.25 x 10 ⁻³
UDP	2.18	2.68 x 10 ⁻³
Nicotinamide ribotide	-1.16	3.75 x 10 ⁻³
Pantothenate	-1.04	4.06 x 10 ⁻³
dCDP	1.44	5.13 x 10 ⁻³
Glucose-6-phosphate	1.09	6.46 x 10 ⁻³
Glycerate-2,3-diphosphate	-1.09	8.09 x 10 ⁻³
Nicotinate	1.78	8.36 x 10 ⁻³
Riboflavin (Vitamin B2)	1.08	0.011
Orotidine-phosphate	1.38	0.011
5-methyl-tetrahydrofolate	-2.88	0.013
2-Deoxyribose-1-phosphate	1.40	0.014
1-methyladenosine	-1.22	0.015
Ceramide	-1.48	0.016
Guanosine	2.41	0.017
Pyridine-2,3-dicarboxylate	1.00	0.027
Stearate	1.64	0.033
D-Glucono-lactone-6-phosphate	1.52	0.036
Dihydroxyacetone phosphate (DHAP)	-1.09	0.038
Pyridoxine	1.51	0.040
Pentose-phosphate	1.85	0.044
dATP	1.17	0.054
Tyrosine	1.57	0.058
ADP	1.74	0.063
D-Hexose-phosphate	-1.05	0.066

Table 30: Continued

Metabolite	Fold change in cells treated with IL-1β+γ-IFN Relative to NT	p-value
Asparagine	-1.47	0.093
NAD	-1.19	0.106
N-acetyl-glutamine	1.23	0.120
1-methylhistidine	1.00	0.134
5'-methylthioadenosine	1.21	0.136
2-Keto-D-gluconate	-1.50	0.139
Glycerate-diphosphate (1,3 and 2,3)	1.19	0.140
Aconitate (<i>cis</i> and <i>trans</i>)	1.51	0.144
Glycerol-3-phosphate	1.70	0.148
Methionine	1.34	0.153
Homoserine	1.34	0.158
Glutamate	1.35	0.162
Carnitine	-1.13	0.168
Cytidine	2.12	0.175
Ornithine	1.62	0.180
Arginine	-1.47	0.204
GABA	1.29	0.228
4-Pyridoxate	1.46	0.229
Choline	1.10	0.238
Acetyllysine	1.32	0.240
5-methyldeoxycytidine	1.37	0.251
Histidine	1.17	0.259
Cysteine	1.25	0.264
Proline	-1.06	0.270
5-Phosphoribosyl-1-diphosphate	1.49	0.276
N-acetyl-glutamate	1.40	0.286
Valine	1.48	0.295
Acetyl phosphate	1.00	0.299
DL-Acetylcarnitine	1.17	0.316
Reduced glutathione	1.17	0.319
Nicotinamide	1.31	0.352
Lysine	1.21	0.354
Glutamine	1.03	0.361
Tryptophan	-1.53	0.365
Fumarate, Maleate, iso-Ketovaleate	1.31	0.369
Phenylalanine	1.72	0.417
S-adenosyl-L-methionine	1.13	0.436
Threonine	1.18	0.452
(Iso)Leucine	1.53	0.454
Adenosine	1.32	0.460
Palmitate	-1.92	0.477
Glycerophosphocholine	1.10	0.478
Aspartate	-1.15	0.484

Table 31: Metabolites Measured

Metabolite	Fold change in cells treated with Camptothecin Relative to NT	p-value
N-Acetylglucosamine-1-phosphate	3.79	1.79 x 10 ⁻⁵
Cysteine	3.59	1.83 x 10 ⁻⁵
1-methylhistidine	5.66	4.83 x 10 ⁻⁵
D-Glyceraldehyde-3-phosphate	1.50	5.23 x 10 ⁻⁵
Pantothenate	2.47	8.07 x 10 ⁻⁵
1-methyladenosine	4.83	8.41 x 10 ⁻⁵
Tryptophan	1.23	3.52 x 10 ⁻⁴
UDP-D-glucose	2.90	4.35 x 10 ⁻⁴
UDP-N-acetylglucosamine	3.10	4.99 x 10 ⁻⁴
Lactate	1.26	6.76 x 10 ⁻⁴
Methylmalnic acid	1.73	9.15 x 10 ⁻⁴
Succinate and Methylmalonate	1.72	1.09 x 10 ⁻³
5-methyldeoxycytidine	2.33	3.55 x 10 ⁻³
5-Phosphoribosyl-1-diphosphate	-1.61	4.71 x 10 ⁻³
Nicotinamide ribotide	-2.92	5.70 x 10 ⁻³
Shikimate-3-phosphate	1.60	6.36 x 10 ⁻³
D-Hexose-phosphate	1.79	7.37 x 10 ⁻³
Nicotinamide	-1.04	7.53 x 10 ⁻³
2-Keto-D-gluconate	-2.09	0.010
5'-methylthioadenosine	1.94	0.011
Glycerol-3-phosphate	2.64	0.012
Ornithine	2.20	0.012
Guanosine	3.02	0.013
Dihydroxyacetone phosphate (DHAP)	1.89	0.015
Pentose-phosphate	2.02	0.018
2-Deoxyribose-1-phosphate	1.43	0.019
N-acetyl-glutamate	1.59	0.020
Citrate	1.56	0.021
Lysine	3.16	0.022
Glutamine	2.65	0.023
ADP	3.92	0.028
Glycerate-2,3-diphosphate	-1.06	0.032
Stearate	-1.26	0.033
UDP	1.87	0.033
GABA	2.29	0.038
Riboflavin (Vitamin B2)	1.69	0.046
Taurine	2.37	0.048
Adenosine	-1.44	0.049
Inosine	1.69	0.050
Orotidine-phosphate	1.12	0.050
Palmitate	-1.08	0.053
Aspartate	1.64	0.062

Table 31: Continued

Metabolite	Fold change in cells treated with Camptothecin Relative to NT	p-value
Reduced glutathione	1.80	0.074
Citraconate	-1.01	0.075
D-Glucono-lactone-6-phosphate	1.01	0.079
TDP	-1.24	0.084
DL-Acetylcarnitine	2.30	0.084
Asparagine	1.67	0.085
Ceramide	-1.14	0.085
Carnitine	1.48	0.089
Glycerophosphocholine	1.70	0.089
Proline	1.86	0.090
dATP	1.33	0.092
Arginine	1.67	0.101
Nicotinate	1.66	0.104
Tyrosine	1.74	0.105
Glucose-6-phosphate	-1.02	0.108
Choline	1.63	0.128
5-methyl-tetrahydrofolate	-2.88	0.130
dCDP	1.21	0.131
Pyruvate	1.04	0.134
Histidine	1.64	0.153
4-Pyridoxate	1.07	0.157
Aconitate (<i>cis</i> and <i>trans</i>)	-1.29	0.193
Citrulline	1.00	0.198
(Iso)Leucine	1.40	0.199
Glutamate	1.59	0.205
Pyridine-2,3-dicarboxylate	1.00	0.206
Acetyllysine	1.67	0.223
Pyridoxine	-1.18	0.224
S-adenosyl-L-methionine (SAM)	2.00	0.225
Malate	1.09	0.236
Threonine	2.37	0.260
Glycerate-diphosphate (1,3 and 2,3)	1.22	0.270
N-acetyl-glutamine	1.61	0.272
Acetyl phosphate	1.00	0.303
Valine	1.34	0.327
Methionine	1.59	0.339
Homoserine	1.59	0.340
Phenylalanine	1.41	0.343
Cytidine	1.74	0.373
NAD	1.07	0.381
Fumarate, Maleate, iso-Ketovaleate	-1.16	0.404
4-Hydroxybenzoate	-1.08	0.482

Vita

Mary Elizabeth Eisenhauer was born May 12, 1987 in Dayton, OH. After moving to Oak Ridge, TN, she graduated from Oak Ridge High School in 2005. She attended Tennessee Technological University where she received her Bachelor's of Science in Chemistry in the spring of 2009. At The University of Tennessee, Knoxville she began her graduate studies in Chemistry, receiving her Master's of Science in Chemistry in December 2011. Remaining at UTK, she began graduate studies in the College of Education, and started teaching for Knox County Schools in August 2011.